Experimental Studies of the Ground State QED Corrections in H- and He-like Uranium

Dissertation

zur Erlangung des Doktorgrades

der Naturwissenschaften

vorgelegt beim Fachbereich Physik

der Johann Wolfgang Goethe-Universität

in Frankfurt am Main

von

Alexandre Gumberidze

aus Kutaisi

Frankfurt am Main 2003

(DF1)

vom Fachbereich Physik der Johann Wolfgang Goethe-Universität
als Dissertation angenommen.

Contents

Chapter 1

Introduction

Our present understanding of electromagnetic interactions is formulated through the theory of quantum electrodynamics (QED). The latter can be regarded as one of the most precisely tested theories of physics. The experimental tests and also the theoretical predictions of QED effects in physics belong to the most stimulating fields in science. During the last years a number of highly subtle setups have been constructed to measure QED effects particularly in strong electromagnetic fields of heavy nuclei. These strong fields provide the unique possibility to test the validity of QED in a regime where ordinary perturbation theory is no longer a suitable tool when considering the external field. As an illustration, in Fig. 1.1 we display the expectation value $< E >$ for the lowest-lying electron state in hydrogen-like ions as a function of nuclear charge Z [1]. The increase of more than six orders of magnitude from $Z = 1$ to $Z = 92$ is not only due to the increasing nuclear charge but also to the closer localization of highly relativistic bound states in heavy hydrogen-like ions. The field strength at the nuclear surface is even higher ($< E > \cong 2 \times 10^{19}$ V/cm). This is only a factor of 2 less than the field strength in superheavy systems with $Z \geq 170$ where spontaneous pair production is predicted to take place if the total charge is confined in a sufficiently small volume for a sufficiently long time [2]. It seems evident that in such strong fields "normal" atomic physics - valid for a hydrogen atom - may be questioned. An accurate knowledge about the validity of QED in strong external fields is also necessary for the detection of new physics beyond QED. Thus it is a primary goal to explore the behavior of electrons in some of the strongest electromagnetic

fields accessible to experimental investigation. The results are important for the energy levels and related x-ray spectra of neutral or singly ionized heavy elements as well.

The advent of powerful ion sources like the Super-Electron Beam-Ion-trap (superEBIT) at Livermore [3] and of heavy-ion storage rings like the ESR at GSI Darmstadt [4, 5] has precipitated both the experimental and theoretical study of very heavy ions with only one or few bound electrons where correlation effects are either absent or under control for specific studies [6]. The QED effects manifest themselves in the Lamb shift of the innermost energy levels of heavy one- and two-electron ions. For hydrogen-like U^{91+}, for example, the Lamb shift of the $1s_{1/2}$ ground-state amounts to approximately 460 eV as compared to 3.4×10^{-5} eV for hydrogen. Other quantities used for tests of QED are the hyperfine splitting of the $1s_{1/2}$ ground state accessible through Laser spectroscopy which can now be performed with high accuracy. Also the Zeeman effect and the corresponding g-factor of the bound electron are governed by QED effects and can be measured with electromagnetic ion traps.

High-precision Lamb shift measurements have been carried out for a number of hydrogen-like ions [7, 8, 9] as well as for helium-like [10] and lithium-like systems [11]. The goal and the main experimental challenge here is to measure the Lamb shift with an accuracy which would allow us to be sensitive to the higher order QED contributions. Also the hyperfine structure measurements on several heavy few-electron highly charged systems have been performed with a precision sufficient to probe QED predictions [12, 13, 14, 15]. For the g-factor measurements have been conducted for the electron bound in hydrogen-like carbon [16], future investigations are planned for the g-factor of bound electrons in the high-Z region (up to hydrogen-like uranium U^{91+}).

In this thesis we will concentrate on the Lamb shift investigations for the heaviest one- and two-electron systems available for experiments, i.e. hydrogen- and helium-like uranium. Whereby the main emphasis of this work is given to the study of ground state ionization energies in He-like uranium. However, because in our experiments the ground state transitions in H-like uranium have been measured at the same time, the topic of the one-electron Lamb shift in the high-Z regime is addressed in addition.

The thesis is structured as follows: First, in chapter two, a review of the theoretical situation will be given. The first and higher order QED corrections (for one as well as for few-electron systems), relativistic many-body perturbation theory (RMBPT) and multi-configuration Dirac Fock (MCDF) calculations (for few electron systems) will be discussed in comparison with recent experimental results. In chapters three and four the experimental apparatus and our measurement of the two-electron Lamb shift in helium-like uranium (U^{90+}) performed recently at the storage ring ESR at GSI will be presented, respectively. Former studies conducted at superEBIT in Livermore [10] will be discussed and the results from both experiments will be given together with the present theoretical values. Data of this kind are particularly interesting in order to test calculations of the tiny two-electron Lamb shift, since by employing our method the dominating one-body parts are completely eliminated and the relative accuracy required for testing the second-order QED contributions is 10^{-3} in comparison with the 10^{-6} necessary to test the QED corrections of the same order in one-electron systems. Besides, in contrast to the one-electron Lamb shift, the two electron effects depend very weakly on the nuclear structure. Therefore these experiments provide a unique test of QED effects in strong fields.

In the fifth chapter, we present an evaluation of the ground state Lamb shift in hydrogen-like uranium from our experimental data. Finally, a summary of the obtained results and an outlook will be given in chapters six and seven, respectively.
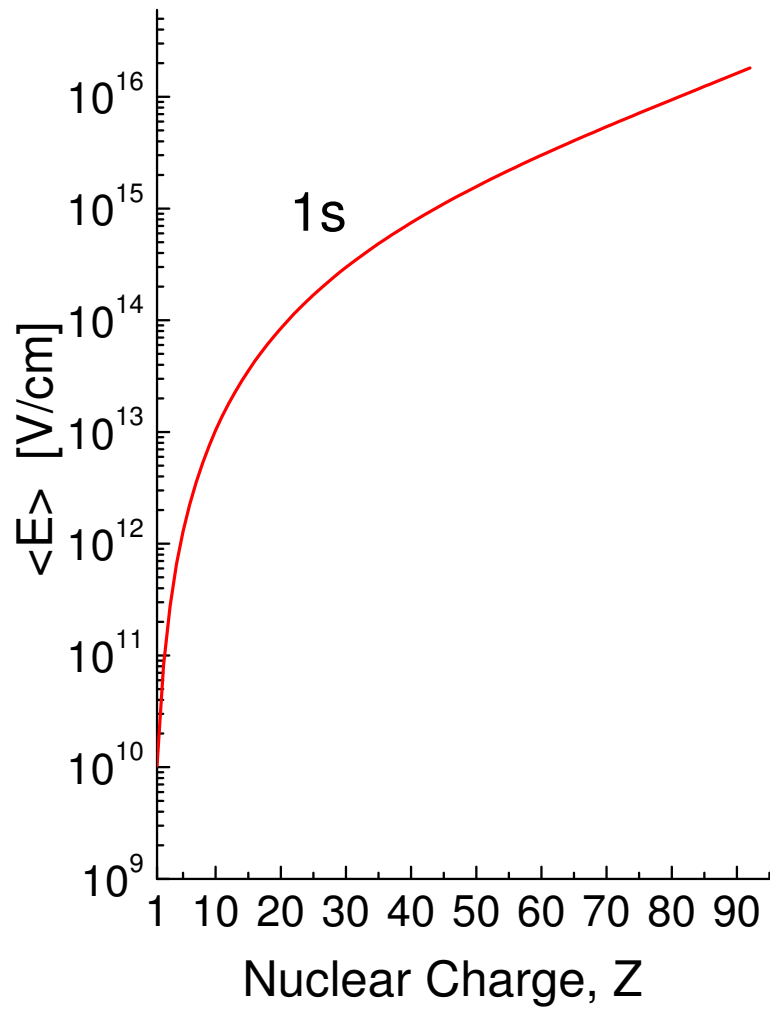
Figure 1.1. Expectation value of the electric field strength for the lowest-lying bound state in hydrogen-like atoms with nuclear charge numbers Z [1].

Chapter 2

QED in highly charged ions

The basic methods of quantum electrodynamics were formulated about 70 years ago in papers of such outstanding theoreticians as Dirac, Jordan, Pauli, Heisenberg, Born, Fock, Wigner, Fermi and others. This theory provided descriptions for the simplest process of creation and annihilation of photons and electron-positron pairs. However, application of these methods to higher orders of perturbation theory gave infinite results. This problem remained unsolved until the late 1940's when Lamb and Rutherford discovered the small difference between the binding energies of the $2s_{1/2}$ and $2p_{1/2}$ states (the so called Lamb shift) [17]. This splitting which was measured to be 1062(5)MHz, could not be explained within the relativistic quantum mechanics (as is known, according to the Dirac equation for the point nucleus these levels must have the same energy while the nuclear size corrections are extremely small for hydrogen). This experiment stimulated theoreticians to complete the creation of quantum electrodynamics since it was believed that this splitting is of quantum electrodynamic origin. The only QED contribution to this splitting which had been calculated at that time was the vacuum polarization contribution. This contribution was too small (-27 MHz) to explain the observed Lamb shift. The self energy contribution had not been calculated because the early quantum electrodynamics gave an infinite result for it. Bethe was the first who evaluated the self energy contribution. Using Kramer's idea of renormalization, he obtained 1040 MHz for this effect. A consequent QED theory was formulated by Dyson, Feynman, Schwinger and Tomonaga (for a historical review of the development of QED see Ref. [18]). They found that

all the divergencies can be removed from the theory by so-called renormaliza-
tion procedure. The main idea of renormalization is the following; parameters
such as the electron mass and the electron charge which originally appear in the
theory are not directly measurable quantities. It was shown that all physical
quantities calculated within QED become finite if they are expressed in terms
of the physical parameters which can directly be measured in experiment. All
calculations in QED are based on the perturbation theory in the fine structure
constant $\alpha \approx 1/137.036$. The individual terms of the perturbation series are
conveniently represented by the so-called Feynman diagrams. Thus, if we want
to calculate the lowest-order contribution to the Lamb shift in a hydrogen-like
atom, we have to evaluate the diagrams depicted in Fig. 2.1 (Fig. 2.1a represents
the self-energy diagram while Fig. 2.1b shows the vacuum polarization diagram).
Classically, the self energy is the interaction of a charge distribution with itself.
In terms of QED, it implies the emission and reabsorption of a virtual photon
by a charged particle. Vacuum polarization describes the coupling of a charged
particle to virtual electron-positron pairs via photon exchange.

Another QED effect consists in a small deviation of the electron g-factor from
its Dirac value. According to the Dirac equation, the free electron g-factor, which
is defined as the ratio of the electron magnetic moment to its mechanical moment,
is equal to 2. QED gives some corrections to this value of which the lowest order
contribution was first derived by Schwinger. He obtained

$$g_{theor} = 2(1 + \alpha/\pi + \ldots) \approx 2 \times 1.00116. \tag{2.1}$$

Schwinger's correction is in a very good agreement with the first experiment by
Kusch and Foley

$$g_{exp} = 2 \times 1.00119(5). \tag{2.2}$$

At present the theoretical and experimental values of the free-electron g-factor,
as well as the Lamb shift in hydrogen are known with much higher accuracy (see,
e.g. [19] and references therein).

As is known, in atoms there is also so-called hyperfine splitting of atomic levels
which is caused by the interaction of the electrons with the magnetic field of the
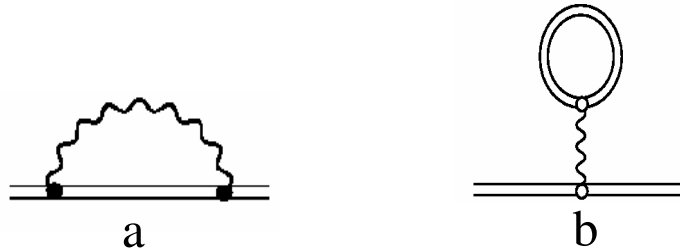
Figure 2.1. Feynman diagrams for the self energy (a) and the vacuum polariza-
tion (b) of order α for a bound electron. To denote the binding state, the electron
lines in the Feynman diagrams are doubled. On the left, an electron emits and
reabsorbs a photon. The loop on the right represents a virtual electron-positron
pair (also in the field of nucleus) that is created and reannihilated.

nucleus. As a result of this interaction, the $1s$ level in hydrogen splits into two
sublevels corresponding to the two possible values of the total moment of the
atom (F=0,1). QED also gives some corrections to this effect (for details see Ref.
[20]).

Before beginning of 1970's the QED corrections were investigated mainly for
low-Z systems such as hydrogen and helium. In addition to α, there is another
small parameter in these systems, which is αZ. As a result, all the calculations
for low-Z systems were based on expansion in α and αZ.

In high-Z systems the parameter αZ is not small and, therefore, the calcu-
lations based on the expansion in αZ are not valid. However, in addition to α,
we have, in few-electron ions, another small parameter which is $1/Z$. The pa-
rameter $1/Z$ reflects the interelectronic-interaction strength ($\sim Z$) with respect
to the electron-nucleus interaction ($\sim Z^2$). On the other hand, the radiation
corrections ($\sim \alpha(\alpha Z)^4$) with respect to the binding energy ($\sim (\alpha Z)^2$) scale like
$(\alpha(\alpha Z)^2)$ (see next section). For very high-Z systems the parameter $1/Z$ be-
comes comparable with α and, therefore, the radiative corrections contribute on
the same level as the interelectronic-interaction corrections. For instance, for

the ground state of helium-like uranium the total first order radiative correction (the self energy plus the vacuum polarization) amounts to 533 eV while the first order interelectronic-interaction correction is 2266 eV. For high-Z few-electron systems, the interaction of the electrons with each other and with the quantized electromagnetic field is much smaller (by factors $1/Z$ and α, respectively) than the interaction with the nucleus. Therefore, it is natural to assume that in zeroth approximation the electrons of the atom interact only with the Coulomb field of the nucleus. The interaction of the electrons with the quantized electromagnetic field is accounted for by perturbation theory.

2.1 Lamb shift in hydrogen-like ions

In the zeroth approximation, the energy levels of a hydrogen atom are derived from the Dirac equation

$$(\alpha \cdot \mathbf{p} + \beta m + V(r))\psi(\mathbf{r}) = E\psi(\mathbf{r}) \tag{2.3}$$

where V(r) is the Coulomb potential of the nucleus. For the point-nucleus case, analytical solution of this equation yields the well known formula for the energy of a bound state:

$$E_{nj} = \frac{mc^2}{\sqrt{1 + \frac{(\alpha Z)^2}{[n-(j+1/2)+\sqrt{(j+1/2)^2-(\alpha Z)^2}]^2}}} \tag{2.4}$$

where n is the principal quantum number and j is the total angular momentum of the electron. QED and nuclear effects give corrections to this formula. The Lamb shift is defined as the difference between the real binding energy and the Dirac-Coulomb binding energy for a point-like nucleus. A schematic diagram of hydrogen-like ions is presented in Fig 2.2.

A dominant nuclear correction results from the deviation of the potential of an extended nucleus from the point like one. To find this correction we must solve the Dirac equation (2.3) with the potential of an extended nucleus and take the difference between the energy obtained and the point nucleus energy (2.4).

The next correction is the QED correction of the first order in α. This correction consists of the self energy (SE) and vacuum polarization (VP) (Fig. 2.1 a,b). The most accurate calculations of the self energy contribution were done by Mohr [21, 22] and by Indelicato and Mohr [23] for point nuclei, and by Mohr and Soff [24] for extended nuclei. A highly efficient procedure for evaluation of the self-energy correction suitable for arbitrary electron states is developed in [25]. The vacuum polarization contribution is conveniently divided into the Uehling part and the Wichman-Kroll part. Calculation of the Uehling part, which gives a dominant VP contribution, causes no problem and was done by many authors. The Wichman-Kroll part was first calculated by Soff and Mohr [27] for extended nuclei and by Manakov et al. [28] for point nuclei. Persson et al. [29] calculated this effect for some specific ions to higher precision.
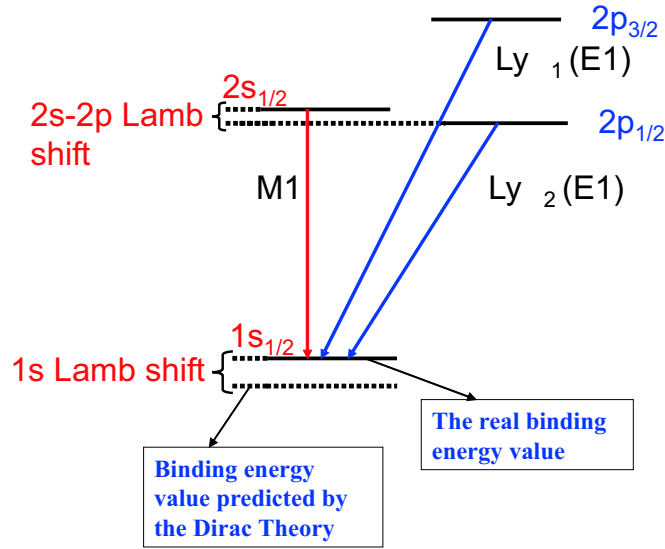
Figure 2.2. A level scheme of hydrogen-like systems together with the energy level shifts which are subsumed as Lamb shift. In addition a schematic presentation of the origin of the Lyman-α transitions is given.

The QED corrections of second order in α are defined by diagrams shown in Fig. 2.3. Until lately, only the VP-VP and SE-VP diagrams have been evaluated (see [30, 31] and references therein). The calculation of all SE-SE diagrams have been completed only recently [32].

All the corrections discussed above are calculated in the approximation in which the nucleus is considered as a source of the external field ("the external field approximation"). The first step beyond the external field approximation consists in accounting for the nuclear recoil correction of the first order in m/M, where M is the nucleus mass. In contrast to the non-relativistic theory where the recoil effect for hydrogen-like atom is accounted for by the reduced mass, a full relativistic theory of the nuclear recoil effect can be formulated only within the QED. For the point nucleus case this problem was solved in [33] where the complete αZ-dependence formulae for the recoil correction were derived. Later these formulae were rederived in simpler ways (see [34] and references therein). The corresponding calculations for the extended nuclei were carried out in [35].
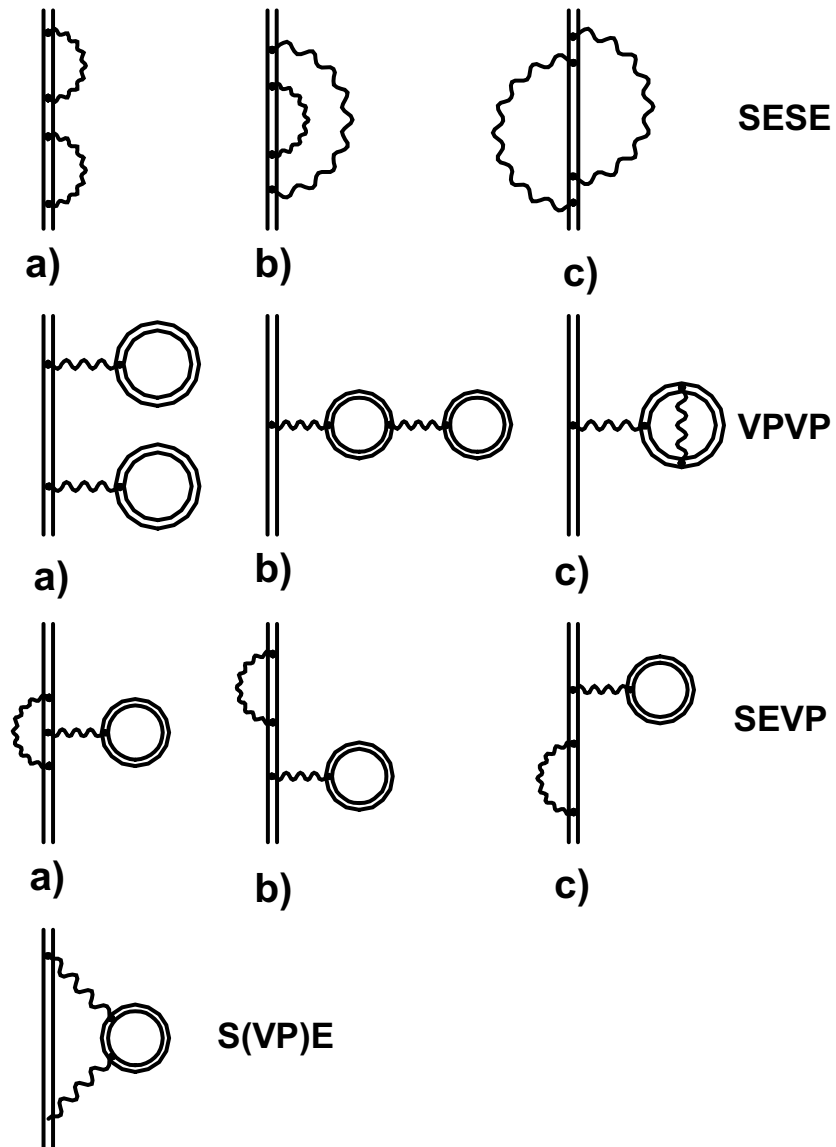
Figure 2.3. Feynman diagrams for the QED-corrections of order α^2 for H-like ions.

Finally, we must take into account the nuclear polarization effect which arises from interactions of the electron with the nucleus where the intermediate states of the nucleus are excited. The energy shift due to this effect was evaluated by Plunien and Soff [36] and by Nefiodov et al. [37].

In one-electron systems the Lamb shift for s-states is commonly presented by the following equation [38, 39]:

$$L = \frac{\alpha}{\pi} \frac{(Z\alpha)^4}{n^3} \cdot F(Z\alpha) \cdot m_0 c^2 \qquad (2.5)$$

where α is the fine-structure constant, n is the principal quantum number, $m_0 c^2$, the electron rest mass, and $F(Z\alpha)$ is a slowly varying function of Z. This function considers all the QED contributions and includes in addition the effect caused by the finite size of the nucleus. Since the Lamb shift scales approximately with Z^4/n^3, all these corrections are largest for the ground-state and for the strong fields at high-Z. For light systems the self energy gives the most important Lamb shift correction. With increasing nuclear charge, however, the influence of the vacuum polarization increases continuously. In Fig 2.4 the contributions of the self energy, vacuum polarization, and of the finite nuclear size to the Lamb shift in hydrogen-like ions are given separately as a function of the nuclear charge. For light one-electron systems as atomic hydrogen, the theory of QED is now well confirmed with extraordinary precision [40]. Here, the experiments are sensitive to the lower orders of the function $F(Z\alpha)$ which for low-Z systems, can be treated by an αZ expansion method. However, for a test of higher order terms, which are not accessible using low-Z ions, the heaviest species such as hydrogen-like uranium are required. At high-Z the influence of the higher order contributions becomes so important that the radiative corrections can no longer be treated by the αZ expansion method but must be calculated to all orders of αZ [22, 41, 42].
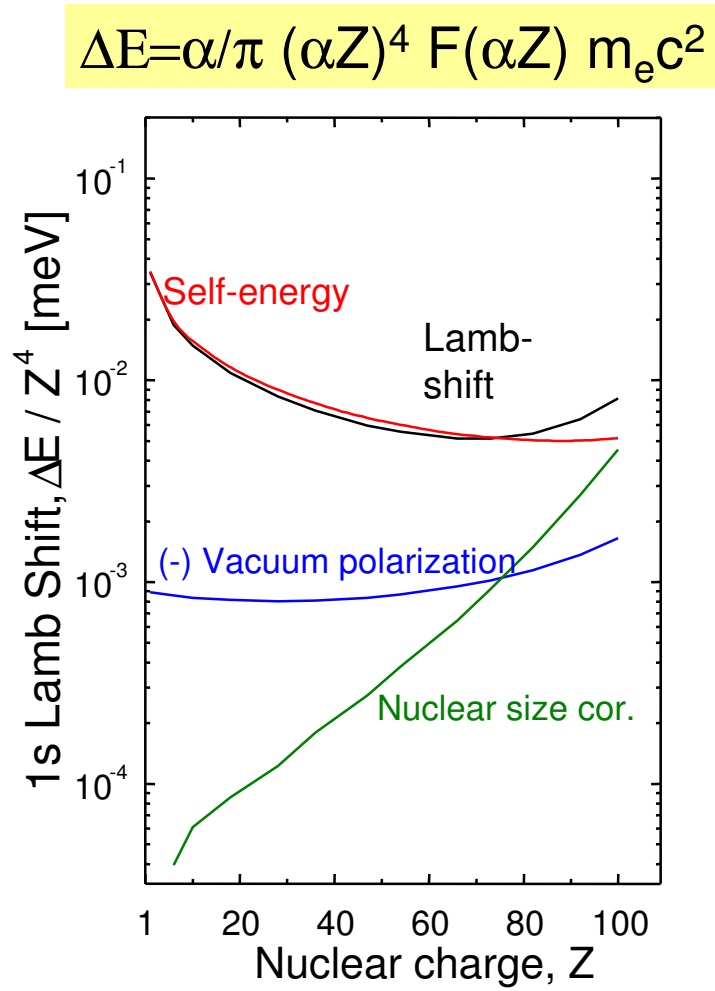
Figure 2.4. The various contributions to the ground state Lamb shift in hydrogen-like ions as a function of the nuclear charge, according to Ref. [39].

2.1.1   Status of the experimental research

For high-Z hydrogen-like ions, the most direct experimental approach for the investigation of the effects of quantum electrodynamics in strong Coulomb fields is a precise determination of the x-ray energies emitted by transitions from bound (and/or continuum) states into the ground state of the ion. In particular, the Lyman transitions are used in this kind of experiments as they appear most intense and well resolved in the x-ray spectra (the origin of the Lyman transitions is shown in Fig. 2.2). The goal of the experiments is to achieve a precision which probes QED contributions which are beyond the one-photon exchange corrections. For the case of uranium where the total 1s Lambs shift contributes approximately 460 eV to the total ground state binding energy of 131.814 keV [42], such a stringent test of QED in strong field requires an absolute experimental accuracy of about 1 eV.

In Fig. 2.5 the experimental results for the ground state Lamb shift in hydrogen-like ions are given and compared with the theoretical predictions [39] (solid line). For comparison, the data shown in the figure are given in units of the function $F(Z\alpha)$ (Eq. 2.5). The solid symbols depict the results from the SIS/ESR facility. Over the whole range of nuclear charges an excellent overall agreement between experiment and theory is observed. For the regime of the high-Z ions ($Z > 54$) most of the results provide a test of the ground-state Lamb shift contribution at the level of 30%. Only the results from the gasjet target (for uranium) and from the electron cooler (for gold and uranium) have a considerably higher accuracy. Up to now most of the Lamb shift experiments for high-Z ions were performed for hydrogen-like uranium. Therefore, In Table 2.1 we show separately the theory of the ground state Lamb shift in $^{238}U^{91+}$ together with the most recent experimental result. All the values are given in eV. Comparison of the theoretical Lamb shift prediction with the result of a recent experiment [43, 44] shows that the present status of theory and experiment provides a test of the QED effects at the first-order in α on the level of 5%.
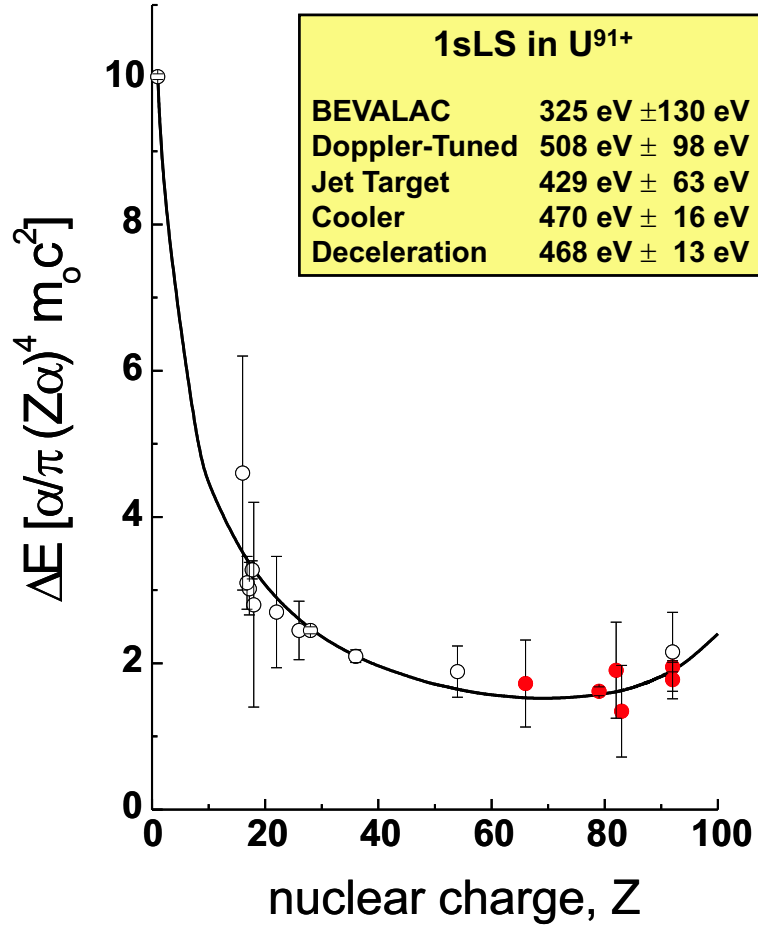
Figure 2.5. All available experimental results for the 1*s* Lamb shift in high-*Z* ions in comparison with theoretical predictions [39]. In the inset the available data for U^{91+} are shown ([7, 9, 44, 45, 46]).

Dirac value	132279.96
Finite nuclear size	198.81
Nuclear Recoil	0.46
Nuclear Polarization	-0.19
VP (see Fig 2.1)	-88.60
SE (see Fig 2.1)	355.05
SESE (see Fig 2.2)	-1.87
VPVP (see Fig 2.2)	-0.97
SEVP (see Fig 2.2)	1.14
S(VP)E (see Fig 2.2)	0.13
Lamb-shift	463.95±0.5
Binding-energy	-131816.01±0.5
Experiment	468±13

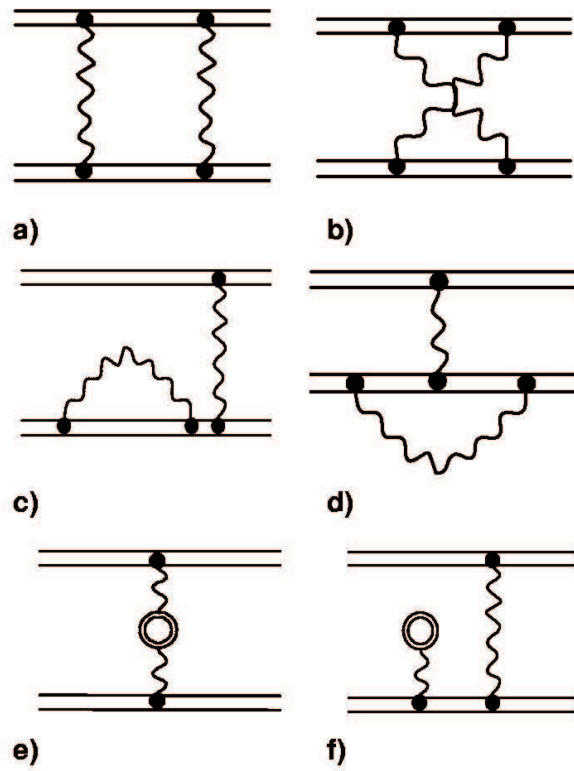**Table 2.1.** The contributions to the $1s$ binding energy in hydrogen-like uranium [32]. The corresponding binding energies for the $2s_{1/2}$ and the $2p_{1/2}$ state amount to -34127.78 eV and -34204.14 eV, respectively [31]. For the $2p_{3/2}$ level the binding energy is calculated to -29640.99 eV [47], whereby the Lamb shift corrections amount to +8.8 eV. The experimental value is taken from Ref. [43].
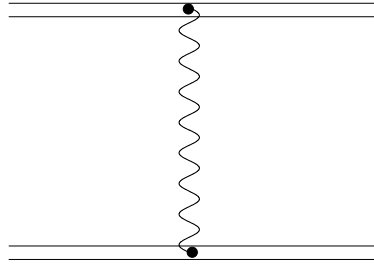
Figure 2.6. One-photon exchange diagram.

2.2 Lamb shift in helium-like ions

In addition to one-electron systems, the study of spectra of helium-like ions has proven to be important for our understanding of relativistic, correlation and QED effects in many-body systems. Recently, there has been a significant progress in theoretical as well as experimental studies of such systems, in particular for the high-Z regime. Various theoretical investigations based on different methods such as the relativistic many-body perturbation theory (RMBPT) [48], multi-configuration Dirac-Fock [49] and the unified method [50], have been performed. For the ground state the progress is in particular impressive, since even the two-electron QED contributions have been evaluated completely up to the second order [51]. To the lowest order in α, the two-electron contribution is determined by the one photon exchange diagram depicted in Fig. 2.6. In the second order in α we have three types of diagrams: two-photon exchange (Fig. 2.7 a, b), self-energy screening diagrams (Fig. 2.7 c, d), and vacuum polarization screening diagrams (Fig. 2.7 e, f). Note, that the claimed theoretical uncertainty for the two-electron QED contributions is very small and, for the particular case of He-like uranium, estimated to be of the order of only 0.1 eV. Most importantly, as has been shown in detail by Persson et al. [51], the two-electron QED effects are almost completely unaffected by the uncertainties of the nuclear charge radius, one of the most serious limitations for the QED tests in high-Z one-electron systems.

Figure 2.7. Feynman diagrams of the second order in α (compare text).

2.2.1   Status of the experimental research

Experimentally, the progress achieved manifests itself by a novel approach where the two-electron contributions to the binding energy in He-like ions can be experimentally isolated. This technique exploits the x-ray transitions from the continuum into the vacant K-shell of bare and H-like high-Z ions in order to measure the ionization potentials of He-like species with respect to that of the H-like ions which gives exactly the two-electron contribution to the ionization potential in He-like ions. This technique was first exploited at the (superEBIT) in Livermore where the two-electron contribution to the ground state binding energy in helium-like systems was measured for various nuclear charges [10].

At superEBIT bare and H-like ions of almost any element can be produced and trapped in an electron beam of arbitrary energy up to 200 keV and currents up to 200 mA [10, 52]. At such collision conditions the fast moving free electrons may undergo a direct radiative recombination transition into the vacant K-shell of the bare and H-like species. Since radiative recombination (RR) is the time reversal of the photoelectric effect, the energy carried away by the photon is just given by:

$$\hbar\omega = E_{kin} + V, \tag{2.6}$$

where E_{kin} denotes the kinetic energy of the electron captured and V is the ionization potential of the ionic system after undergoing radiative capture. Since both the bare and H-like ions are simultaneously trapped, i.e. both ion species are interacting with the same electron beam, the difference in the photon energies between radiative transitions into the bare and H-like ions is independent of the electron beam energy. It corresponds just to the difference between the ionization potentials of the H- and He-like species formed by the RR process which gives exactly the two-electron contribution to the ground state binding energy in He-like ions. Most important, all one-electron contributions to the binding energy such as the finite-nuclear size corrections and the one-electron self-energy cancel out completely in this type of experiment [51]. A schematic presentation of this experimental situation at the EBIT is shown in Fig. 2.8.

By applying the experimental method described above, data were obtained
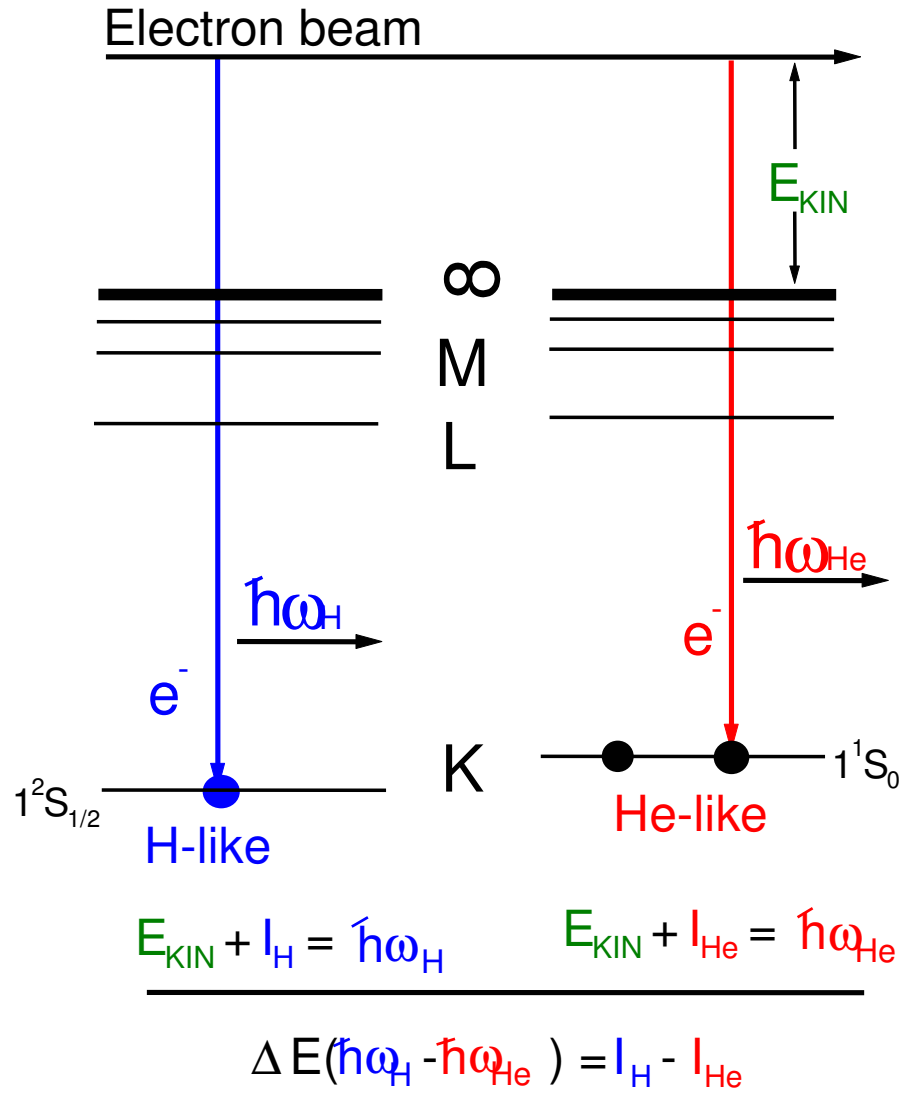
Figure 2.8. Schematic presentation of the RR process of free electrons into the initially bare and H-like ions. The energy difference $\hbar\omega_H - \hbar\omega_{He}$ gives exactly the two-electron contribution to the ionization potential in He-like ions.

for Ge (Z=32), Xe (Z=54), Dy (Z=66), W (Z=74), Os (Z=76) and Bi (Z=83). In the experiment, the electron-beam/ion interaction zone was viewed by a solid state Ge(i) detector (for a detailed description of the data evaluation applied see Ref. [10]). In Fig. 2.9, sample spectra for the x-ray regime of RR into the vacant K-shell of germanium, xenon and bismuth are given separately. In all cases, the RR line splitting between RR into the bare and H-like ions appears well resolved. In table 2.2 the results from this experiment are presented together with the various contributions to the two-electron part of the binding energy in helium-like systems. The experimental uncertainty quoted in the table is entirely determined by counting statistics. The predictions are based on relativistic many-body perturbation calculations (RMBPT) which take into account the non-QED part of the electron-electron interaction to all orders [51]. In particular, all two-electron QED contributions are considered for the first time complete to second order in α. As can be deduced from the experimental and theoretical results presented in table 2.2 the experimental data provide already a meaningful test of the many-body non-QED part of the electron-electron interaction. Moreover, the data are already at the threshold of a sensitive test of the two-electron QED contributions. However, at high nuclear charges such as $Z = 83$ it turned out that the production efficiency for bare ions is not sufficient and the results suffered by counting statistics. This can be observed from the spectra in Fig. 2.9, where one clearly sees a decrease of the relative intensity of the peak for the bare ions with increasing Z due to the rapid decrease of the K-shell ionization cross section for electron impact which scales as $1/Z^4$. For example at $Z = 83$, a statistical accuracy of 14 eV has been achieved which has to be compared with the predicted 2eQED contributions of 4.2 eV. Consequently, currently there is no hope to extend the experimental studies at the superEBIT to elements such as uranium.

This limitation is not present at the ESR storage ring. Very recently, we started our study of the two-electron contributions to the ground state binding energy in helium-like uranium in an experiment conducted at the electron cooler of the ESR storage ring. The aim of our present experimental study is to measure precisely the two-electron contribution to the ionization potential in He-like uranium of about 2.2 keV with an accuracy better than 5 eV [26]. Since two-electron QED effects are calculated to contribute 7 eV, such an experimental study would
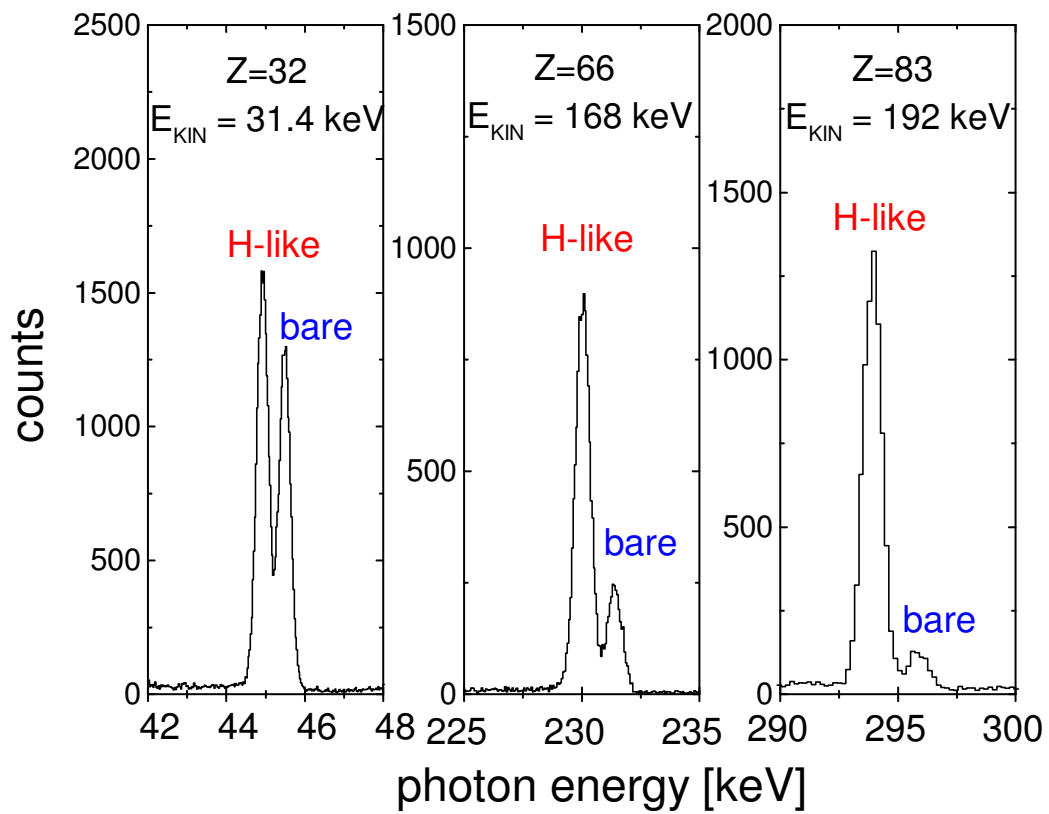
Figure 2.9. Sample K-shell RR line for germanium (Z=32), dysprosium (Z=66) and bismuth (Z=83) at the superEBIT [10, 52].

therefore provide the very first test of higher-order QED corrections (higher order in α) for the domain of high-Z ions.

Nuclear Charge	1st order RMBPT (eV)	$\geq 2^{nd}$ order RMBPT (eV)	NR (eV)	2eSE (eV)	2eVP (eV)	Total theory (eV)	Experiment (eV)
32	567.61	-5.2	0.0	-0.5	0.0	562.0	562 ± 1.6
54	1036.56	-7.01	0.2	-1.8	0.2	1028.0	1027.2 ± 3.5
66	1347.45	-8.56	0.4	-3.2	0.6	1336.6	1341.6 ± 4.3
74	1586.93	-9.87	0.6	-4.6	0.9	1573.9	1568 ± 15
83	1897.56	-11.73	0.9	-6.7	1.6	1881.5	1876 ± 14
92	2265.87	-14.11	1.3	-9.7	2.6	2246.0	

Table 2.2. The individual two-electron contributions to the ground state binding energy in some He-like ions [51] in comparison with the experimental results from superEBIT [10] (NR: non-radiative QED as defined by Persson et al. [51]; 2eVP: two-electron vacuum polarization; 2eSE: two-electron self energy; Total theory: predicted difference in the ionization potentials between the H- and He-like systems).

Until recently, the only available technique for the study of ground state energies of He-like ions has been the spectroscopy of $K\alpha$ transitions. Due to the strong $1/n^3$ scaling of the leading QED effects (see equation 2.5), this method tests the total ground state QED contributions by assuming that the energies of the excited states can be calculated precisely. For He-like Ge^{30+} a Bragg crystal spectrometer was used in a previous EBIT measurement to obtain an accuracy of 0.2 eV for the $1s2p(^1P_1) - 1s^2(^1S_0)$ transition which enables a distinction between different theories [53]. These transitions has also been measured in He-like Kr^{34+} with an accuracy of 0.3 eV [54].

At higher Z, all available He-like transition energy measurements have been done using high-velocity accelerator beams capturing electrons from neutral target atoms. These experiments must deal with large Doppler shifts and suffer from the fact that the observed $K\alpha_1$ and $K\alpha_2$ lines both contain two transitions that are unresolved in existing experiments. In spite of these problems, uncertainties as low as 60 eV have been achieved for He-like bismuth [55] and uranium

[56] and 3.5 eV for xenon [57]. In order to outline the advantage of the present relative measurement with respect to the standard $K\alpha$ spectroscopy technique, where the absolute ground state binding energies are deduced, we give in table 2.3 the one- and two-electron contributions for the ground state binding energy in He-like uranium.

One-electron contr. [32]	-131816.01	Two-electron contr. [51]	2246
Self energy:	355.05	2nd order	-14.16
Vacuum polarization:	-88.60	2e Lamb shift:	-7.1
Nuclear size:	198.81	non-radiative QED	1.3

Table 2.3. Total one- and two-electron contributions to the ionization potential of He-like uranium (in eV). In addition some important correction terms are quoted.

As seen from the table the second order two-electron contribution and in particular the two-electron QED correction are considerably smaller than the one-electron QED terms and the nuclear size effect. Within their experimental precision the available experimental data for $K\alpha$ transitions probe essentially these one-electron contributions. In contrast, the energy differences measured in the superEBIT (and in the present) experiment isolate the true two-electron contributions and all the one-electron contributions cancel out completely. This is of particular relevance with respect to the nuclear effects. For the heaviest H-like systems the uncertainty introduced by these effects dominates the total error in the theoretical ground state binding energy [39]. In the case of uranium it may prevent probing of the QED corrections on an absolute level of precision of better than ± 1 eV. For hydrogen-like uranium, Franosch and Soff [58] have estimated that the error introduced by the nuclear size correction amounts to 0.36 eV. This uncertainty corresponds to the difference between the size effects for homogeneously charged sphere model and a Fermi distribution. Persson et al. [51] have applied the same technique for the ground state of He-like uranium. Their calculations reveal that the size effect causes only an uncertainty of 16 meV for the two-electron contribution. In general, they found a very weak dependance of these contributions on the nuclear structure, e.g. a change of the root-mean-

square nuclear radius for uranium of $R = 5.86$ fm by 1 % causes a variation of the two-electron contribution of less than 0.1 eV [51] .

2.3   Decay rates in heavy few-electron ions

This chapter cannot be closed without a few comments on the structure and the decay rates of heavy few-electron systems. In low Z H-like ions the $2\,^2S_{1/2}$ level is metastable and decays by a two-photon emission ($2E1$-decay) [59, 60]. However, for very high Z the $M1$ decay is already a prompt decay and faster than the $2E1$ branch [61, 62]. Fig. 2.10 shows the decay scheme and the corresponding transition rates as a function of Z. (The region accessible to lifetime measurements applying beam-foil techniques is typically in the order of nano-seconds and above.) For the heaviest ions like U^{91+} we have to keep in mind that the $Ly\alpha_2$ line ($^2P_{1/2} \rightarrow GroundState$) is blended by the M1 transition ($^2S_{1/2} \rightarrow GroundState$).

For He-like ions the situation is more complex. As the atomic structure changes drastically with Z, two schematic decay schemes - roughly applicable to Ar^{16+} and U^{90+}, respectively - are given in Fig. 2.11 on top of the graph with corresponding transition rates. Whereas for the light He-like species the intercombination lines (triplet - singlet transitions) are at least metastable, the triplet decay rates increase dramatically due to the relativistic effects for the heavy ions so that for U^{90+} practically all excited L states (except the $^3P_0$ state) decay promptly to the ground state. ($^3S_1 : M1$ decay $\sim Z^{10}$; $^1S_0 : 2E1$ decay $\sim Z^6$; $^3P_1 : E1$ decay $\sim Z^{10}$; $^3P_2 : M2$ decay $\sim Z^8$; see Refs [61, 62] and references therein). For heavy He-like ions like U^{90+} one will find two ground state transition x-ray lines, the $K\alpha_1$ and $K\alpha_2$ lines. Each line comprises two components; the $K\alpha_1$ line is composed by the ground state transitions from $^1P_1$ and $^3P_2$ states and the $K\alpha_2$ line by the ones from $^3S_1$ and $^3P_1$ states. Also the continuous spectrum from $2E1$ decay of the $^1S_0$ level may be slightly blended by contributions from $E1M1$ decay of the $^3P_0$ state.
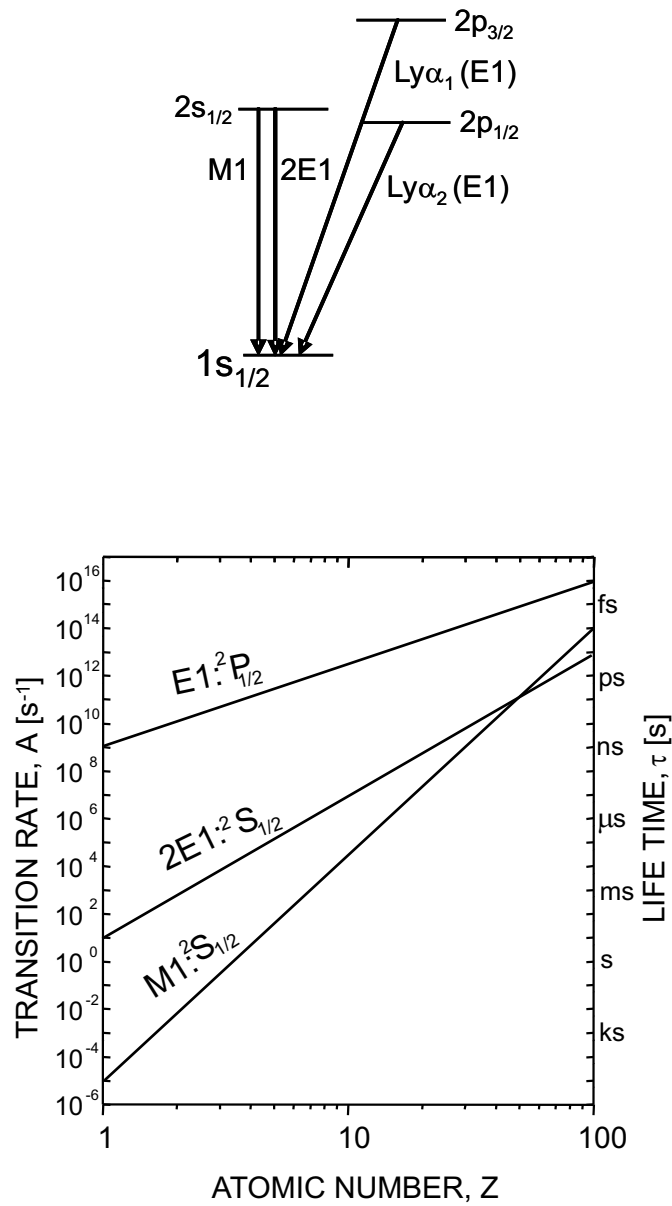
Figure 2.10. Levelscheme (top) and transition rates (bottom) for the first excited levels in H-like ions. Transition rates are given as function of the atomic number.
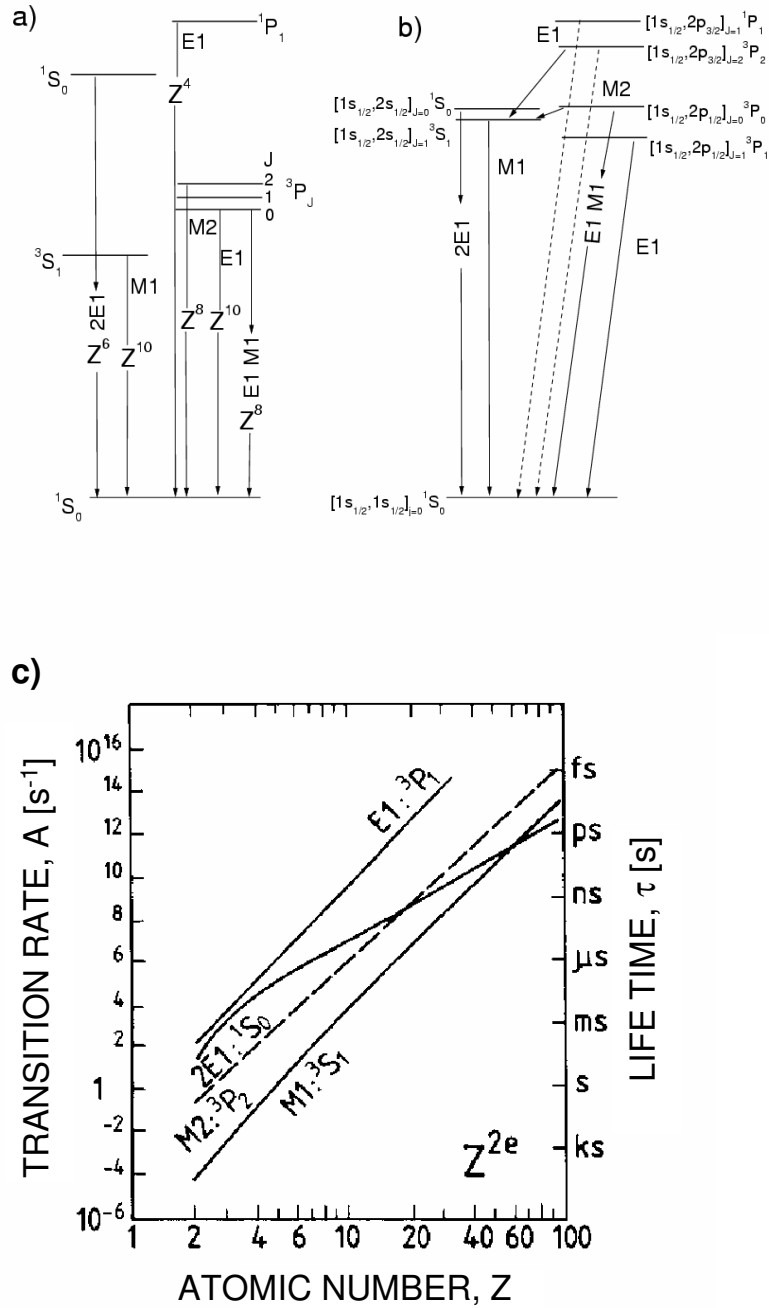
Figure 2.11. The decay of the first excited levels in He-like ions. Schematic level diagrams of low (a) and high (b) Z He-like ions. The transition rates are given as function of Z (c).

Chapter 3

The experimental environment

The production and cooling of intense beams of fully stripped ions, as introduced by heavy-ion storage rings and in particular by the storage ring ESR , constitutes an important step for accurate precision spectroscopy of atomic transitions in the realm of high-Z systems. The ESR storage ring with its brilliant beams of cooled heavy-ions provides unique conditions for this kind of precision investigations. Fig. 3.1 shows the layout of the heavy-ion synchrotron/storage ring facility.

The highly-charged ions can be accelerated in the heavy ion synchrotron SIS (circumference 216 m), to the final energies of up to 1 GeV/u. These beams can then be provided for experiments after slow (or fast) extraction at the caves in the target area, at the fragment separator (FRS), or they can be extracted into the transfer line towards the ESR. In the transfer line the ions pass through a thick stripper foils. From the emerging charge state distributions, the fraction of bare ions is magnetically separated and injected into the storage ring. Note that for the case of uranium ions where the K-shell binding energy amounts to ≈ 130 keV, a beam energy of at least 300 MeV/u is required in order to produce bare ions with sufficient intensity, a beam energy which corresponds approximately to $\beta = 0.6$, where β denotes the ion velocity in units of the speed of light. Fig. 3.2 shows a schematic sketch of the ESR storage ring (circumference of 108 m, magnetic rigidity of 10 Tm) and its main components such as the electron cooler device, the internal gasjet target, and the rf-cavities.

In the storage ring, the injected hot ion beam with a typical emittance of about 5 π mm mrad is very efficiently cooled by Coulomb interaction with the
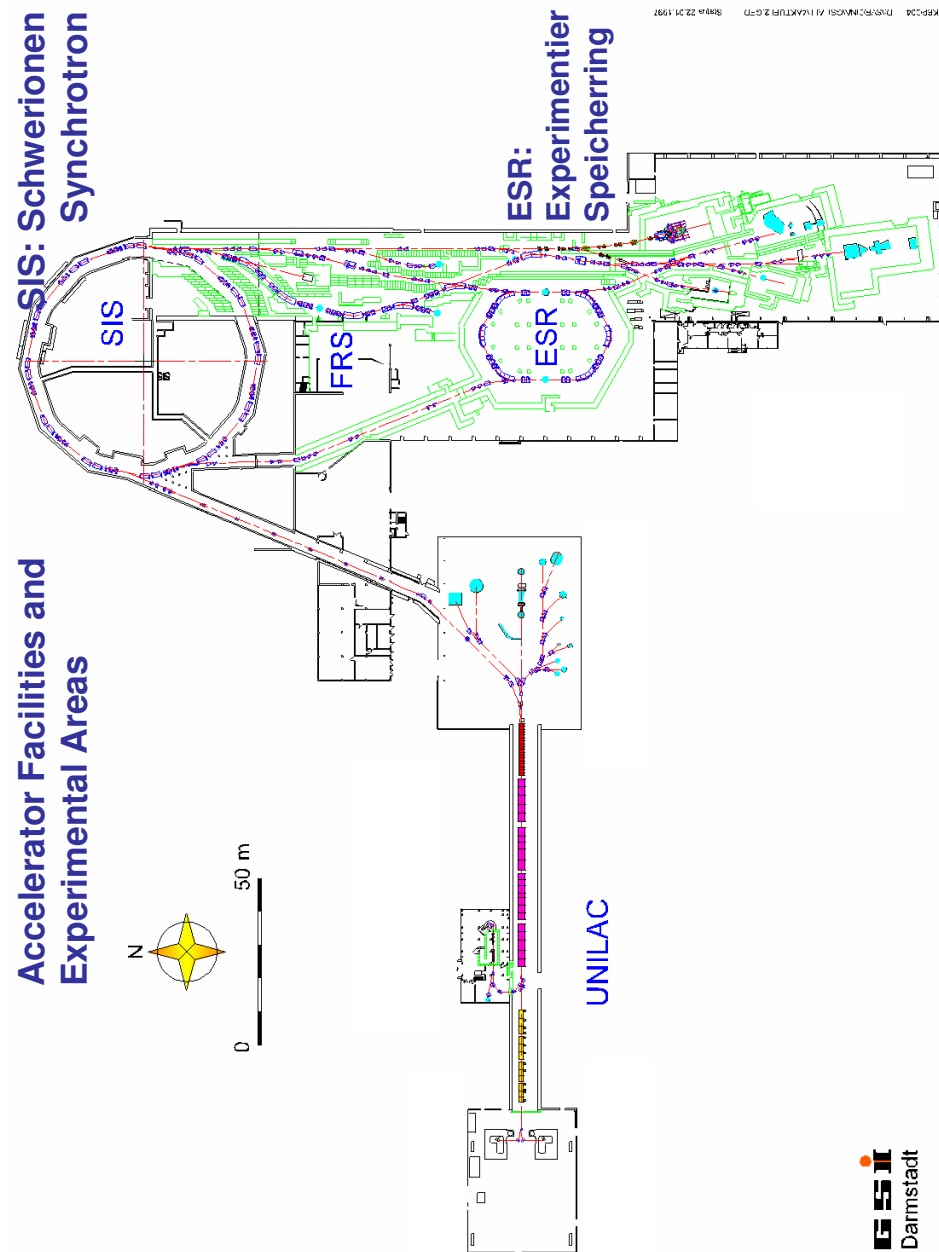
Figure 3.1. Layout of the heavy ion synchrotron/storage ring facility SIS/ESR at Darmstadt.
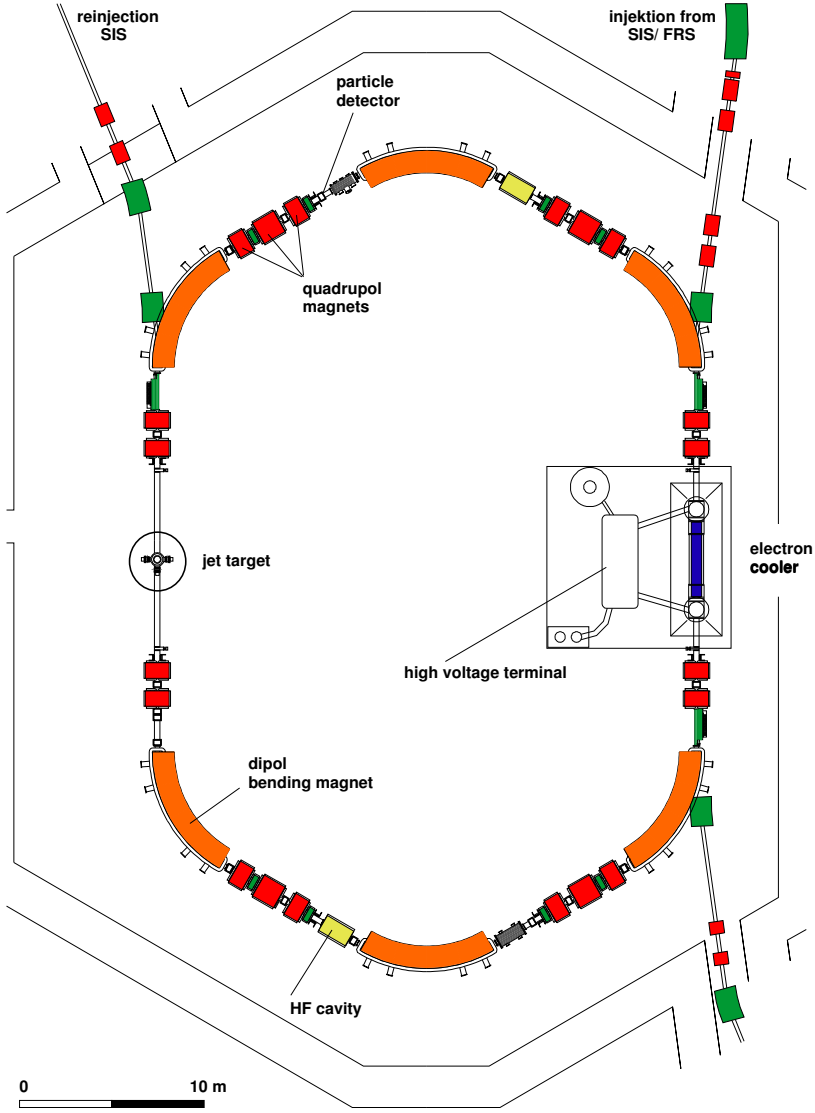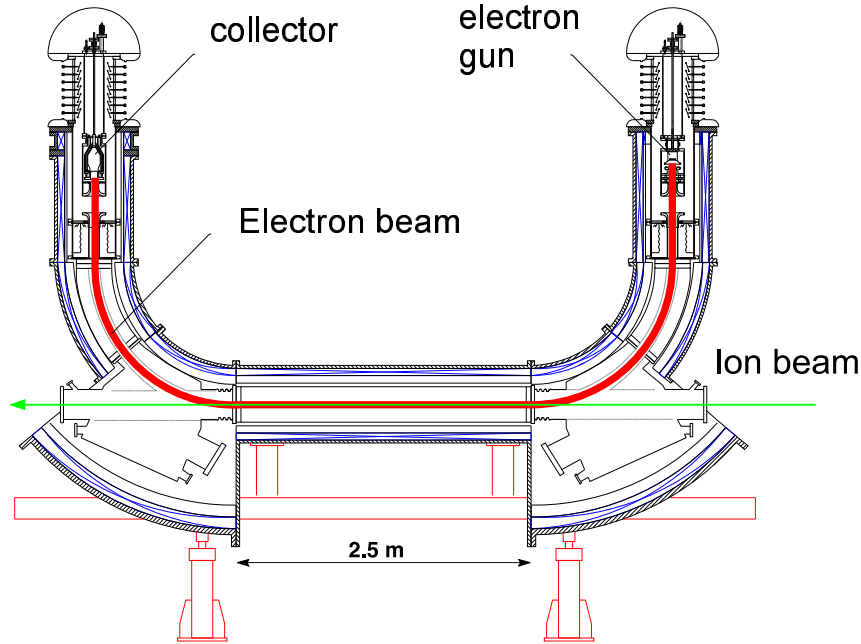
Figure 3.2. The experimental storage ring ESR.

Figure 3.3. Schematic figure of the ESR electron cooler.

cold co-moving electrons in the 2.5 m long electron cooler section (see Fig. 3.3). For this purpose electron currents of typically 100 to 300 mA are applied. This cooling technique leads to an emittance of the stored beam of less than 0.1 π mm mrad and to a small beam size with a typical diameter of less than 5 mm. In particular, electron cooling guarantees a well defined constant beam velocity, generally of the order of $\Delta\beta/\beta \approx 10^{-5}$. It reduces the relative longitudinal momentum spread of the injected ion beam of $\Delta p/p \approx 10^{-3}$ to about 10^{-5}. This can be read from the signal of a pickup via Schottky noise spectrum of the circulating ions. As an example, a Schottky frequency spectrum of an uncooled ion beam in comparison with a cooled one is given in Fig. 3.4.

Here, however, it is important to note that both the transverse emittance and the relative momentum spread of the stored beam depend on the number of stored ions and the applied cooler current [63]. Within the last years the maximum possible number of ions was improved significantly (see Fig. 3.5). For high-Z
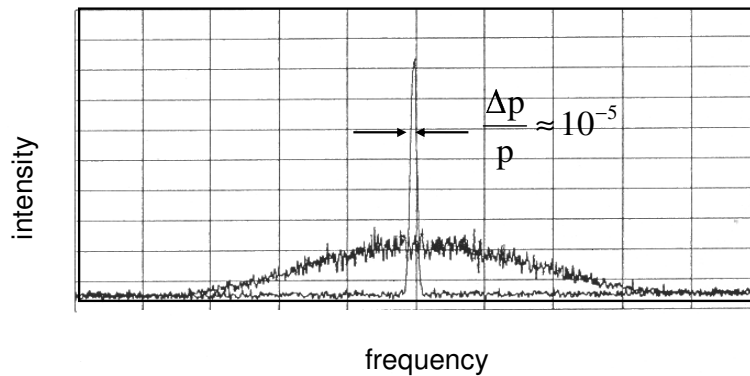
Figure 3.4. Schottky frequency spectrum for a circulating beam of U^{92+} ions at 295 MeV/u. The broad distribution refers to the non-cooled beam, measured directly after injection into the ESR. The narrow distribution reflects the momentum profile of a continuously cooled ion beam.

ions, e.g. uranium, more than 10^8 ions can be stored routinely. This number is still below the upper limit of particles which can be stored in principle. These limits are due to the space charge potential of the stored ion beams and restrict the number of stored ions e.g. for the case of bare uranium at 556 MeV/u to 9.3×10^9 and at 50 MeV/u to 4.4×10^8, respectively [64].

Besides the electron cooler device, which can be considered also as a dense electron target ($\sim 10^7 electrons/cm^3$) the ESR is equipped with a gasjet target. Here, various gas targets such as CH_4, N_2, Ar or even heavier targets can be used with areal densities of about $10^{12} particles/cm^2$ and a diameter of about 5 mm. Both experimental areas can be viewed by x-ray detectors. It should be added that at both of these target areas laser beams can be merged collinearly with the ion beam.

In both of the experimental places charge changing processes may take place which change the magnetic rigidity of the ions concerned. These charge-changed
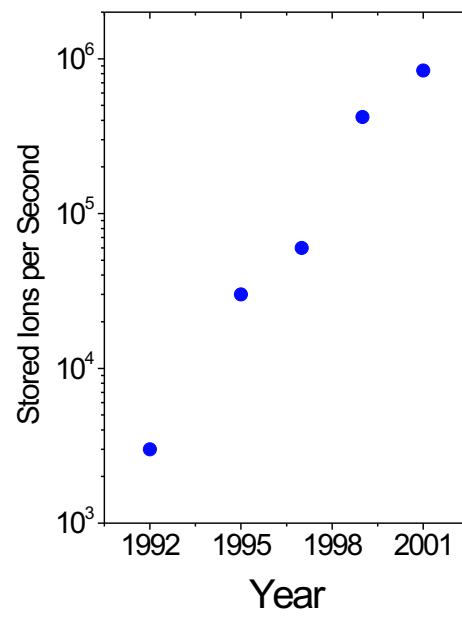
Figure 3.5. Number of stored ions in the experimental storage ring ESR [65].

ions can be measured in position sensitive multiwire particle detectors inserted during running in vacuum sealed pockets which have thin particle windows (Fig. 3.6, 3.7).
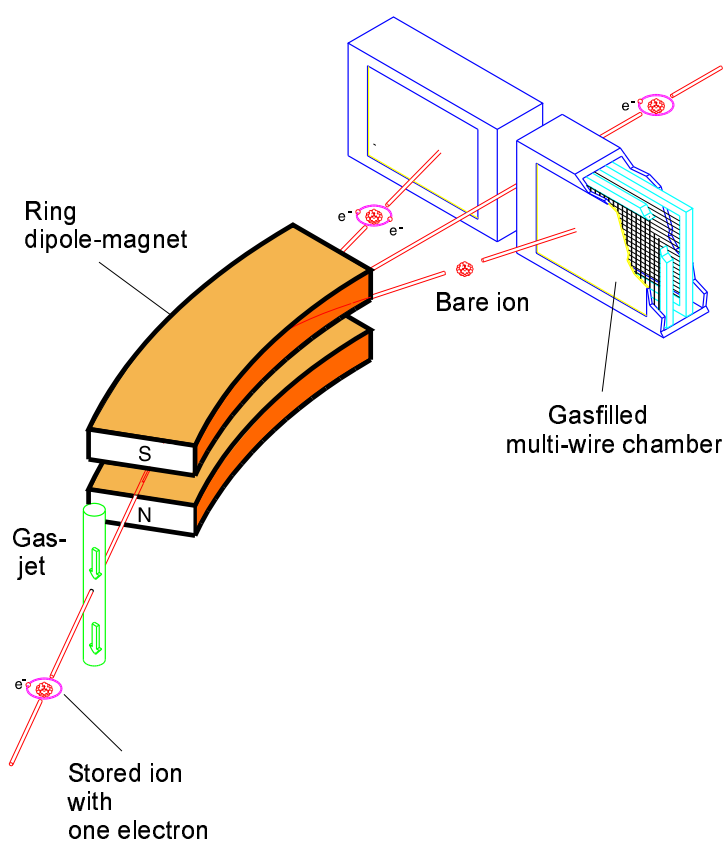
Figure 3.6. Principle of charge-exchange experiments at the internal jet-target illustrated for the case of stored H-like ions. The primary beam of stored ions at charge-state Q crosses a perpendicularly oriented molecular or atomic supersonic gas beam. The ring dipole magnet serves as a magnetic spectrometer for changes of magnetic rigidity, here electron capture (Q-1) and ionization (Q+1) [65, 66].
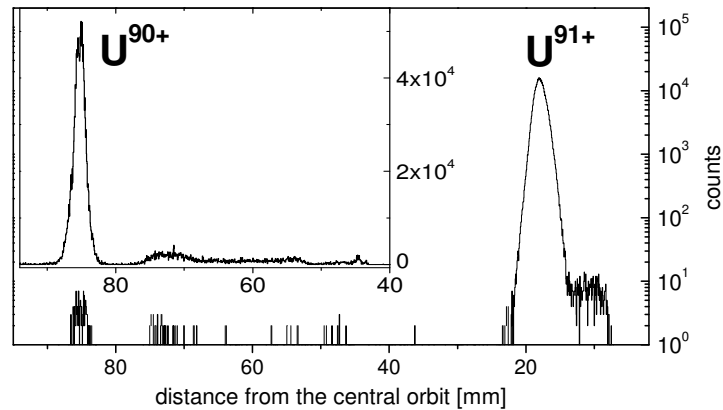
Figure 3.7. Charge state spectrum of uranium ions with initial charge of 92 after passage through a thin *Ar*-target. The detector (MWPC) is mounted behind the dipole magnet downstream to the internal target [65, 66].

3.1   X-ray Spectroscopy at the ESR

The individual Lamb shift experiments conducted up to now applied quite different techniques and methods. The underlying principle of all Lamb shift investigations at high-Z, however, is the same for all experiments and it can be summarized as follows:

- production of the bare ion species,

- storing and cooling inside the storage ring,

- population of excited levels via electron capture,

- detection of transitions from continuum and bound states to the ground state,

- determination of the line centroids,

- transformation of the results into the emitter frame.

3.1.1 The Experimental Challenge: Doppler Corrections

Both the gasjet-target and the electron cooler can be applied for an intense production of characteristic Lyman-α radiation of the circulating high-Z ions. At the gasjet target, capture of bound target electrons into the fast moving, bare projectiles populates excited levels of H-like ions and finally results in emission of Lyman photons. At the electron cooler side, the free electrons are captured via radiative recombination (i.e. the time reversed photo ionization process) into the bare ions, populating also excited levels of the H-like species formed by the capture process. By cascades, many of such events lead to Lyman-α photon emission. Although the ESR provides brilliant, monochromatic beams, the main problem encountered is still caused by the uncertainties introduced by the Doppler shift corrections, because the x-rays are emitted by ions moving with velocities of about 60% of the speed of light. In order to derive the transition energy in the emitter frame, the transition energy measured in the laboratory system must be corrected for the relativistic Doppler shift given by

$$E = E_{lab} \cdot \gamma \cdot (1 - \beta \cos \theta_{lab}). \tag{3.1}$$

Here, E and E_{lab} are the x-ray energies in the emitter system and in the laboratory frame, respectively, θ_{lab} denotes the laboratory observation angle, and γ is the relativistic factor. In Fig. 2.5 (a,b) the ratio E_{lab}/E is plotted as a function of observation angle for two different beam energies. The final uncertainty of the x-ray energy in the emitter frame is determined by the uncertainties in the absolute value of β and of the observation angle θ_{lab}. The influence of the latter on the final result depends crucially on the beam velocity and the observation angle chosen. This can easily be seen from the derivative of Eq. 3.1 given by

$$(\frac{\Delta E}{E})^2 = (\frac{\beta \sin \theta_{lab}}{1 - \beta \cos \theta_{lab}} \Delta \theta_{lab})^2 + (\gamma^2 \frac{\cos \theta_{lab} - \beta}{1 - \beta \cos \theta_{lab}} \Delta \beta)^2 + (\frac{\Delta E_{lab}}{E_{lab}})^2 \tag{3.2}$$

For instance, due to the $\sin \theta_{lab}$ term, the uncertainty in $\Delta \theta_{lab}$ does not affect the final result at observation angles close to 0° and 180°. Here, the error due to $\Delta \beta$ is largest. Also, by choosing $\beta = \cos \theta_{lab}$ the uncertainty caused by $\Delta \beta$ can be minimized, but now the uncertainty introduced by $\Delta \theta_{lab}$ is maximal (see Fig. 2.5 (c,d)). In practice a velocity-sensitive measurement at the electron cooler
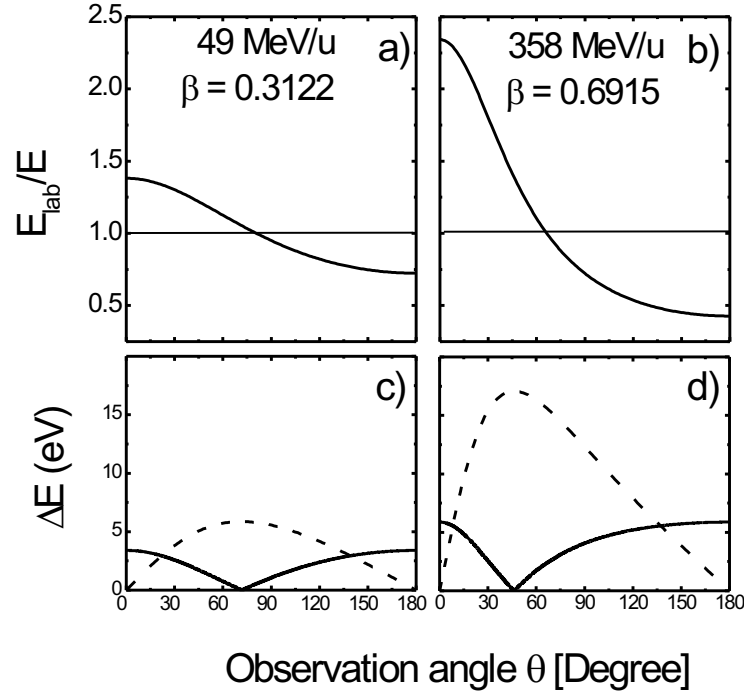
Figure 3.8. a), b) The ratio E_{lab}/E as a function of the observation angle for two beam energies; c), d) The uncertainty of the photon energy in the emitter frame caused by the uncertainties of the β (*solid line*) and the observation angle (*dashed line*). Assumed uncertainties of the β and θ values are $\Delta\beta = 3 \cdot 10^{-5}$ and $\Delta\theta = 0.01^o$, respectively.

and an angular-sensitive geometry at the gas-jet target can be realized. This way absolute observation angles are either not critical or they are spectroscopically determined by using several detectors viewing the same interaction zone. For completeness it is important to note that $\Delta\theta_{lab}$ and $\Delta\beta$ can also be interpreted as widths. Hence Eq. 3.2 describes also the Doppler width observed in the laboratory frame.

3.2 X-ray spectroscopy at the electron cooler

In order to understand spectra emitted via interaction of the stored ions with electrons at the cooler, it is necessary to know the cross-sections for the charge changing processes which take place at this experimental area. In the following a brief survey of the basic relevant recombination processes will be given.

3.2.1 Recombination processes

The main purpose of the electron cooler in a storage ring is cooling of the ion beam (for details of the electron cooling we refer to [67, 68]). However, due to a high quality, dense electron beam the electron cooler can be used as an excellent free electron target to study the electron-ion interactions at low relative energies.

When the electron cooler operates at the cooling energy $E_c = (m/m_i)E_i$, where E_i is the ion energy and m and m_i are the electron and the ion masses, respectively, the electrons interact with ions, essentially, in the limit of zero relative kinetic energy, which has only thermal energy spread (temperature) of about 0.1 eV transversally, and 1 meV longitudinally. The density of electrons in the cooler electron beam is, typically, of the order of $10^7 cm^{-3}$. Additionally, the vacuum in the electron cooler is usually in the 10^{-11} mbar range. These unique properties of the electron beam in the cooler, combined with the availability of heavy ion beams in the storage ring, offer nearly ideal experimental condition to study various aspects of electron-ion interaction.

In an electron cooler an ion can recombine with a free electron by one of three basic interaction processes: the radiative recombination (RR), dielectronic recombination (DR), and collisional (three-body) recombination (TR). These processes are schematically shown in Fig. 3.9.

In radiative recombination an ion A^{q+} captures a free electron with emission of a photon. This can be written as:

$$A^{q+} + e \rightarrow A^{(q-1)+} + \hbar\omega \tag{3.3}$$

where q stands for the ion charge state. Energy conservation requires that

$$T_e = \hbar\omega - \mid \epsilon_n \mid \tag{3.4}$$
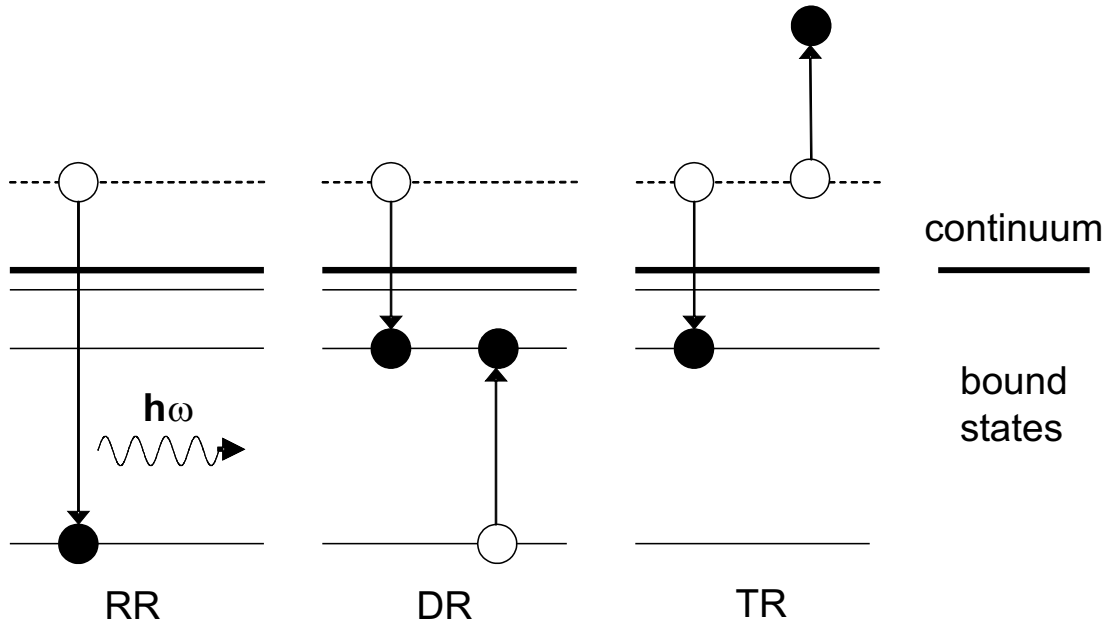
Figure 3.9. Electron-ion recombination processes: radiative recombination (RR), dielectronic recombination (DR) and collisional (three-body) recombination (TR).

here T_e is a kinetic energy of the electron in a final state, $\hbar\omega$ is an energy of the emitted photon and $|\epsilon_n|$ is a binding energy of the electron in the final state. For low energy electrons, as in the cooling of ion beam in the electron cooler, simple estimation based on Kramers work [69] shows that the recombination cross section scales inverse proportionally both to n and the electron energy E. For higher electron energies the cross section decreases with n and energy even faster, namely as $1/n^3 E^2$. Consequently, in radiative recombination mostly the low n-states are populated. First measurement of the radiative recombination rate has been done by Andersen et al. [70, 71] in the electron cooler in a single pass experiment. In this experiment the recombination rates for bare He^{2+}, C^{6+} and F^{9+} ions were measured for relative electron energies 0-1 eV. This experiment showed a good agreement with the prediction of the recombination rates from Stobbe theory [72], when a correction for the field-ionization effect due to the analyzing electric field was taken into account.

Recombination rates measured by this group for non-bare ions [73, 74] showed,

generally, larger discrepancies with the theory, but the calculations used only an approximate approach of the effective charge. Later recombination rates measured at the TSR storage ring [75, 76] at cooling conditions showed substantial discrepancies ($\sim 50\%$) with Stobbe theory, which could be attributed to a stronger field-ionization effect in ring experiments. Similar results were obtained at GSI in a merged beams experiment for non-bare ions [77, 78]. A possibility to study the radiative recombination at storage rings equipped with an electron cooler opens new interesting experimental fields. Because the RR is the time reversed photoionization, the study of this process in highly charged ions can give, via the principle of detailed balance, some insight in photoionization of few-electron excited states, which is not accessible to study in synchrotron radiation facilities. The spectroscopy of photons emitted from RR in the electron cooler shows very narrow peaks (of order of 0.1 eV) at the photon energies corresponding to the electron binding energies in the final states. A precision spectroscopy of x-rays from RR of few-electron ions with electrons can give access for measuring accurately the electron binding energies in one- and few-electron systems. This is very important for studying the QED, relativistic and electron correlation effects.

From the three recombination processes, the RR is the most relevant for our investigation based on x-ray spectroscopy. Therefore, a further theoretical discussion of the radiative recombination will be given in the next subsection (3.2.2).

For ions possessing electrons it is possible that when a free electron is captured another bound electron is excited simultaneously forming thus a doubly excited state (Fig. 3.9). If this intermediate state then decays radiatively below the first ionization threshold, the ion is stable against the autoionization and the dielectronic recombination (DR) is completed [79]. This two-step process may be written as follows:

$$A^{q+} + e \rightarrow A^{(q-1)+}(nl, n'l') \rightarrow A^{(q-1)+} + \hbar\omega \qquad (3.5)$$
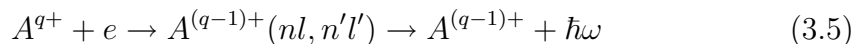
Due to energy conservation, the kinetic energy of the free electron E plus its binding energy in the final state must equal the excitation energy of the bound electron $\Delta E_{n'l'}$, i.e. $E + E_{nl} = \Delta E_{n'l'}$. This process is thus a resonance one and the positions of these DR resonances and their intensities give information about doubly excited states $(nl, n'l')$. High energy resolution in a merged electron-ion

beam experiment in the electron cooler, being of the order of a fraction of eV, gives a possibility to perform precision spectroscopy of doubly excited states formed in DR process. The electric field due to the electron beam space charge influences the DR resonances by mixing the l-states. Also, the magnetic fields, both in the cooler and the ring bending magnets, which are converted into the electric fields in the moving (ion) frame, change a rate of the observed charge-changed recombination products due to the field-ionization effects [80]. Consequently, a role of the external fields on DR process can be studied in the cooler storage rings as well. First measurements of the DR have been performed in merged beam, single-pass experiments [81, 82]. These and further experiments using cold ion beams in storage rings [75, 83, 84, 85, 86] yielded a lot of very interesting results on spectroscopy of doubly excited states in few-electron atoms. Dielectronic recombination for higher energies ($\sim keV$) has also been studied successfully using the electron-beam ion trap (EBIT) ion source [87].

At very low electron energies and high electron densities, as in the case of low-temperature dense plasma, the electron-ion recombination is dominated by the pure three-body collisional recombination. In this process a capture of a free electron is associated with excitation of other free electron in continuum (Fig. 3.9). This may be written in a following way:

$$A^{q+} + e + e \rightarrow A^{(q-1)+} + e \qquad (3.6)$$

The collisional recombination rate α_{coll} depends on the electron density since two electrons are involved in the process, and scales with the ion charge as q^3. For the bare ions the recombination rate is given by the following formula [88]:

$$\alpha_{coll} = 2.0 \cdot 10^{-27} n_e Z^3 / (kT)^{9/2} [cm^3/s] \qquad (3.7)$$

where n_e is the density (in cm^{-3}) and electron beam temperature kT is given in eV. In a more detailed discussion of the collisional recombination in a low-temperature plasma one has to take into account also other processes which may occur in such media, namely the re-ionization (inverse of the collisional recombination), collisional excitation and deexcitation, radiative deexcitation and the radiative recombination. The net result of chain of these processes is called the

collisional-radiative recombination [89]. This rather complicated process, which plays an important role in astrophysics, was a subject of a few studies [88, 89, 90]. Here we will only mention the most important features of the collisional-radiative recombination. First of all, mostly very high n-states, with a narrow spread around some n_b (called a "bottleneck") are populated in this process [91, 92]. This is due to the fact that the decay rate has a minimum (around n_b), because the radiative decay rates decrease with n, while the collisional deexcitation rates increase with n rapidly. A position of the "bottleneck" for hydrogenic plasma and the electron densities typical for the cooler ($\sim 10^7 cm^{-3}$), according to Ref. [92], is located around $\epsilon_b \approx 0.5$, in terms of the reduced energy $\epsilon = Z^2 R/n^2 kT$, where R is the Rydberg constant. With this one finds that n-states around $n_b \approx (2Z^2 R/n^2 kT)^{1/2}$ are populated in collisional-radiative recombination. For cooling condition, where typically $kT \approx 0.1$ eV, one obtains $n_b \approx 16Z$, but such high Rydberg states can be field-ionized in motional electric field in bending magnet in experiments in storage rings. For this reason it was expected that the collisional-radiative recombination should not influence the measured recombination rates. However, recent experimental data [77, 78] indicate a contribution of the collisional-radiative recombination to the measured rates.

3.2.2   Radiative recombination

First theoretical treatment of the radiative recombination was given by Kramers [69] in 1923. Using the ideas underlying the correspondence principle he derived, on the semiclassical ground, the following expression for the recombination cross section, $\sigma_n^k(E)$, into a fixed n-state:

$$\sigma_n^k(E) = \frac{32\pi}{3\sqrt{3}}\alpha^3 a_0^2 \frac{Z^4 Ry^2}{nE(n^2 E + Z^2 Ry)} \tag{3.8}$$

Here α is the fine structure constant and a_0 stands for the Bohr radius. For practical reasons we note that $\frac{32\pi}{3\sqrt{3}}\alpha^3 a_0^2 = 210.5$ barns. Kramers formula predicts surprisingly well the main features of the recombination process. For low energy electrons $E \ll E_{nl}$ the cross section scales as $\sigma_n^k \sim Z^2/nE$. In the high energy limit, $n^2 E \ll Z^2 Ry$, Eq. 3.8 shows that the recombination into Rydberg states scale as $1/n^3$. Quantum mechanics developed in the twenties showed that the Kramers RR cross section agree within 20% with quantum mechanical predictions, with largest discrepancies found for low n-states. Due to its simplicity the semiclassical Kramers formula is still widely used, with quantum mechanical correction known as the Gaunt factor [93].

The development of the quantum mechanics gave an appropriate ground for the theoretical description of the radiative recombination. Early studies of the subject using quantum mechanics were performed by Oppenheimer [94], Wessel [95], Stueckelberg and Morse [96], Gordon [97], and finally by Stobbe [72] in 1930. He derived, in nonrelativistic dipole approximation, the general quantum mechanical expression for the radiative recombination cross section for an arbitrary nl-state. In the later works, mostly related to the astrophysical aspects, the numerical calculation of the RR cross sections were performed. In this context one has to mention papers by Bates et al. [98], Burgess [99] and Seaton [100].

Bethe and Salpeter discussed the radiative recombination process in their classical textbook "Quantum Mechanics of One- and Two-Electron Atoms" [101]. They showed that the Kramers formula for RR cross section can be obtained on quantum mechanical ground in the limit of high n-states.

In 1992, M. Pajek and R. Schuch [102] gave compact analytical results for state selective cross sections for radiative recombination of free electrons with

bare ions, in the low-energy limit. They calculate the asymptotic expressions for the dipole matrix elements when $E_e/E_{nl} \ll 1$, where E_{nl} is the binding energy of the (n, l) state, showing that in this limit the RR cross section scales as $1/E_e$ and giving a simple analytical result for a fixed arbitrary (n, l) state:

$$\sigma_{nl}(E_e) \approx \frac{E_{nl}}{E_e}\sigma(n, l) \tag{3.9}$$

where $\sigma(n, l)$ is introduced as the reduced RR cross section

$$\sigma(n, l) = \frac{\pi^2}{3}\alpha^3 a_0^2[(l + 1)c_{l+1}^2(n, l) + lc_{l-1}^2(n, l)] \tag{3.10}$$

In recent years an exact relativistic formulation [103] has been implemented that takes into account a relativistic motion of the electron both in the bound and in the continuum state subject to the Coulomb field of the nucleus. Moreover, all multipoles in the electron-photon interaction, i.e. retardation effects are included. In the following, we will compare state selective total and angular differential cross section of the Stobbe theory, evaluated according to the technique proposed by Burgess [104] with the corresponding result of the exact theory [103]. Such a comparison is of special interest for the low energy regime and high projectile charges, collision conditions as they do exist at electron cooler devices at storage rings. At such conditions the standard methods applied treat recombination also in the dipole or Born approximation but apply additional approximations in order to avoid the evaluation of the bound-free matrix elements for the high excited states (see e.g. *Bethe-Salpeter* formula). In contrast, the technique of Burgess allows one to evaluate the recombination cross section within the Stobbe theory for any arbitrary projectile states without any other approximation (see Fig. 3.10).

As demonstrated in Ref. [105, 106] it is very suitable for a fast computation of the integrals involved in the RR rate coefficient expression involving any arbitrary projectile states and electron beam temperatures. As an example, for a low nuclear charge $Z = 10$, a principal quantum number $n = 5$ and a low projectile energy of 0.1 MeV/u, it turns out that the Stobbe theory treatment and the relativistic formulation yield the same result within very close limits, as to be expected. However, retaining low relative velocities but choosing a high nuclear
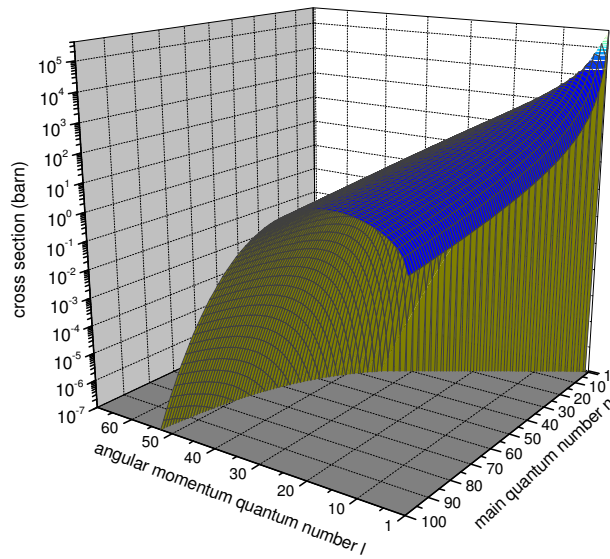
Figure 3.10. State selective cross section for radiative recombination into bare uranium at 0.1 MeV/u (corresponding to an electron kinetic energy of 54.86 keV) as a function of principal and angular momentum quantum number [105].

charge such as $Z = 92$, we obtain sizeable differences in the cross sections, for a detailed comparison of total and angular differential RR cross sections at cooler energies we refer to [105].
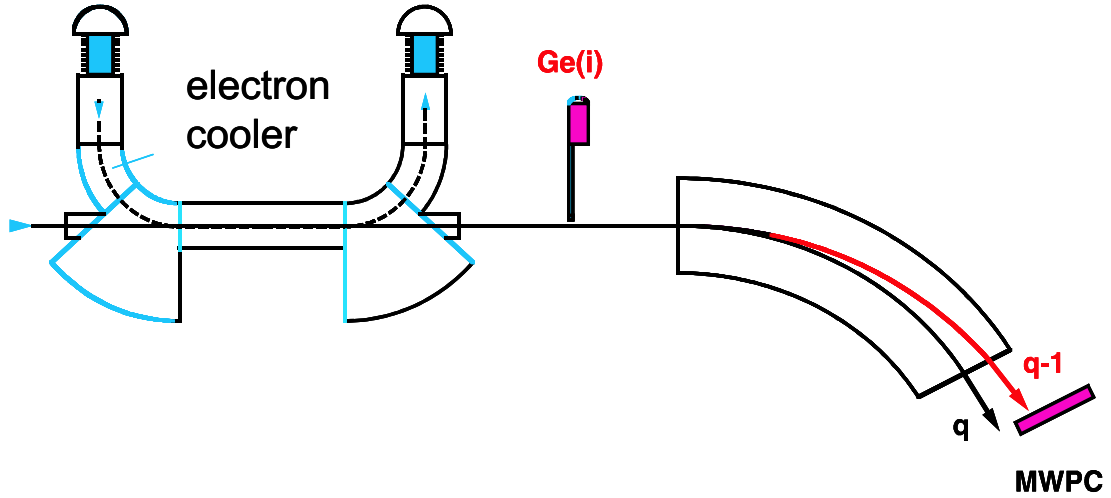
Figure 3.11. Experimental set-up at the electron cooler (see e.g. Ref. [8]).

3.2.3 Experiments at the electron cooler

The experimental setup for the measurements of x-ray radiation at the electron cooler device is shown in Fig. 3.11 [8]. At the electron cooler, the ion-beam/electron-beam interaction region is viewed by a solid state Ge(i) detector at an observation angle of about 0.55^o, i.e. close to 0°, where a slight uncertainty in the observation angle does not affect the final precision (see above). The detector is mounted 4.2 m downstream of the midpoint of the 2.5 m long straight electron cooler section which results in a solid angle of about $\Delta\Omega/\Omega = 4 \times 10^{-5}$. The x-rays are produced by electron capture into the bare projectiles and recorded in coincidence with the down-charged ions. For this purpose a position sensitive multi-wire detector is installed behind the first dipole magnet, located downstream from the cooler section. As a result, very clean conditions for x-ray spectroscopy are present at the cooler section. By using this experimental set-up, Lamb shift experiments have been performed for H-like Au^{78+} and U^{91+} at specific beam energies of 298 MeV/u and 321 MeV/u, respectively [8, 9]. As an example, the x-ray spectrum for initially bare uranium ions undergoing electron capture in the cooler is shown in Fig. 3.12.
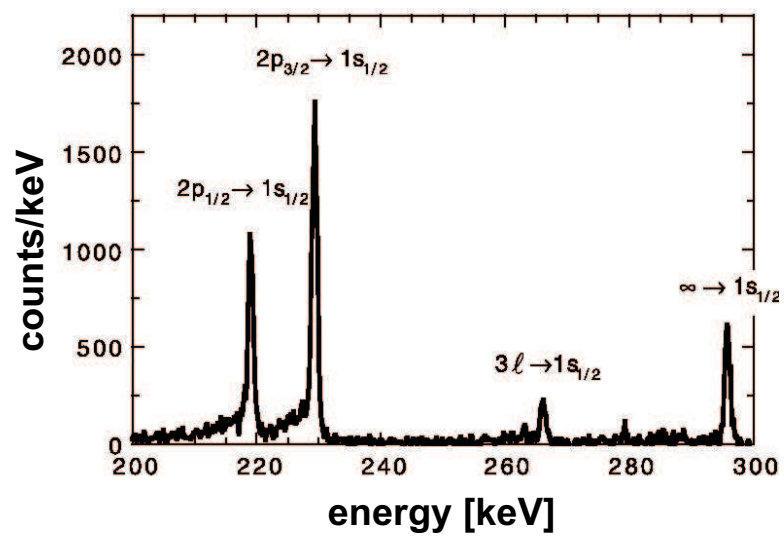
Figure 3.12. Coincident x-ray spectrum of U^{91+} measured at the electron cooler for an ion-beam energy of 321 MeV/u at 0° observation angle [8].

Chapter 4

Measurement of the Two-electron Lamb Shift for the Ground State of He-like Uranium

In August 2001, we carried out our investigation of the two-electron contributions to the ground state binding energy in helium-like uranium at the ESR storage ring at GSI Darmstadt using the experimental technique established at the superEBIT (see above). For this purpose we used the experimental setup at the electron cooler section, a setup which has already been used in former $1s$ Lamb shift experiments (see Figs. 3.11 and 4.1).

4.1 Experiment

For the experiment bare and H-like uranium ions extracted out of the SIS were injected into the ESR at an energy of 360 MeV/u and subsequently decelerated down to 43.59 MeV/u. Directly after the injection from the SIS (before the deceleration) the ions were first cooled at the high energy, then electron cooling was switched off, the coasting beam was bunched and the deceleration mode was applied. At the low energy the electron cooling was switched on again and the measurement cycle started. The cooler current and voltage applied after deceleration were about 100mA and 23kV respectively. As it was already mentioned above, electron cooling guarantees a well defined constant beam velocity, gener-

ally of the order of $\Delta\beta/\beta \approx 10^{-5}$ as well as a reduction of the beam emittance. The accumulated ion currents in the ESR were about 3-4 mA and 550-600 μA before and after the deceleration, respectively. In order to exclude the data which might have been influenced by the complicated beam-handling procedures during injection and deceleration, no x-ray spectra were recorded during the beam accumulation periods. Only after the completion of a whole cycle (including deceleration) a measurement was started. The measuring time per cycle was limited by the capture rate in the cooler to typically few minutes.

X-rays emitted via radiative recombination in the cooler were detected by a segmented germanium detector consisting of four individual strips (Fig. 4.2). An active area and a thickness were $1560mm^2$ (which corresponds to $390mm^2$ for one strip) and 15 mm respectively. The detector was mounted in a pocket behind a 0.1 mm thick stainless steel window which separated the vacuum in the ESR ($\leq 10^{-10}$mbar) from atmosphere. The transmission of the window for x-rays with energies above 100 keV exceeds 97%. The efficiency of the detector for x-rays between 15 and 350 keV was determined using calibrated radioactive sources. The energy resolution was about 700 eV at x-ray energies of about 170 keV for all strips. The whole assembly was mounted 4.1 m downstream of the midpoint of the 2.5m long straight cooling section and could be moved vertically by means of a stepping motor. During the measurement the detector was placed close to the ion beam so that the observation angles of the ion-beam/electron-beam interaction zone were 0.35^o, 0.53^o and 0.71^o for strip number 1, strip number 2 and strip number 3 respectively. Strip number 4 did not see the interaction zone (inside the straight cooler section). The shift of the observed photon energy between two neighboring strips due to the Doppler effect amounted to about 1 eV. The Doppler broadening was negligible due to the observation angle of close to 0°.

The x-rays were recorded in delayed coincidence with down-charged uranium ions, as produced by the capture of one electron in the cooler. The down-charged ions were registered in a gas-filled multiwire proportional counter (MWPC) which was installed in a pocket behind the first dipole magnet downstream of the electron cooler (compare scheme of the experimental set-up displayed in Fig. 3.11). During the periods of beam accumulation, the detector was pulled out of the

beam pipe for beam injection. Before the start of the measurement, the detector was moved to such a position that down-charged particles could be detected without disturbing the orbit of bare projectiles.

Because the key feature of the experiment is a relative measurement of RR into the K-shell of initially bare and H-like uranium, we changed during the experiment three times between the two charge states. Compared to a simultaneous storage of both charge states, also possible at the ESR, this applied method has the advantage to allow us to measure the x-ray emission in coincidence with the down-charged ions. However, it is necessary to note that in contrast to the superEBIT experiment the RR transition into the initially bare and H-like ions is measured in alternate order in our case. Consequently, the requirement of the experiment is that both the bare and H-like species must travel with identical energies. Moreover, within the cooler section, the trajectory for both ion species must be the same. Since the beam energy at the ESR is determined by the cooler voltage, identical beam energies for both ion species are guaranteed. Also, the trajectories of the ion beams inside the cooler section are well controlled. Even, a slight misalignment between the beams of bare and H-like ions (e. g. 1 mm) does not affect the final accuracy of the experiment. Here, we profit from the 0° geometry of our x-ray setup which is rather insensitive to an uncertainty in the observation angle (see Fig. 3.8). In particular the experiment benefits from the recent established deceleration technique [43]. At low energies, all uncertainties associated with Doppler corrections are strongly reduced compared to high-energy beams. Note, the accuracy in the Doppler shift corrections of about $\Delta E/E \approx 5 \times 10^{-5}$ at the ESR is determined by the uncertainty in the determination of the absolute velocity. However, because an energy difference of approximately 2.2 keV (emitter frame) has to be determined, this uncertainty would introduce an error of less than ± 0.1 eV and can therefore be neglected.

Figure 4.1. Photo of the experimental setup at the ESR electron cooler.
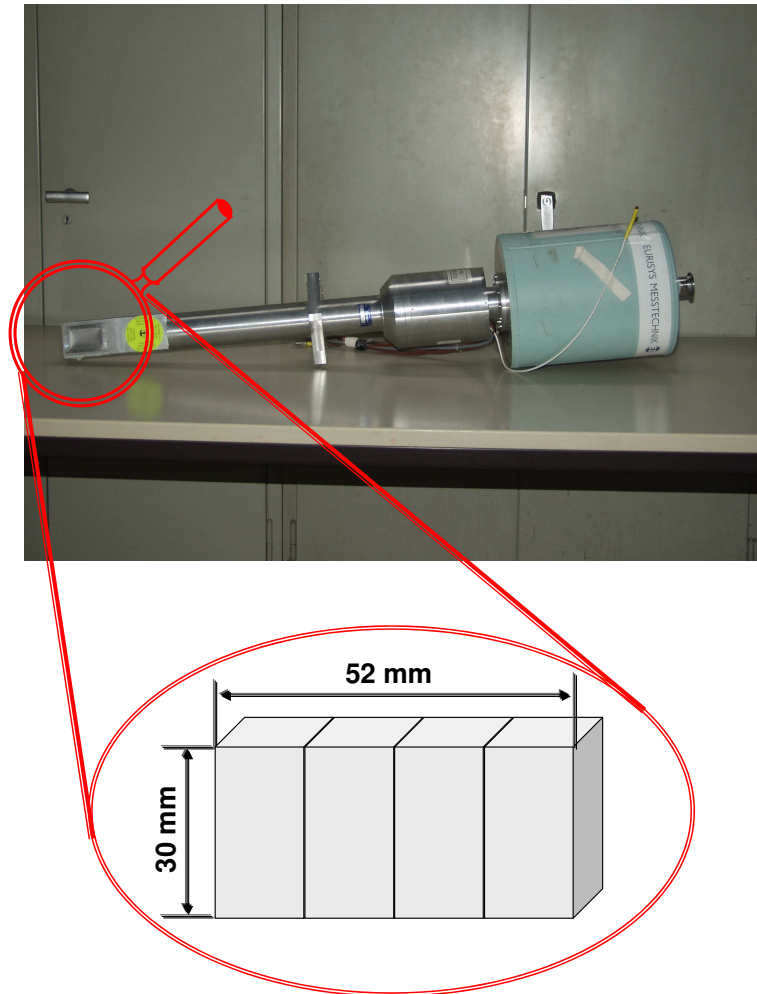
Figure 4.2. The four-fold germanium detector as used in the cooler experiment.

### 4.1.1   Comparison between the experimental situations at the superEBIT and at the ESR electron cooler

Here we would like to summarize (and compare) some of the key features of the experimental environments at the electron cooler and at the supeEBIT.

The superEBIT

- Ions are at rest in the laboratory system (no uncertainties coming from Doppler effect),

- simultaneous storage of the bare and H-like species,

- no x-ray particle coincidences,

- relative energy of the electrons with respect to the ions (in the laboratory system) of about 200 keV.

The electron cooler

- Ions are moving in the laboratory system with an energy of 43.59 MeV/u,

- observation of the electron-beam/ion-beam interaction zone from about 0° angle with respect to the beam axis,

- application of the deceleration mode, which together with latter feature results in negligible Doppler uncertainties,

- non-simultaneous storage of the bare and H-like species,

- x-ray particle coincidences,

- relative energy of the electrons with respect to the ions is essentially 0 eV (see Fig. 4.3). Because of this, the energy of the K-RR photon is considerably smaller as compared to the one at the superEBIT. This implies a better detection efficiency along with a better energy resolution.
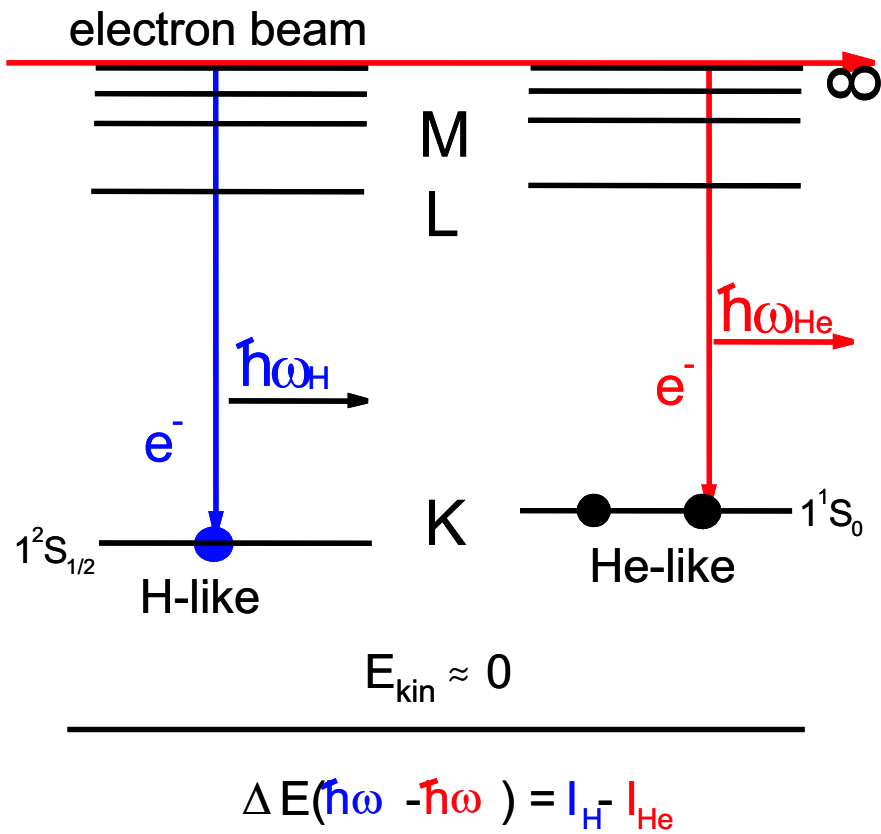
Figure 4.3. Schematic presentation of the RR process in the electron cooler (compare Fig. 2.8).

4.2   The X-ray Spectra

In Fig. 4.4 calibrated x-ray spectra are displayed as observed for initially bare and H-like uranium ions at an energy of 43.59 MeV/u. The spectra are almost background free, since they were recorded in coincidence with down-charged ions. The most intense lines observed can be attributed to direct transition of electrons into the K-shell of the projectile ions (K-RR) and to characteristic $L \longrightarrow K$ (Lyman α) transitions. due to the observation angle of approximately 0°, the characteristic Lyα transitions and the K-RR line with energies of about 100 and 130 keV in the emitter frame, are blue shifted and appear at energies close to 130 and 170 keV respectively. Note, that the radiative recombination process at low relative velocities (which is indeed the case in the electron cooler) populates predominantly high-n, l states (see Fig. 3.10). This fact explains the distinctive tails in the low energy side of the Lyman transitions which are observed in the x-ray spectrum (see Fig. 4.4). The cascades following electron capture into highly excited levels may lead to delayed Lyman emission, which then takes place within the 3 m long distance between the end of the electron cooler and the Ge(i) detector. Such events are registered at observation angles up to 9° which gives rise to an appreciable Doppler shift towards lower energies (see Fig. 4.5) [8, 9]. One should note here that the tails of Lyα transition lines, caused by cascade feeding of the L-shell levels are consequently not present in the case of the RR photon emission.

A further important aspect of our study is that due to the low β-value of 0.29 and the experimental time resolution of about 20 ns (which is mainly determined by the x-ray detector time resolution), photon events which occurred inside the cooler section can be distinguished from events where the emission took place just in front of the x-ray detector. For the latter x-ray events, the set-up possess a comparably large solid angle and the photon energies appear markedly shifted leading to the low-energy tails of the Lyman radiation. In Fig. 4.6 we depict a two dimensional scatter plot of the observed x-ray energy versus the coincidence time (between photon and particle detection) together with the corresponding time and energy spectra.

It is evident that the events which are associated with the delayed Lyman emis-

sion have different coincidence time as compared to the ones stemming from the prompt emission inside the cooler. As a consequence, application of a condition on the coincidence time spectrum excludes most of the cascade contributions leading to the low-energy tails in the corresponding energy spectrum (see Fig. 4.7).

An additional important aspect of the experiment is that due to the beam energy of 43.59 MeV/u, the bremsstrahlung intensity is strongly reduced compared to the high beam energies [8, 9], since a much lower electron current ($\approx$ 100 mA) and the cooler voltage ($\approx$ 23 kV) are applied (at high energies of about 300 MeV/u the values of the corresponding parameters amount to 300 mA and 150 kV). This leads, except of a strongly reduced bremsstrahlung intensity, to a strongly reduced bremsstrahlung cutoff (20 keV instead of 150 keV). These experimental conditions allowed us to observe for the very first time RR transitions into the L-shell as well as the Balmer radiation located at the low energy part of the spectra (see Fig. 4.4). In Fig. 4.8 the Balmer spectrum observed for the bare uranium projectiles is depicted.

In order to compare the observed experimental data with theoretical predictions, a spectrum simulation was performed (see e.g. Ref. [108]). It considers the RR process by application of the dipole approximation. For bound-bound transitions and states below $n = 10$ the relativistic transition rates were used taking into account higher-order multipoles (M1, E2, M2). In contrast, for all the higher states we restricted the calculations to nonrelativistic electric-dipole transitions. For the final comparison with the simulation, the experimental spectrum was corrected from the detector efficiency and from transmission through the $100\mu m$ stainless steel window. The result of the comparison is shown on Fig. 4.9. The theoretical spectrum appears to describe well the experimental one. We would like to emphasize that in order to reproduce our experimental data observed at the electron cooler (where the relative energy of ions and electrons is essentially 0 eV), it is necessary to consider the excited states with n at least up to 100 or even higher, in contrast to the high energy regime where taking into account states with n up to 20 already gives a very good agreement with the experimental spectrum [107, 108]. This is shown in Fig. 4.10, where the experimental Balmer spectrum is compared with the theoretical spectra calculated by

inclusion of excited states up to 20, 40, 60 and 80.

In the high energy part of the observed x-ray spectra the transitions for the K-RR show up which are of particular interest for the current study (see Fig. 4.4). As it was already mentioned above, the photons emitted by radiative recombination into the ground state of bare and H-like projectiles can be exploited for a determination of the two-electron contribution to the ground state binding energy in He-like uranium; the difference in the centroid energies for such radiative recombination transitions equals to the difference in the ionization potential between the H- and He-like ions formed by the recombination process (see Fig. 4.3) which gives exactly the two-electron contribution to the ground state energy of He-like uranium. In order to achieve the desirable precision, a determination of the x-ray line centroids to an accuracy on the order of few percent from the FWHM of the peak is required. In the next section the data evaluation procedure and possible sources of different uncertainties will be discussed.
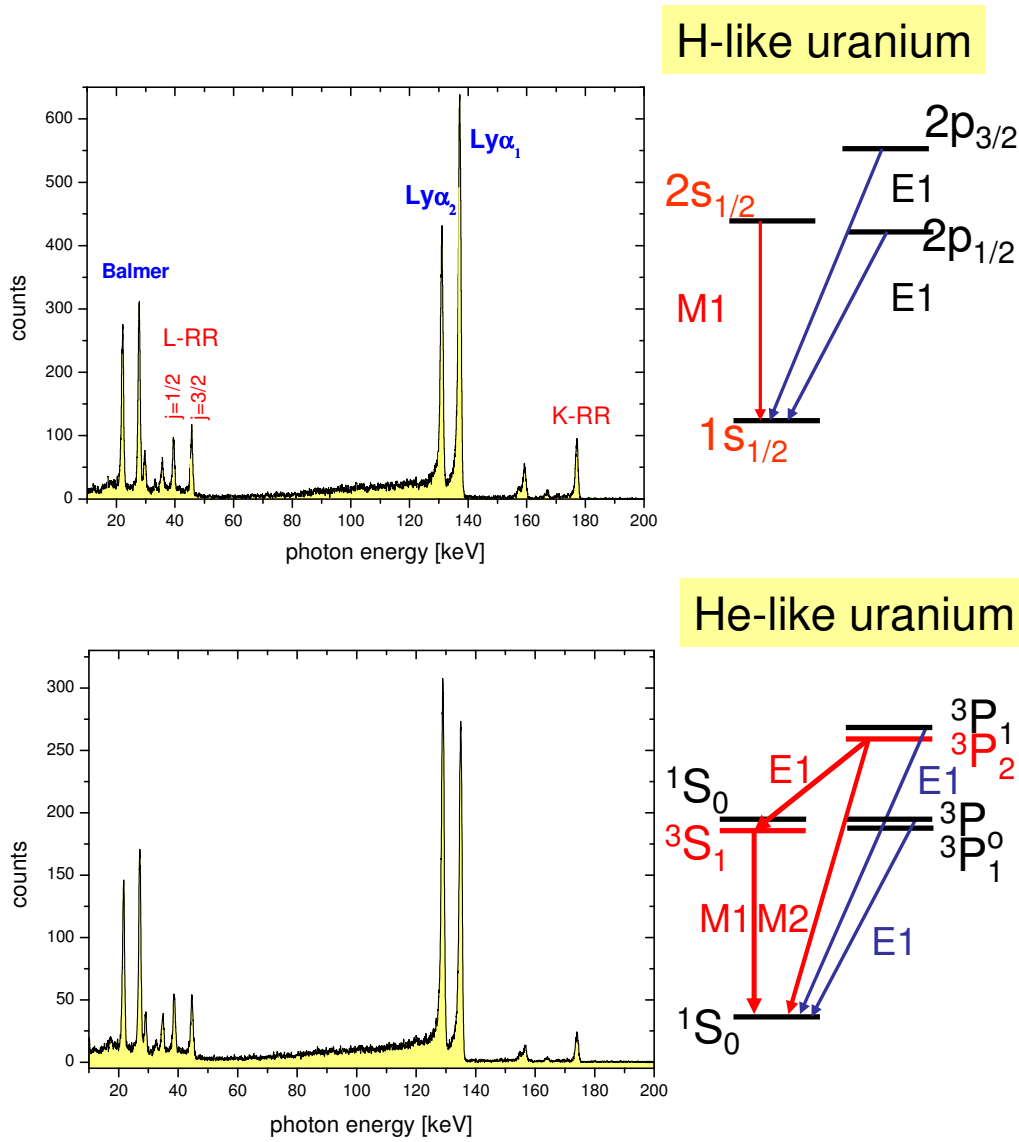
Figure 4.4. X-ray spectra for H-like and He-like uranium as observed for decelerated ions at the electron cooler of the ESR storage ring. The x-ray spectra are measured in coincidence with down-charged uranium ions. For data accumulation, an effective beam time of 4 days has been used.
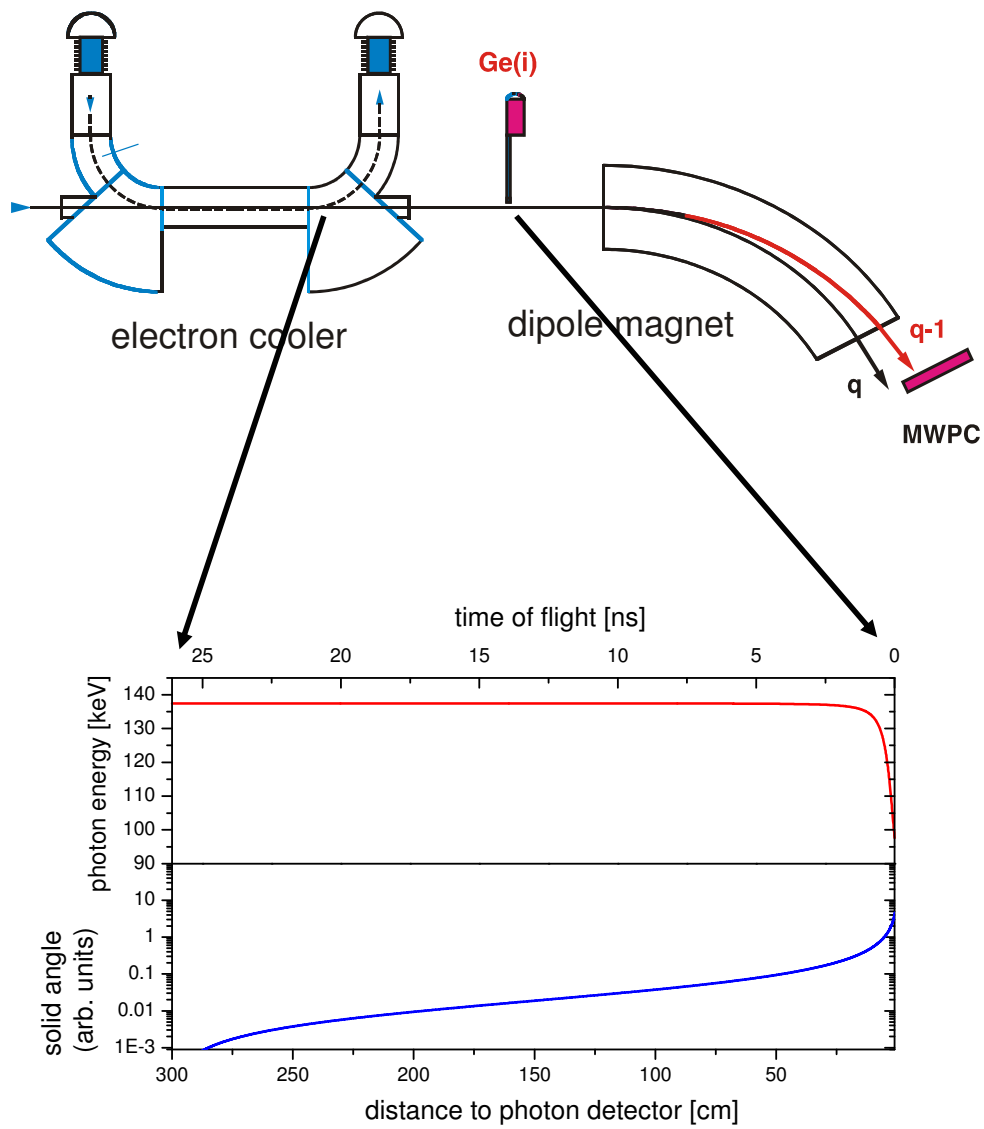
Figure 4.5. The geometry of the experimental setup at the ESR electron cooler.
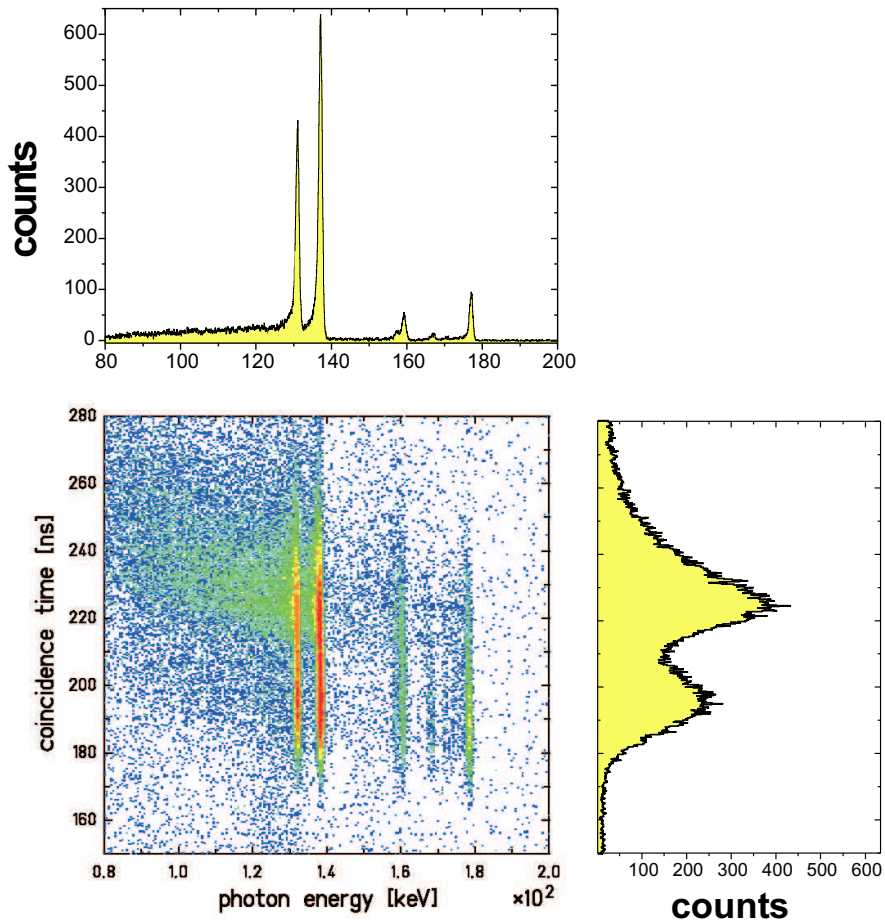
Figure 4.6. Two dimensional scatter plot of the observed x-ray emission versus the coincidence time. The latter refers to the time difference between photon and particle detection. The pronounced structure observed in the time spectrum allows us to disentangle between photon emission which has occurred inside the electron cooler section and such events where the emission takes place just in front of the x-ray detector.
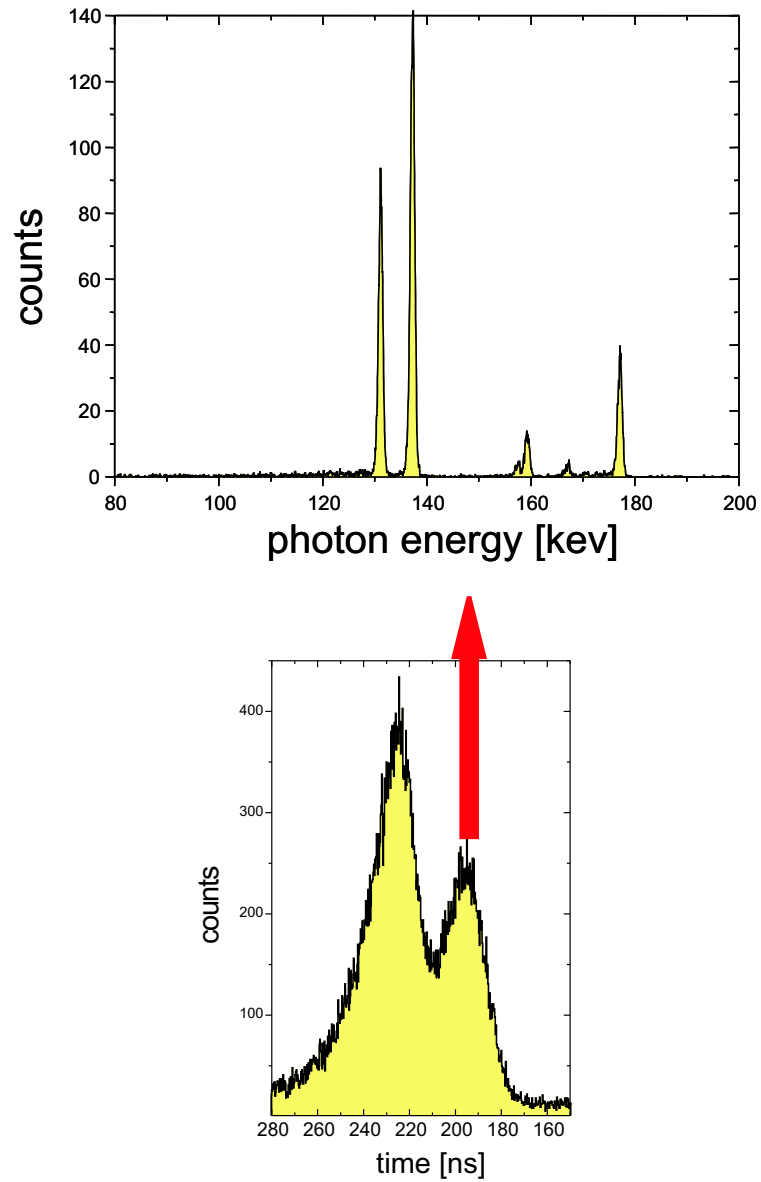
Figure 4.7. X-ray (energy) spectrum (top) accumulated with a condition on the coincidence time spectrum (bottom).
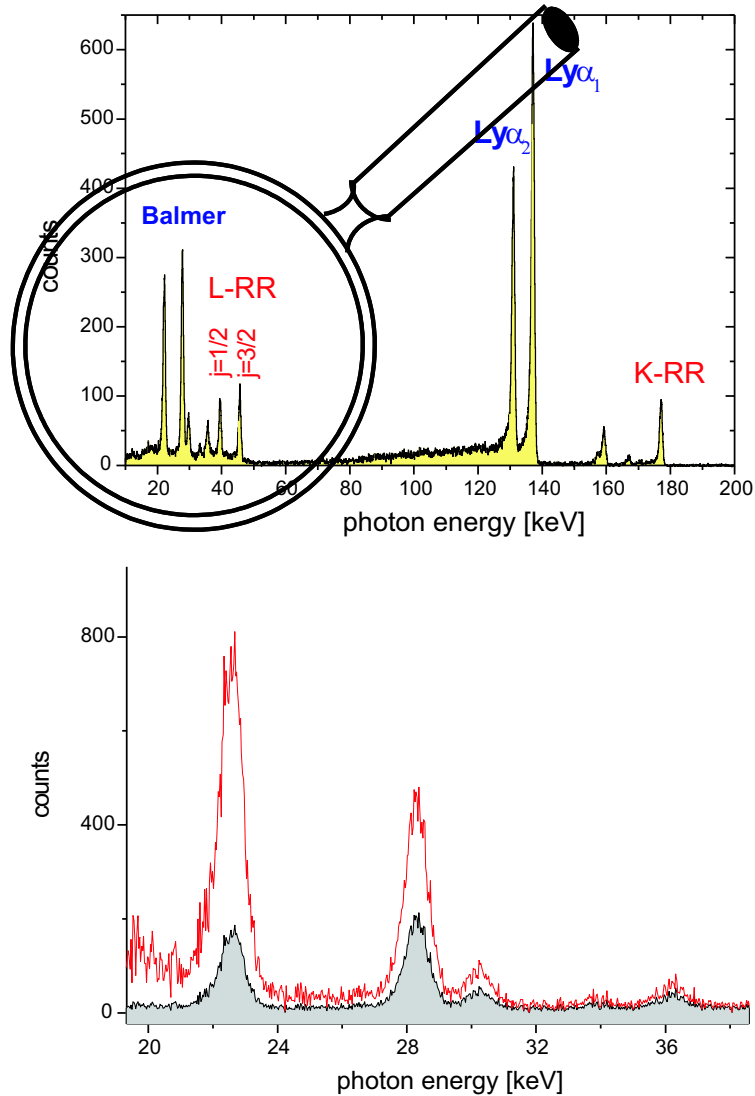
Figure 4.8. The Balmer radiation located at the low energy part of the spectrum observed for U^{92+} (top). In the bottom part an expanded low energy region is presented; the shaded area shows the Balmer spectrum as observed in the experiment (without the transmission correction) whereas the unshaded area refers to the corresponding spectrum corrected for a transmission through the 100 μm stainless steel window.
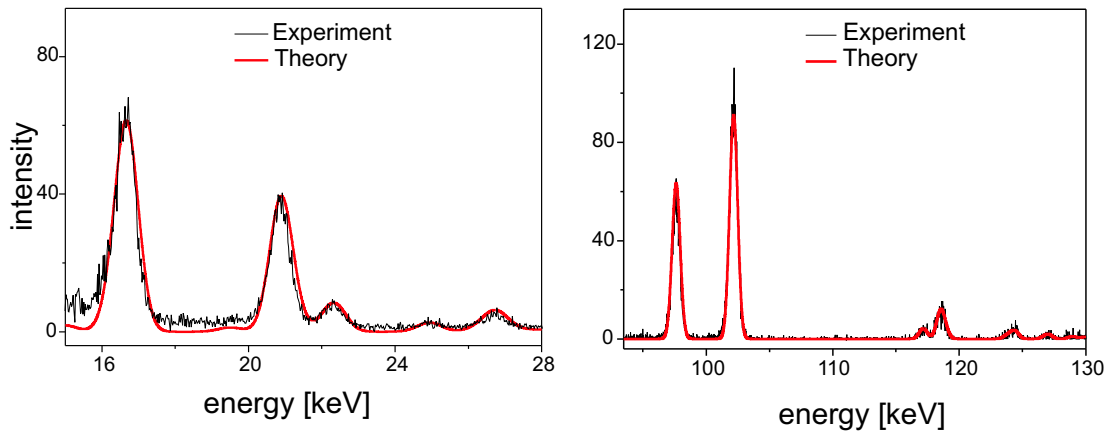
Figure 4.9. Comparison of the X-ray spectrum recorded for RR into the bare uranium with the spectrum simulation. On the left and the right side the Balmer and the Lyman transitions are presented, respectively. Note, for comparison no fitting of the theoretical spectra to the experimental results has been applied.
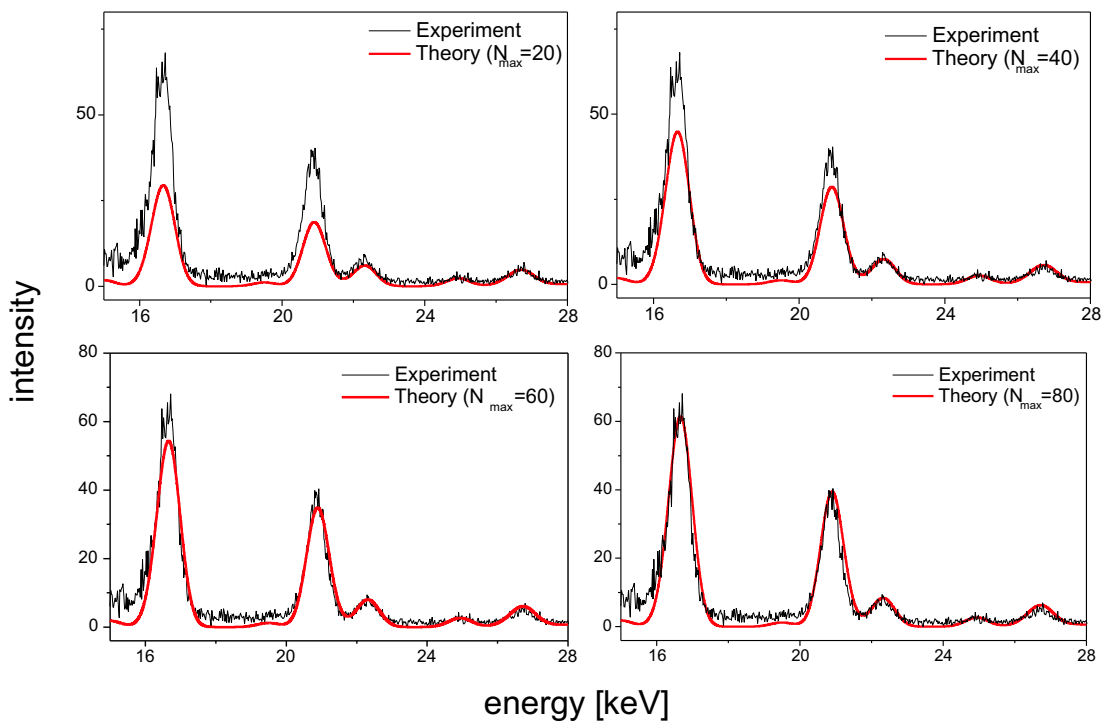
Figure 4.10. Comparison of the experimental Balmer spectrum recorded for RR into the bare uranium with the theoretical spectra calculated by inclusion of excited states up to 20, 40, 60 and 80, respectively.

4.3 Data evaluation and error analysis

Several sources of systematic error were considered and dealt with using consistency checks and data collection procedures as described below. In the end the overall uncertainties in our results are dominated by the statistical uncertainty in the line positions and the contribution of the systematic errors is minor.

4.3.1 Detector geometry

Previous studies have shown that the centroid positions of γ-ray peaks in germanium detectors can depend on the incident photon direction [109]. Our detector directly faced the ion-beam/electron-beam interaction zone and the calibration source was placed in front of the detector as well (in contrary to the experiment at the superEBIT where the source was placed in an annulus that subtended a half angle of approximately 3.5^o with respect to the detector axis [10]). So, the uncertainty in the determination of the peak centroids due to the different geometry was excluded. Note that this type of error could influence a measurement of a large energy difference, but it would not contribute to the measured closely spaced K-RR lines.

4.3.2 Spectator electrons

In our experiment the ionization potentials are deduced from radiative recombination peak energies assuming that electrons are captured into the ground states of bare and H-like ions. The centroid energy of these peaks could be affected by the presence of additional electrons in high Rydberg levels, an effect observed for $K\alpha$ transitions in hot plasmas [110]. However, this should not influence our measurement since the K-RR photon emission was measured in coincidence with the down-charged ions. But, this effect could play a role if the electron present in a high Rydberg state is field-ionized in the dipole magnet before a down-charged ion is detected (see Fig. 3.11). Nevertheless, this should affect both K-RR lines (for bare and for H-like ions) in the same way and therefore should not influence a difference between their centroid positions. Furthermore, we assume that possible contributions of direct transitions from high Rydberg levels to the ground

state are negligible in our measurement, since the Rydberg states with very high angular momentum are populated via the RR process at very low relative energies (see Fig. 3.10) and therefore, the direct transitions to the ground state are forbidden by the dipole selection rules.

### 4.3.3   Peak shape and fitting function

The fitting function consists of a Gaussian peak shape with a shelf on the low energy side [10, 111]. The position, amplitude and the width of the Gaussian were free parameters during the fitting procedure. As an illustration, the result of such a fit is shown on Fig. 4.11. As a consistency check the fitting was performed using different routines.

4.3.4   Energy calibration

Although the intrinsic resolution of Ge(i) detector used in the experiment for the energy range of relevance is about 700 eV, small energy difference between two close spaced lines can be determined with high accuracy [109]. In order to take advantage of this property, the projectile energy of 43.59 MeV/u was chosen. At this particular beam energy the Doppler shift close to 0° allowed us to park the 177.21 keV γ-line of ^{169}Yb, used for calibration, just in between the K-RR lines for H-, and He-like uranium. This is shown in Fig. 4.12. Note, that the calibration line of 130.52 keV is also parked near to the characteristic Lyman lines.

The energies of ^{169}Yb calibration lines are known to 0.8 eV or better, [112] (see Fig. 4.13).

During the experiment the calibration source was frequently placed in front of the detector in order to gain control over possible drifts. During the data analysis the calibration behavior as a function of time was analyzed. The data were divided into individual groups and were analyzed separately. After this, results deduced from each of the individual data sets were compared and checked for consistency. As an example, we present in Fig. 4.14 the outcome obtained from 3 different subgroups for the strip number 1. Afterwards, by combining together the results from the different data sets the final numbers (for each of the
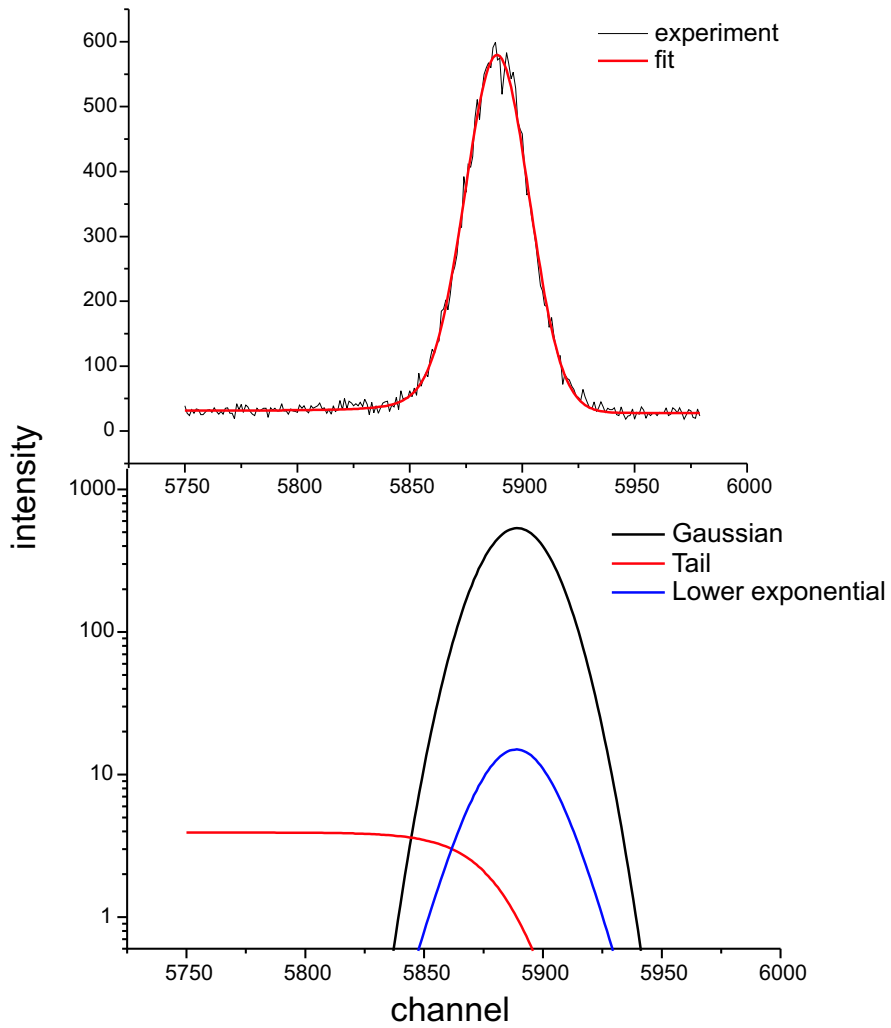
Figure 4.11. Upper part: The fit of 177.2 keV γ-line of ^{169}Yb source used for calibration. Lower part: individual components of the fit function.
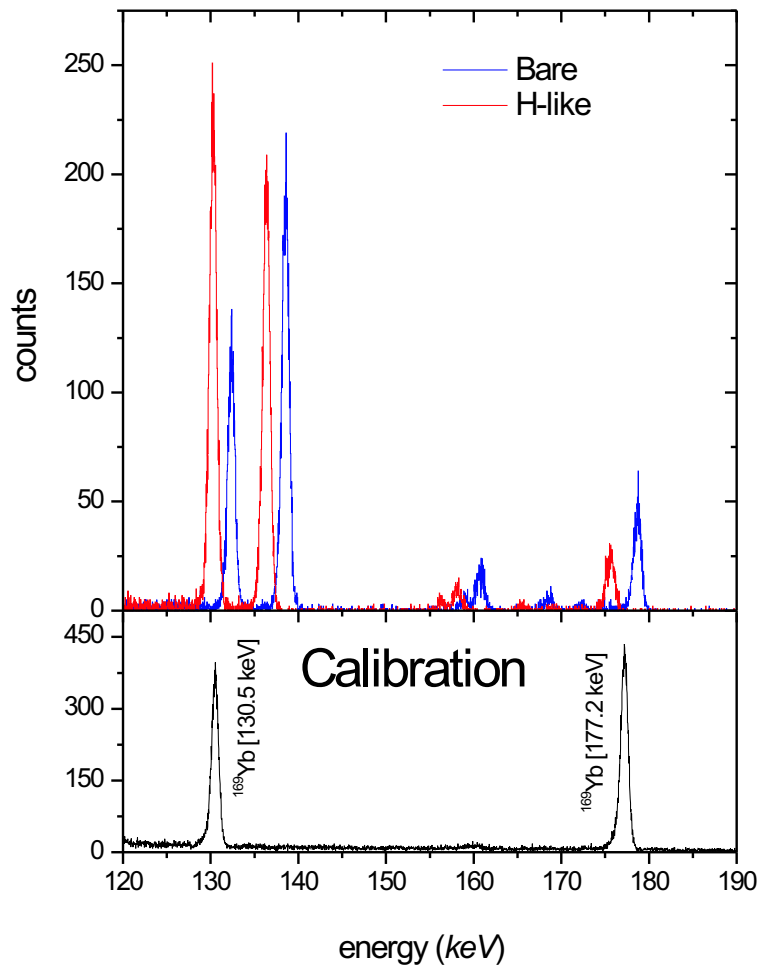
Figure 4.12. X-ray spectra for H- and He-like uranium as measured at the ESR electron cooler together with the calibration spectrum.
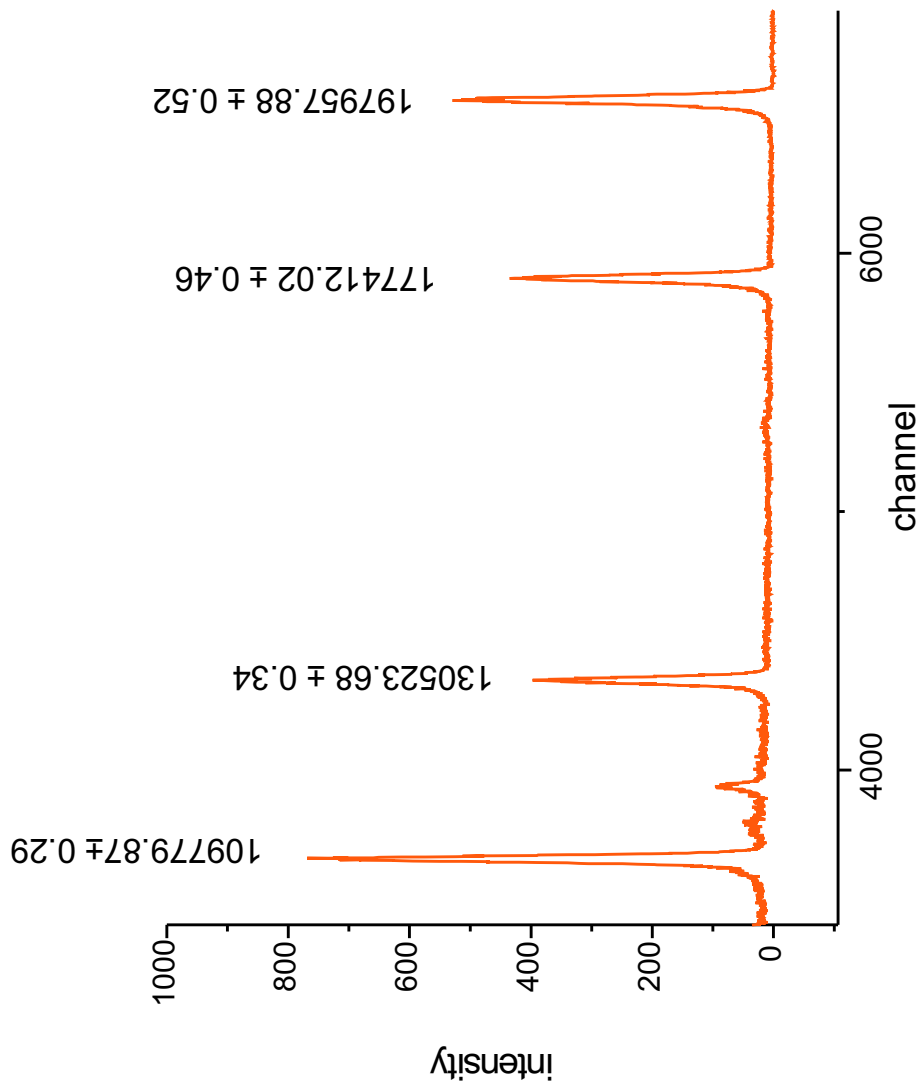
Figure 4.13. The Spectrum of the [169]Yb radioactive source used for calibration as recorded by our Ge(i) detector. The energy values are given in eV (taken from [112]).
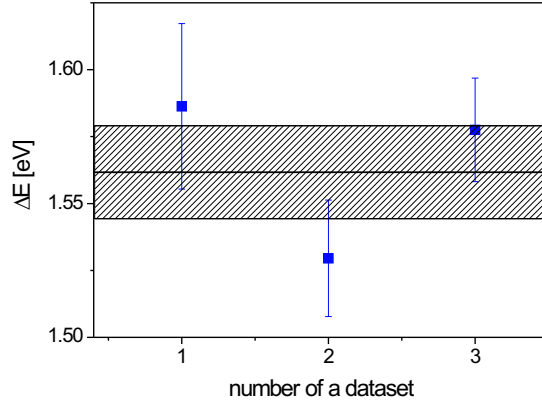
Figure 4.14. The difference between positions of the calibration line at 177.21 keV and the K-RR into the bare uranium for different data sets (compare text). The line in the middle and the shaded area refer to the weighted mean and to the standard deviation of the three values, respectively.

strips) were obtained. They are given in the table 4.1.

STRIP	K-RR H-like	K-RR He-like	ΔE
1	1.562 ± 0.013	-1.498 ± 0.017	3.059 ± 0.022
2	1.574 ± 0.010	-1.455 ± 0.014	3.029 ± 0.017
3	1.624 ± 0.016	-1.475 ± 0.032	3.098 ± 0.036

Table 4.1. The results obtained for each of the individual strips; K-RR H-like: the K-RR photon energy relative to the 177.21 keV γ-line of ^{169}Yb for radiative recombination into initially bare uranium, K-RR He-like: the same as K-RR H-like, but for RR into initially H-like uranium, ΔE: the difference between the K-RR photon energies for radiative recombination into the bare and into the H-like uranium. (all numbers are given in keV).

4.3.5 The transformation into the emitter frame

In order to obtain the difference between ionization potentials for H- and He-like uranium, the energy difference between the K-RR lines for capture into bare and into H-like uranium ions, extracted from the x-ray spectra (observed in the laboratory system) has to be transformed into the rest frame of the ions. (see Eq. 3.1 in the chapter 3). According to the formula the energy in the emitter frame depends on the observation angle (in the laboratory system) and on the β value of the projectile. The observation angles for strip number 1, strip number 2 and strip number 3 were 0.35^o, 0.53^o and 0.71^o, respectively. The value of β was determined from the electron cooler voltage since the velocity of the cooling electrons defines the velocity of the stored ions. The voltage (U) is connected with β via the following relation

$$(\gamma - 1)mc^2 = eU_e \tag{4.1}$$

where e and mc^2 are the charge and the rest mass of electron, respectively. U_e is the voltage U of the high-voltage generator corrected by the potential depression due to the space charge of the electron beam and by the small work function in the cathode. For the beam energies of relevance it is given by the following formula

$$U_e = U \times 1.0011 - 375 \times I_c[A] \tag{4.2}$$

where the first term is a correction resulting from calibration (see below) and the last term represents the space charge correction.

Uncertainties of the observation angle and of the velocity contribute to the overall error of the K-RR energy difference in the emitter frame according to the Eq. 3.2 in the chapter 3. The uncertainty of the angle $\Delta\theta$ is given by the precision of positioning the x-ray detector which is about ±1mm. The resulting uncertainty of the observation angle is $\Delta\theta = \pm0.02^o$. Due to the 0° experimental geometry, this gives (for all strips), according to the Eq. 3.2, a relative uncertainty of less than 2×10^{-6} (corresponding to the absolute uncertainty of 0.004 eV) in the determination of the energy difference. However, the price to be paid for the 0° geometry is a maximum contribution to the uncertainty of the x-ray energy

from the error of the β. Here, we profit from the applied deceleration technique as well as from a precise calibration of the electron cooler voltage. According to Eq. 4.1, the uncertainty in the β is related to the uncertainty of the electron cooler voltage by the following relation

$$\Delta\beta = \frac{1}{\beta\gamma^3}\frac{e}{mc^2}\Delta U_e \tag{4.3}$$

This gives an uncertainty $\Delta\beta$ of about $5.8 \cdot 10^{-6}\Delta U_e$ for $\beta = 0.29565$. The high-voltage generator of the electron cooler has been calibrated by the PTB (Physikalisch-Technische Bundesanstalt) so that the voltage can be determined with an accuracy of better than ±5 V (at a voltage setting of 23 kV). Taking into account this value for ΔU_e, results in $\Delta\beta = 2.885 \cdot 10^{-5}$. Finally, according to the Eq. 3.2, this value of $\Delta\beta$ gives (for all strips) a contribution of less than $3.16 \cdot 10^{-5}$ (corresponding to 0.0711 eV) to the total uncertainty of the measured K-RR energy difference. In table 4.2, we present results of the K-RR energy differences for each of the strips, together with the error contributions resulting from the Doppler transformation into the ion reference (emitter) frame.

STRIP	ΔE_{lab}	ΔE_{em}	σ_θ	σ_β	σ_s
1	3059.24	2255.61	0.002	0.071	16.07
2	3029.11	2233.41	0.003	0.071	12.67
3	3098.31	2284.44	0.004	0.071	26.24

Table 4.2. ΔE_{lab}: the difference between the K-RR photon energies for capture into the bare and into the H-like uranium as measured in the laboratory frame; ΔE_{em}: the same as ΔE_{lab}, but in the emitter frame; σ_θ: the uncertainty resulting from an error in the observation angle ($\Delta\theta$); σ_β: the uncertainty resulting from an error in the β value of the moving ions ($\Delta\beta$); σ_s: the statistical uncertainty resulting from the error in the K-RR line centroid determination (all values are given in eV).

The final result for the two-electron contribution to the ground state binding energy in He-like uranium was obtained to be 2248 ± 9 eV as a weighted mean of three independent values (see Fig. 4.15).
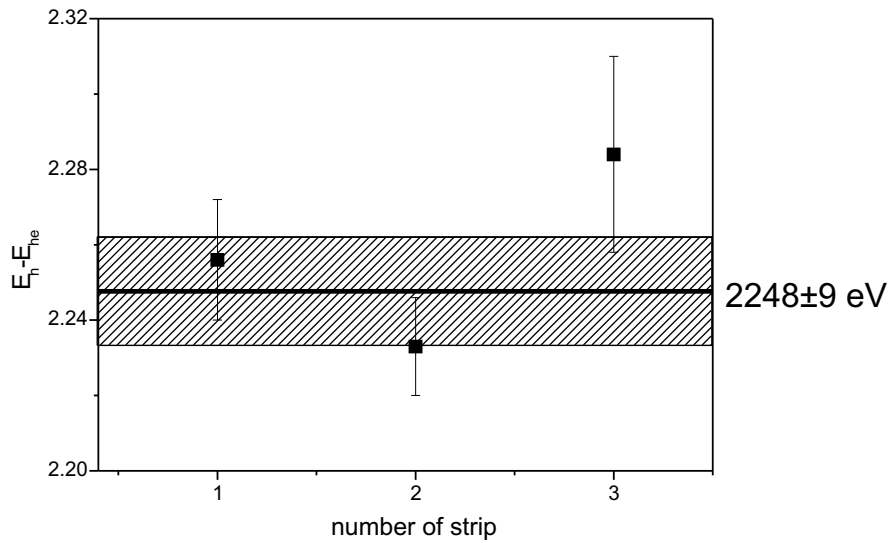
Figure 4.15. The experimental value for the difference in the ionization potential between H- and He-like uranium, i.e. two-electron contribution to the K-shell binding energy of the He-like uranium obtained as a weighted mean of the three independent values (one for each of the strips).

We conclude that the systematic uncertainty from all sources of error is small compared to the statistical uncertainty of the peak centroid determination. Therefore the quoted accuracy of ± 9 eV is entirely statistical.

4.4 Result and discussion

Several different theoretical approaches have been applied to helium-like ions. The "unified" method of Drake uses a relativistic $1/Z$ expansion [50]. This approach is known to be incomplete at the level of $(Z\alpha)^4$, so it is expected to be most accurate at low-Z with an uncertainty that grows like Z^4. The multiconfiguration Dirac-Fock (MCDF) [49] and relativistic many-body perturbation theory (MBPT) [48, 113] approaches are more appropriate for high-Z systems. Recently an all-order technique for relativistic MBPT has been applied to He-like ions [48]. For ground state, in addition, all two-electron QED contributions have been evaluated up to the second order in [51]. Results of these theoretical approaches are compared with our measured two-electron contribution to the ground state binding energy of He-like uranium in table 4.3. In the case of the unified and all-order MBPT method only the total ionization energies are available. Therefore in order to compare with the experimental result it is necessary to subtract the (more accurate) one-electron contribution. We used hydrogen-like energies given by [39] for this purpose. Within the experimental uncertainty, general agreement exists between the experimental result and the predictions of all the theories. However, our result favors the many-body perturbation theories and the MCDF treatment over the unified theory. In fact, as it was already mentioned above, the MBPT calculations are more appropriate for high-Z systems.

EXPERIMENT	RMBPT [48]	UNIFIED [50]	MCDF [49]	RMBPT + QED [51]
2248 ± 9	2249	2256	2244.5	2246

Table 4.3. Two electron contribution to the ground state binding energy of He-like uranium (in eV).

In order to elucidate in more detail the achieved experimental sensitivity, we compare in table 4.4 our result with the individual two-electron contributions as calculated in [51] (results obtained at the superEBIT are presented for comparison as well). In the context of relativistic MBPT, the uncertainty of our measurement is smaller than the second-order many body contribution so the experimental

results are sensitive to this part of the theory. Moreover, our accuracy is of the same size as the second-order two-electron self energy contribution. Here, we would like to stress that in our experiment contributions of possible systematic error sources are essentially eliminated and our result is only limited by counting statistics.

Nuclear Charge	1st order RMBPT (eV)	$\geq 2^{nd}$ order RMBPT (eV)	NR (eV)	2eSE (eV)	2eVP (eV)	Total theory (eV)	Experiment (eV)
32	567.61	-5.2	0.0	-0.5	0.0	562.0	562 ± 1.6
54	1036.56	-7.01	0.2	-1.8	0.2	1028.0	1027.2 ± 3.5
66	1347.45	-8.56	0.4	-3.2	0.6	1336.6	1341.6 ± 4.3
74	1586.93	-9.87	0.6	-4.6	0.9	1573.9	1568 ± 15
83	1897.56	-11.73	0.9	-6.7	1.6	1881.5	1876 ± 14
92	2265.87	-14.11	1.3	-9.7	2.6	2246.0	2248 ± 9

Table 4.4. Comparison of our experimental result for $Z = 92$ with the RMBPT calculations of Persson [51] and results from the superEBIT experiment [10].

Chapter 5

1s Lamb Shift in H-like uranium

5.1   The method

As it was already mentioned, for high-Z ions one of the most reliable approaches for the investigation of the QED effects (Lamb shift) is a precise determination of the x-ray energies emitted by transitions from bound (and/or continuum) states into the ground state of the ion. In the last chapter a measurement of the two-electron contribution to the ground state binding energy of He-like uranium was presented, where the K-RR (direct transitions from continuum to the ground state) line centroids were exploited in order to obtain the value for the difference between the ground state binding energies of H- and He-like uranium which, in turn, gives a direct access to the two-electron contribution. Besides the K-RR, intense characteristic $L \rightarrow K(Ly\alpha)$ transitions show up in the observed spectra (see for example, Figs. 4.4 and 4.7). These characteristic transitions (as well as the K-RR) can be used for obtaining a value for the ground state Lamb shift in hydrogen-like uranium. Assuming that energies of the L-shell states are precisely known from the theory [47], the ground state Lamb shift can be deduced by comparison of the observed $L \rightarrow K$ transition energies to the ones predicted by the Dirac theory. This is illustrated in Fig. 5.1. However, it should be noted that only the $Ly\alpha_1$ centroid energy allows a direct comparison with the ground state Lamb shift prediction due to the fact that only the $2p_{3/2} \rightarrow 1s_{1/2}$ transition contributes to the observed line whereas the $Ly\alpha_2$ line has contributions from two; the $2p_{1/2} \rightarrow 1s_{1/2}$ and the $2s_{1/2} \rightarrow 1s_{1/2}$ transitions. They can not be

79
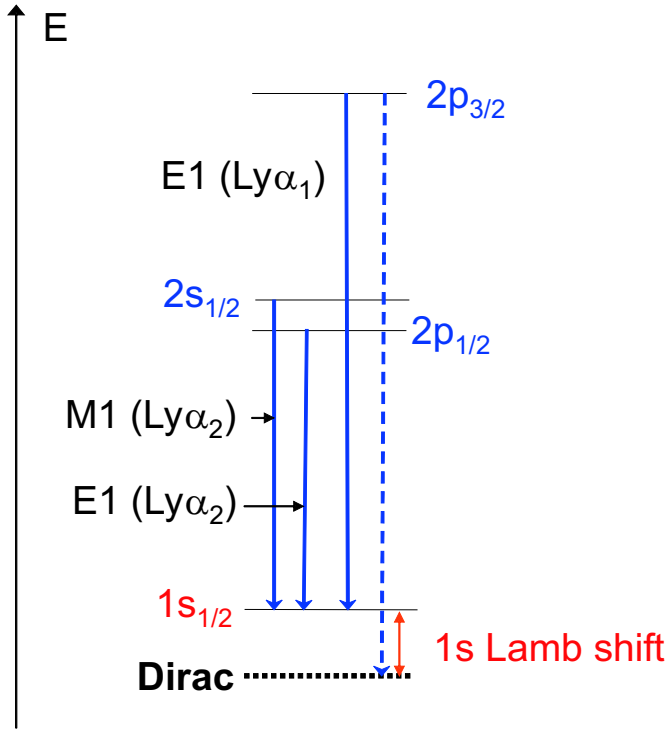
Figure 5.1. The ground state Lamb shift together with the schematic presentation of the various $L \rightarrow K(Ly\alpha)$ transitions.

resolved experimentally since the line spacing between $2s_{1/2}$ and $2p_{1/2}$ amounts to 70 eV, whereas the intrinsic resolution of the detector used is about 700 eV for the energies of relevance.

5.2   Data evaluation

In order to obtain the $Ly\alpha_1$ centroid energy we have used a similar technique as for the case of the two-electron contribution measurement, described in the section 4.3. Of course, everything stated above (chapter 4) concerning the experimental setup, calibration and other experimental details holds true for the present case as well . As we have already noted, at our beam energy of 43.59 MeV/u, the two calibration lines of ^{169}Yb (177.21 and 130.52 keV) were situated near to the K-RR and $Ly\alpha_1$, respectively. This allowed us to determine the small energy differences (between the x-ray and the calibration lines) with high accuracy. In the present case (for the $Ly\alpha_1$ centroid determination) the γ-line at 130.52 keV was used. We have divided the data into subgroups and analyzed separately (similar to the

two-electron contribution evaluation case). The transformation into the emitter frame was performed in the same way as well (see section 4.3). We will come back to this point later in this section. In table 5.1 we present the results obtained for the different data sets (for the strip number 1) together with a mean value.

Dataset	$\mathbf{Ly\alpha_{1,lab}}$	$\mathbf{Ly\alpha_{1,em}}$
1	138577.0 ± 10.6	102174.1 ± 7.8
2	138587.7 ± 9.7	102181.9 ± 7.1
3	138562.2 ± 9.8	102163.2 ± 7.2
Mean	138575.7 ± 5.8	102173.1 ± 4.3

Table 5.1. Outcomes from the different data sets for strip number 1; $Ly\alpha_{1,lab}$: the $Ly\alpha_1$ centroid energy in the laboratory frame, $Ly\alpha_{1,em}$: the $Ly\alpha_1$ centroid energy in the emitter frame, Mean: a weighted mean of the three values. (all results are in eV).

As a next step, the results derived from the individual data sets were combined in order to deduce the $Ly\alpha$ energy values for each of the strips. This is shown in Fig. 5.2 where the result for the $Ly\alpha$ energy for the strip number 1 is obtained as a weighted mean of the three results (from the individual subgroups). Afterwards, we deduced values for the $1s$ Lamb shift for every strip as a difference between the measured $Ly\alpha_1$ energy and the one predicted by the Dirac theory. They are given in table 5.2.

STRIP	1s Lamb Shift [eV]	σ [eV]
1	465.9	4.3
2	458.1	3.7
3	458.3	6.2
Mean	460.9	2.5

Table 5.2. The $1s$ Lamb shift values for the individual strips deduced from the $Ly\alpha_1$ centroid energies.

Finally the $1s$ Lamb shift value of 460.86 ± 2.5 eV was obtained from the $Ly\alpha_1$
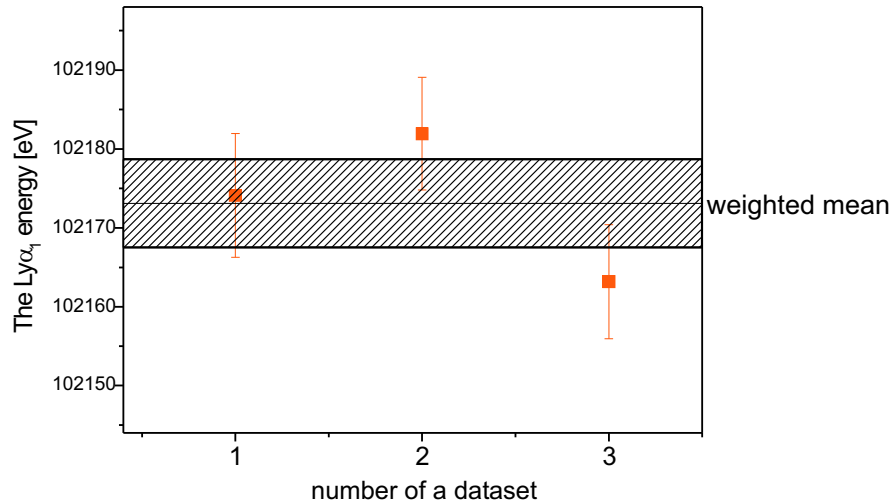
**Figure 5.2.** The $1s$ Lamb shift values from three different data sets for strip number 1. The line in the middle and the shaded area refer to the weighted mean and to the standard deviation of the three values, respectively.

centroid energies as a weighted mean of the three values for individual strips (see Fig. 5.3).

Here we present a few comparisons (checks);

The value for the ground state Lamb shift can also be deduced from the centroid energy of the K-RR line, since the energy of a photon, emitted via radiative recombination in the electron cooler, equals to the ground state binding energy of the ion. Therefore, the Lamb shift is just a difference between the observed K-RR photon energy and the Dirac value for the K-shell binding energy. Since we have already obtained the K-RR centroid energy for the measurement of the two-electron contribution (chapter 4) it can be directly exploited in order to deduce the value for the $1s$ Lamb shift in H-like uranium. The results for each of the strips are presented in table 5.3. In Fig. 5.4 we compare the values for the $1s$ Lamb shift deduced from the K-RR and $Ly\alpha_1$ line centroids. As can be seen from the figure, a good overall agreement exists between the two results.

We have already mentioned that the binding energy value for the $2p_{3/2}$ state is exactly known from theory. According to [47], it equals to -29640.99 eV (which already includes the Lamb shift correction of 8.8 eV). The experimental value for the $2p_{3/2}$ binding energy can be obtained by noticing that it is just the difference
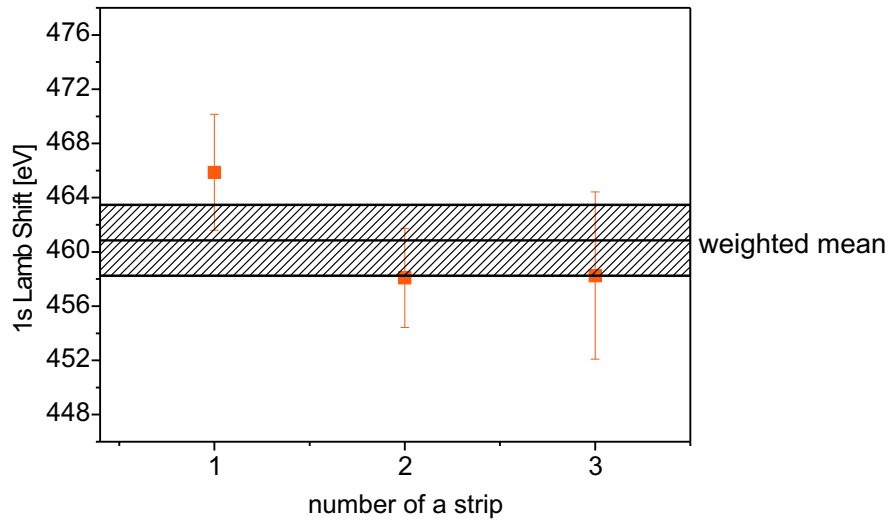
Figure 5.3. The ground state Lamb Shift in H-like uranium obtained as a weighted mean of the three values (for three strips).
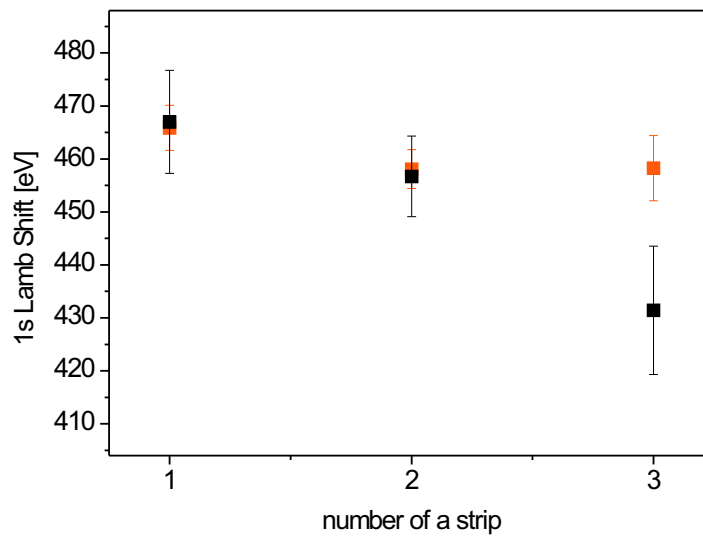
Figure 5.4. Comparison between the values for the ground state Lamb Shift deduced from the K-RR (black squares) and the $Ly\alpha_1$ (orange squares) centroid energies.

| STRIP	1s Lamb shift [eV]	σ [eV]
1	467.0	9.7
2	456.7	7.6
3	431.4	12.1
Mean	454.9	5.4

Table 5.3. The $1s$ Lamb shift values deduced from the K-RR line centroids for the individual strips.

between the ground state binding energy and the $Ly\alpha_1$ $(2p_{3/2} \rightarrow 1s_{1/2})$ transition energy. Hence, the binding energy of the $2p_{3/2}$ state simply equals the difference between the centroid energies of the K-RR and the $Ly\alpha_1$ lines (see Fig. 5.5). Comparing the experimental result for the $2p_{3/2}$ binding energy (obtained as a difference of K-RR and $Ly\alpha_1$ centroid energies) with the theoretical one can serve as consistency check, since the theoretical value is known with a very high level of confidence (contribution of the QED effects is very small). In table 5.4 we present our experimental values for the $2p_{3/2}$ binding energies for the individual strips. The final experimental result for the $2p_{3/2}$ binding energy (obtained as a weighted mean) agrees very well with the theoretical prediction including QED corrections.

STRIP	$2p_{3/2}$ Binding energy	
1	29639.9 ± 10.6	
2	29631.8 ± 8.3	
3	29667.5 ± 13.3	
Mean value:	29641.3 ± 5.9	**Theory:** 29640.99

Table 5.4. The experimental values for the $2p_{3/2}$ binding energy for the individual strips. The final result (a weighted mean) is presented in comparison with the theoretical value [47] as well (all numbers are in eV).

As it was already shown, we deduced two independent values for the ground state Lamb shift in hydrogen-like uranium from the centroid energies of the $Ly\alpha_1$
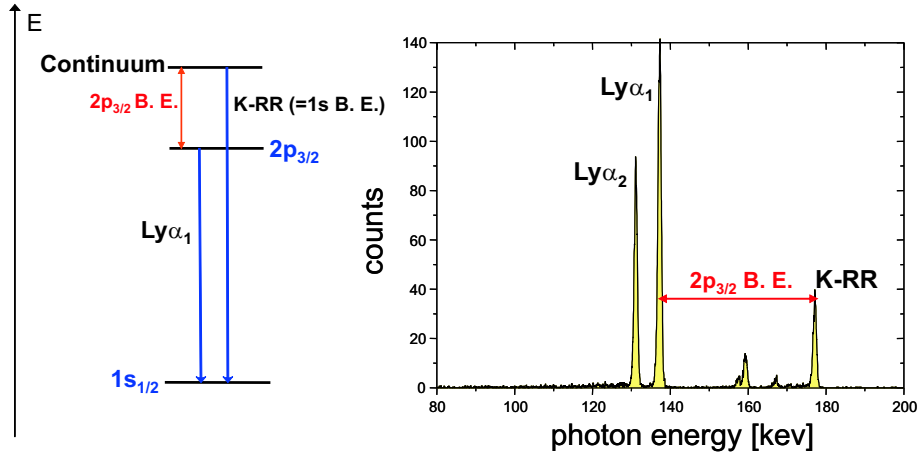
Figure 5.5. Left side: schematic presentation of $L \to K$ and K-RR transitions in hydrogen-like ion; Right side: the corresponding lines as observed in the experimental spectrum. (B. E.=Binding Energy).

and K-RR lines. The weighted mean of these two values is 459.8 ± 2.3 eV. (see table 5.5). The quoted error is entirely statistical. However, for obtaining the final uncertainty, a contribution from the Doppler transformation has to be added as well. The error resulting from an uncertainty in the observation angle gives a negligible contribution (of about 0.1 eV) to the total uncertainty. However, an uncertainty resulting from an error in the cooler voltage of ± 5 V (and correspondingly in the β value) amounts to 3.5 eV. According to this, the final result for the 1s Lamb shift is $459.8 \pm 2.3 \pm 3.5$ eV. To estimate the final accuracy, the two uncertainties are added quadratically (in accordance with Eq. 3.2) giving ± 4.2 eV.

From the Lyα_1	From the K-RR	Mean value
460.9 ± 2.5	454.9 ± 5.4	459.8 ± 2.3
The final result for the 1s Lamb shift	459.8 ± 4.2	

Table 5.5. The final result for the ground state Lamb shift in H-like uranium.
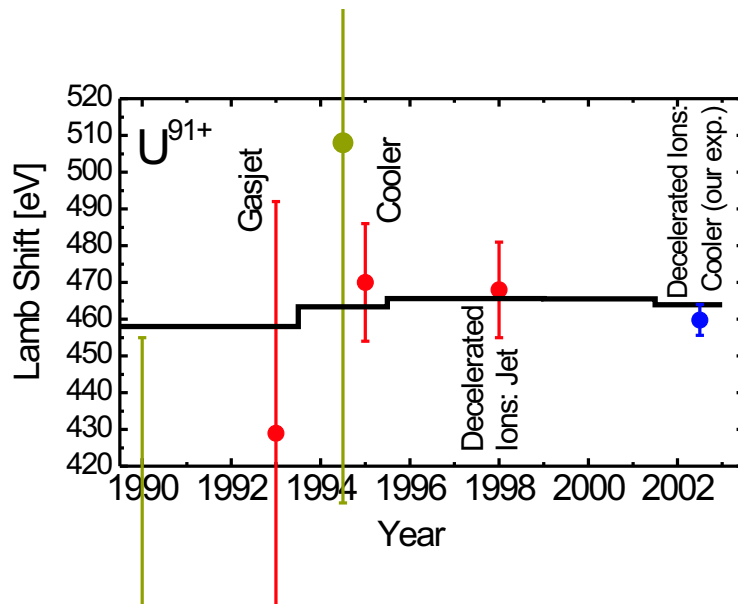
Figure 5.6. Experimental results for the ground state Lamb shift in hydrogen-like uranium in comparison with theory (solid line). The blue point refers to the result of our experiment, the red points are values obtained at the ESR storage ring [7, 9, 44] and the green points are results from experiments conducted at the BEVALAC accelerator [45, 46].

5.3   Comparison with theory

In Fig. 5.6, our experimental result for the ground-state Lamb shift in hydrogen-like uranium is presented together with available results from other experiments [7, 9, 44, 45, 46] and compared with different theoretical predictions [31, 32, 39, 41, 114] (solid line). The figure demonstrates the substantial improvement by almost two orders of magnitude achieved at the ESR storage ring as compared to earlier experiments conducted at the BEVALAC accelerator [45, 46]. Note, that the theoretical predictions are also changing in time. Our value is consistent with results from the former experiments. In order to emphasize the achieved experimental precision, we compare, in table 5.6 our result for the 1s Lamb shift in H-like uranium with the newest theoretical value. Different contributions to the total theoretical Lamb shift are listed separately as well. The theoretical value was calculated including all second order (in α) contributions which until

recently were the largest sources of the theoretical uncertainties [115, 116, 117]. Our result is sensitive to the first order (in α) QED contributions at the 1.5% level. Moreover, only a slight improvement in accuracy would be sufficient in order to accomplish a meaningful test of the recently calculated second order QED contributions [32]. One should note, however that the finite nuclear size effect contributes more than 40% to the total Lamb shift correction. Although the uncertainties introduced by the latter effect (0.3 eV [41]) are much smaller than the present experimental accuracy, they may prevent, for the particular case of uranium, a direct test of QED with a precision of 1 eV or better. For this purpose, an experiment using ^{208}Pb appears to be most appropriate because the extended nuclear size of this double magic nucleus is much better known.

Finite nuclear size	198.81
Nuclear Recoil	0.46
Nuclear Polarization	-0.19
VP (see Fig 2.1)	-88.60
SE (see Fig 2.1)	355.05
SESE (see Fig 2.2)	-1.87
VPVP (see Fig 2.2)	-0.97
SEVP (see Fig 2.2)	1.14
S(VP)E (see Fig 2.2)	0.13
Total Lamb shift	463.95±0.5
Experiment	459.8±4.2

Table 5.6. Comparison of the ground state Lamb shift value obtained in our experiment with various individual contributions to the theoretical prediction [32].

Chapter 6

Summary

In summary, the cooled heavy-ion beams of the ESR storage ring offer excellent experimental conditions for a precise study of the effects of QED in the ground-state of high-Z one- and two-electron ions. This has been demonstrated within the series of experiments conducted at the electron cooler device as well as at the gasjet target.

In this work we have used a recently developed experimental approach to obtain the first direct measurement of the two-electron contributions to the ground state binding energy of helium-like uranium. By employing our method, all one-electron contributions to the binding energy such as finite-nuclear size corrections and the one-electron self energy cancel out completely. Note, this is a distinctive feature of this particular kind of QED test and is in contrast to all other tests of bound state QED for high-Z ions such as $1s$ Lamb shift (in one-electron systems), g-factor of bound electrons, or hyperfine splitting. Compared to former investigations conducted at the superEBIT in Livermore we could already substantially improve the statistical accuracy and extend studies to the higher-Z regime. Moreover, our result has reached a sensitivity on specific two-electron QED contributions. Our value agrees with the theoretical predictions within the experimental uncertainty. Similar to the superEBIT experiment possible sources of systematic errors are essentially eliminated and the final result is limited only by counting statistics.

For the case of the $1s$ Lamb shift in hydrogen-like uranium, the achieved accuracy of ± 4.2 eV is a substantial improvement by a factor of 3 compared to

the most precise value up to now [44] (see Fig. 5.6). Our result already provides a test of the first-order QED contributions at the 1.5% level and only a slight improvement is required in order to achieve a sensitivity to QED contributions beyond first-order SE and VP.

Chapter 7

Outlook

It was shown above that in our experiment, for the measurement of the two-electron contribution, possible sources of systematic errors are essentially eliminated (or negligible) and the final result is limited only by statistical uncertainty in the peak centroid determination. Accordingly, a further more extended experimental run would provide us with a further improvement of the experimental accuracy.

In the case of the $1s$ Lamb shift, one of the main limiting factors for a further improvement in the experimental precision is the systematic uncertainty stemming from an error in the determination of the beam velocity (the β value). By using decelerated beams, a further progress towards an absolute accuracy of 1 eV may be anticipated. For this purpose, we have recently conducted a test run at the ESR electron cooler for the beam energy of 20 MeV/u. As an example, spectra recorded in this experiment for recombination into U^{92+} is shown in Fig. 7.1. A peculiarity of the experiment is a simultaneous observation of the ion-electron interaction zone from two, 0 deg (forward) and 180 deg (backward) angles. This could provide us with a possibility to considerably reduce the uncertainty resulting from an error in the β value and may path the way towards 1 eV precision.

Alternatively, future experiments may also use a highly redundant setup at the jet-target and will focus in addition on decelerated ions combined with the crystal spectrometers [118, 119] or bolometers [120, 121] which presently are under commissioning at the ESR.
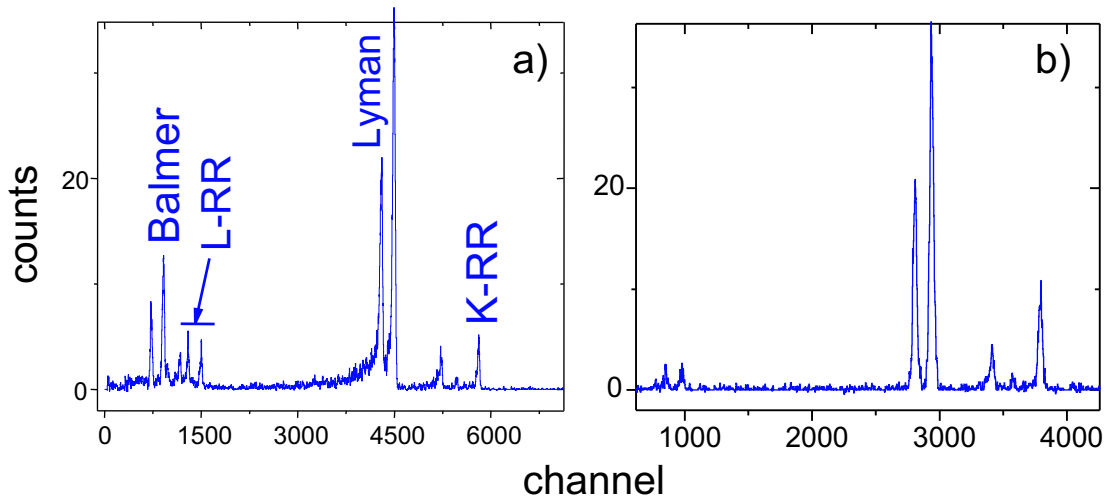
Figure 7.1. a) Coincident x-ray spectrum for the recombination into U^{92+} measured at the electron cooler for an ion-beam energy of 20 MeV/u at 0° observation angle, b) Coincident x-ray spectrum recorded at an observation angle of 180°. Note that in the latter spectrum there are no tails present for the Lyman lines. This result is in agreement with the assumption that the tails are generated by delayed transitions which take place out of the electron cooler and just in front of the x-ray detector (see chapter 4).

As an example, a new kind of x-ray spectrometer, set up in the FOcussing Compensated Asymmetric Laue (FOCAL) geometry, has been developed for this purpose [119] (Fig. 7.2). The spectrometer serves in measuring small wavelength differences between the fast moving x-ray source, represented by the circulating ions in the ESR, and a stationary calibration source. It is designed for energies between 50 and 100 keV or wavelengths between 25 and 12 pm leading to Bragg angles of less than 4° for a Si(220) crystal. In a future experiment, this focussing transmission crystal spectrometer will be combined with a segmented germanium x-ray detector. Such a position-sensitive detector permits the measurement of an energy spectrum wide enough to investigate the interesting energy regime simultaneously. In addition, the good energy resolution enables discrimination against background events of the recorded spectra arising from various sources. Very recently such a microstrip detector system, developed at the Forschungszentrum Jülich [122] (see Fig. 7.3), with a position resolution of close to 200 μm has be-
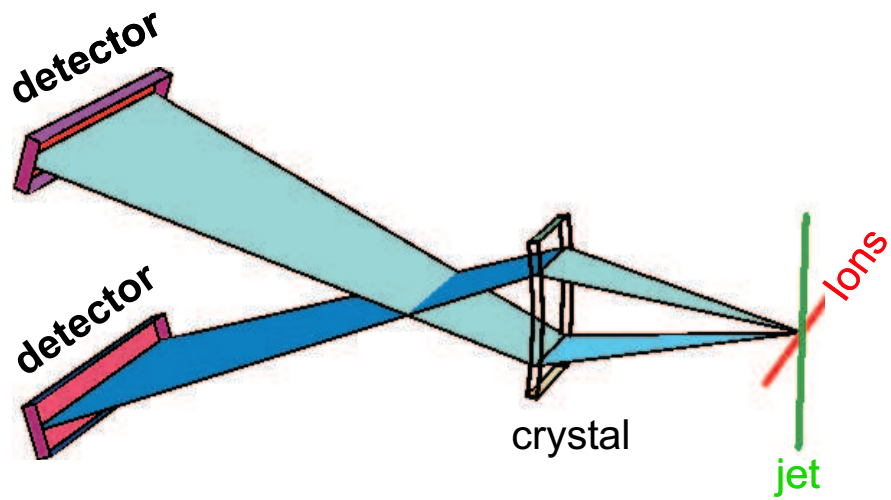
Figure 7.2. Experimental arrangement of the FOCAL spectrometer at the ESR jet target.[119].
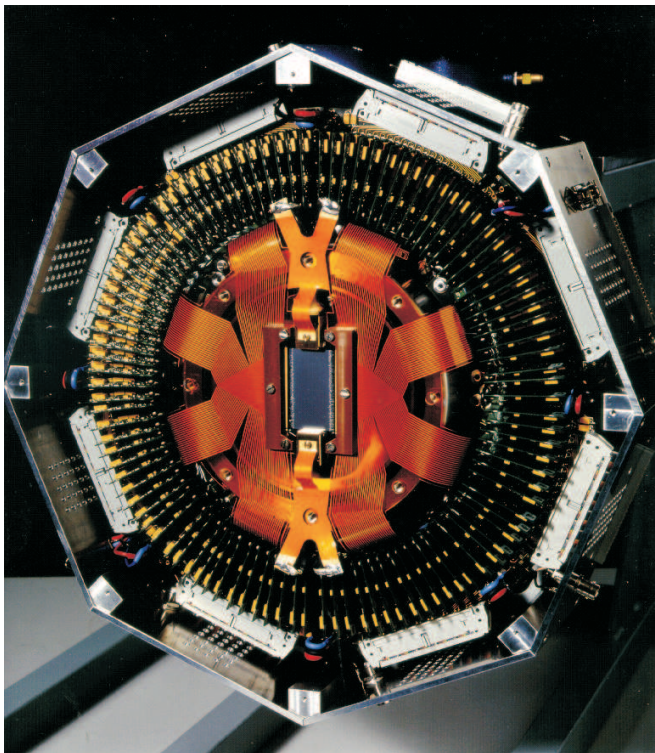
Figure 7.3. The main part of the germanium microstrip detector system without the cryostat-cap and the cover for the electronics [122].
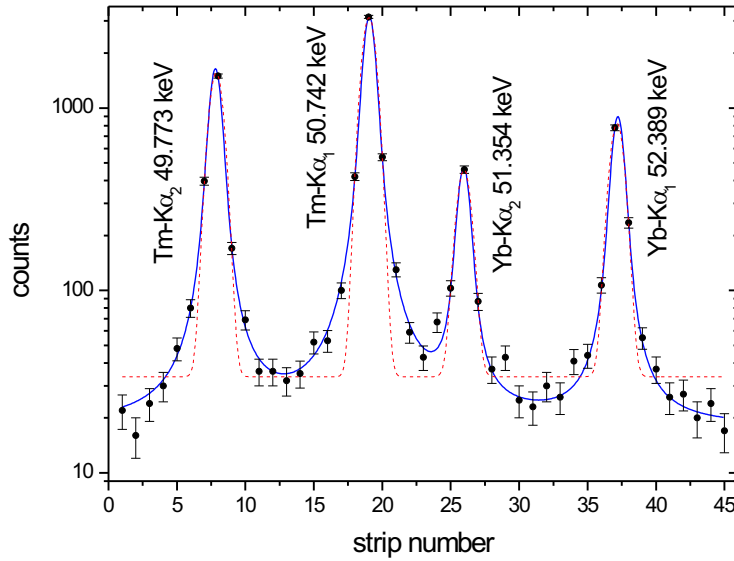
Figure 7.4. Result obtained with the germanium microstrip detector mounted at the FOCAL spectrometer. The intensity pattern as a function of the position (energy) identifies well resolved the two components of the Kα-doublet of Tm as well as those of Yb [122]. The solid line refers to a least square fit by using Voigt profiles and the dashed line refers to Gaussian distribution.

come available and has been tested in combination with the FOCAL spectrometer using an intense radioactive ^{169}Yb source. Even without any strict conditions on the photon energies for the individual strips, the intensity pattern observed with the microstrip detector as function of the position (i.e. strip number) identifies clearly the two x-ray lines of the Kα-doublet from Tm and Yb (Fig. 7.4) which are separated by approximately 970 eV and 1030 eV, respectively. This demonstrates that in combination with the FOCAL spectrometer [119], an energy resolution better than 100 eV can be achieved along with high detection efficiency.

In conclusion, considering the experimental progress described above, an achievement of 1 eV precision for the measurement of the ground state Lamb shift in H-like uranium can be expected within the next few years.

Chapter 8

Zusammenfassung

Den Schwerpunkt der vorliegenden Arbeit bilden Experimente zur Überprüfung der Quantenelektrodynamik (QED) im Grenzbereich extrem starker elektromagnetischer Felder, wie sie in den schwersten Atomen vorliegen. Zwar gilt die Quantenelektrodynamik (QED) als eine der am Besten überprüften Theorien der Physik. Für den Bereich extrem starker elektrischer Felder, denen die am Stärksten gebundenen Elektronen im schweren Atomen ausgesetzt sind, werden allerdings Effekte höherer Ordnung vorhergesagt, die sich vor allem auf die Bindungsenergien auswirken. Eine präzise experimentelle Überprüfung dieser Korrekturen steht aber bislang noch aus. Auf Grund ihrer einfachen Struktur sind für eine solche Überprüfung Atome mit nur einem oder zwei Elektronen besonders geeignet, bei denen die Spektroskopie der Röntgenübergänge einen direkten Zugang zu den dort vorliegenden Bindungsenergien liefert. Für solche spektroskopische Untersuchungen an den schwersten Ein- und Zwei-Elektronensystemen bietet die Experimentier-Speicherringanlage für hochgeladene Ionen – ESR – bei der GSI in Darmstadt ideale Voraussetzungen.

Bei denen im Rahmen dieser Arbeit am ESR durchgeführten Experimenten lag das Hauptaugenmerk auf einer präzisen Vermessung des Beitrags der Elektron-Elektron-Wechselwirkung zum Ionisationspotenzial im He-ähnlichen Uran, d.h den schwersten Zwei-Elektronensystemen, die gegenwärtig Experimenten zur Verfügung stehen. Diese repräsentieren die einfachsten atomaren Vielteilchensysteme, in denen aber auf Grund der hohen Kernladung zugleich relativistische Effekte, Korrelationen und QED-Beiträge eine wichtige Rolle spielen. Hingegen

und im Unterschied zu den Ein-Elektronen-Systemen spielen hier Korrekturen, die auf die Ausdehnung des Kerns zurückzuführen sind, eine stark untergeordnete Rolle. Auf Grund des gewählten Experimentieraufbaus konnten zudem die Grundzustandübergänge für H-artiges Uran vermessen werden, so dass ebenso präzise Informationen für die Grundzustandsenergie des Urans mit nur einem Elektronen gewonnen werden konnten.

Für die Untersuchung des He-ähnlichen Urans am Experimentierspeichering ESR wurde eine neuartige Experimentiermethode aufgegriffen, die erst kürzlich in einem Experiment an einer elektronstrahlbetriebenen Falle für hochgeladene Schwerionen (EBIT, 'Electron Beam Ion Trap') eingeführt wurde. Hierbei wird die radiative Rekombinationsstrahlung, die bei dem Einfang eines freien Elektrons in den Grundzustand der Ionen auftritt, ausgenutzt. Die Energie dieser Strahlung ist somit proportional zur Bindungsenergie des eingefangenen Elektrons im Endzustand. Vergleicht man die Energie der Rekombinationsstrahlung für den Einfang in nackte Ionen mit der für den Einfang in die H-ähnlichen Ionen, so ist die zu beobachtende Differenz der Photonenenergien ausschließlich auf die unterschiedlichen Ionisationspotenziale der beiden Ionensorten zurückzuführen. Somit wird in diesem Experiment das Ionisationspotenzial der He-ähnlichen Ionen mit dem der H-ähnlichen Ionen verglichen und das Experiment liefert eine direkte Messung des Beitrags der Elektron-Elektron-Wechselwirkung zum Ionisationspotenzial He-ähnlicher Ionen.

Das Experiment wurde am Elektronenkühler des ESR-Speicherrings durchgeführt, wobei der Photonennachweis mittels eines Ge(i)-Detektors erfolgte, der die Elektronen-Ionen-Wechselwirkungszone unter einem Beobachtungswinkel nahe Null Grad einsah. Es muß hervorgehoben werden, dass es sich bei den im ESR gespeicherten Ionen um schnelle, sich relativistisch bewegende Teilchen handelt und die relativistische Dopplertransformation generell eine besondere experimentelle Herausforderung darstellt. Dies macht eine besonders präzise Bestimmung der Ionengeschwindigkeit und des Beobachtungswinkels generell zwingend erforderlich. Der Vorteil der 'Null Grad'-Geometrie am Elektronenkühler des ESR besteht darin, dass kleine Unsicherheiten in der Bestimmung des absoluten Beobachtungswinkels nahezu keinen Einfluß auf das Messergebnis haben, was bereits in früheren Experimenten am Elektronenkühler des ESR erfolgreich ausgenutzt wer-

Z	Erste Ordnung RMBPT (eV)	Zweite Ordnung RMBPT (eV)	NR (eV)	2eSE (eV)	2eVP (eV)	Total Theorie (eV)	Experiment (eV)
83	1897.56	-11.73	0.9	-6.7	1.6	1881.5	1876 ± 14
92	**2265.87**	**-14.11**	**1.3**	**-9.7**	**2.6**	**2246.0**	**2248 ± 9**

Tabelle 8.1. Vergleich der experimentellen Ergebnisse für den Zwei-Elektronenbeitrag zum Ionisationspotenzial in U^{90+} (diese Arbeit) mit den theoretischen Vorhersagen (für Details vgl. Kapitel 4). Die Spalten NR ('non-radiative QED'), 2eSE (Zwei-Elektronen Selbstenergie) und 2eVP (Zwei-Elektronen Vakuumpolarisation) beziehen sich auf die spezifischen Zwei-Elektronen-Strahlungskorrekturen. Zudem ist ein früheres Ergebnis, das an der SuperEBIT gewonnen wurde [10], aufgeführt.

den konnte. Auf Grund der Eigenschaften der Dopplertransformation hat die Unsicherheit in der Bestimmung der absoluten Ionengeschwindigkeit maximalen Einfluß auf das Messergebnis. Besonders hervorzuheben ist, dass im Rahmen der hier durchgeführten Untersuchung erstmalig für ein Experiment am Elektronenkühler abgebremste Schwerionenstrahlen eingesetzt wurden, wodurch die Ionengeschwindigkeit von ca. 70% Lichtgeschwindigkeit auf etwa 20% Lichtgeschwindigkeit reduziert werden konnte. Als Folge wurden nicht nur die Unsicherheiten, wie sie aus der Dopplertransformation resultieren, wesentlich verringert. Vielmehr konnte nun die Messung bei einer entsprechend niedrigeren Kühlerspannung und einem vergleichsweise geringen Kühlerstrom durchgeführt werden. Hierdurch konnte der Bremsstrahlungsuntergrund, der von den Kühlerelektronen hervorgerufen wird, drastisch abgesenkt werden. Schließlich sei noch angemerkt, dass während des Experiments mehrmals zwischen den Ladungszuständen 92+ auf 91+ für den primären, gespeicherten Ionenstrahl gewechselt wurde, um den Einfluß möglicher systematischer Fehlerquellen zu reduzieren bzw. besser zu kontrollieren.

Für den Zwei-Elektronenbeitrag zum Ionisationspotenzial im He-ähnlichen Uran konnte aus dem Experiment ein Wert von 2248 eV gewonnen werden, wobei eine Genauigkeit von 9 eV erreicht wurde. Für den Grundzustand in He-ähnlichen Ionen stellt dieses Ergebnis die bislang genaueste Bestimmung des Zwei-Elektronenbeitrags dar, wobei eine Sensitivität erreicht wurde, die erstmals an die
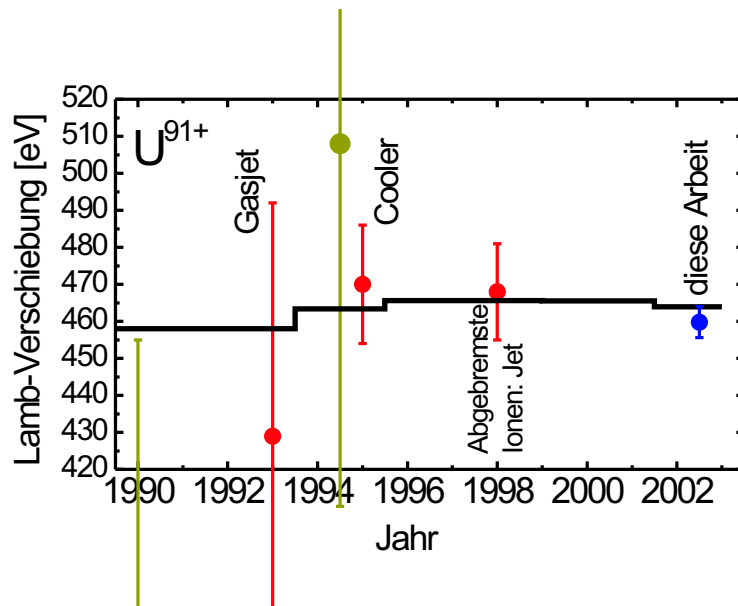
Abbildung 8.1. Experimentelles Ergebnis für die 1s-Lamb-Verschiebung im H-ähnlichen Uran (blau Punkt: diese Arbeit) im Vergleich mit theoretischen Vorhersagen. Zudem sind alle in der Literatur vorliegenden experimentellen Daten für die 1s-Lamb-Verschiebung in U^{91+} abgebildet (rote Punkte: ESR-Daten [7, 9, 44]; grüne Punkte: Daten vom BEVALAC Beschleuniger [45, 46].

Größe der spezifischen Zwei-Elektronen-QED Beiträge heranreicht (2eSE: Zwei-Elektronen Selbstenergie; 2eVP: Zwei-Elektronen Vakuumpolarisation). Dies ist aus Tabelle 8.1 zu entnehmen, in der das erreichte experimentelle Resultat im Vergleich zu der theoretischen Vorhersage von Person et al. [51] wiedergegeben ist, das im Rahmen der 'relativistic many body perturbation theory' gewonnen wurde. Generell sei hier betont, dass es im Rahmen dieser Arbeit erstmals gelang, die vorliegenden Daten für das Ionisationspotenzial schwerer He-ähnlicher Ionen auf U^{90+} zu erweitern, wobei das vorliegende Resultat die früheren Messungen (s. Tabelle 8.1) um einen Faktor Zwei an Sensitivität übersteigt. Der Vergleich mit der theoretischen Vorhersage liefert eine gute Bestätigung für die Theorie der QED für Vielteilchensysteme im Bereich extrem starker Felder.

Neben der Bestimmung des Zwei-Elektronenbeitrags zum Ionisationspotenzial in U^{90+} konnte durch das Experiment auch eine Bestimmung für die 1s-Lamb-Verschiebung für das H-ähnliche Uran gewonnen werden. Hierzu diente neben der

radiativen Rekombinationsstrahlung eine Auswertung der sehr intensiven charakteristischen $2p_{3/2} \rightarrow 1s_{1/2}$ Ly-α_1 Strahlung (ca. 102 keV im Emittersystem). Aus einem Vergleich der Messergebnisse mit den Vorhersagen der Dirac-Theorie für einen punktförmigen Urankern folgt für die $1s$-Lamb-Verschiebung ein Wert von 459.8 eV mit einer Genauigkeit von 4.2 eV. Der Fehler setzt sich hierbei zum Einen aus der statistischen Genauigkeit für die Schwerpunktbestimmung der Röntgenübergänge von 2.3 eV zusammen. Zum Anderen folgt ein wesentlicher Beitrag aus der Genauigkeit, mit der die absolute Ionengeschwindigkeit bestimmt wurde, was sich in einem Fehler von 3.5 eV niederschlägt. Der eigentliche Fehler für den experimentellen Lamb-Shift-Wert folgt hieraus durch quadratische Addition zu 4.2 eV. Dieses sehr präzise Ergebnis, dass die bislang vorliegenden experimentellen Resultate um einen Faktor Drei an Genauigkeit übertrifft, ist Folge der Kombination aus Abbremstechnik und der 'Null Grad'-Detektorgeometrie. In Abbildung 8.1 ist das aus dieser Messung hervorgegangene Messergebnis zusammen mit allen anderen experimentellen Daten dargestellt, die mittlerweile für den $1s$-Grundzustand im U^{91+} vorliegen. Zudem sind ebenso die theoretischen Vorhersagen als Funktion der Jahreszahl wiedergegeben (durchgezogene Linie). Wie aus der Abbildung zu entnehmen ist, befindet sich auch das Ergebnis dieser Arbeit in sehr guter Übereinstimmung mit der theoretischen Vorhersage. Insbesondere kann nun für den konkreten Fall der $1s$-Lamb-Verschiebung in wasserstoffähnlichem Uran der QED-Beitrag auf dem Niveau von 1.5% als gesichert angesehen werden. Hierdurch erfährt die Theorie der Quantenelektrodynamik in sehr starken Coulomb-Feldern eine hervorragende Bestätigung. Zudem ist das erreichte Ergebnis an der Schwelle zur Überprüfung selbst höherer QED-Beiträge, die für den Bereich hoher Kernladungszahlen erst kürzlich theoretisch vorhergesagt wurden und ein Größe von ca. +1.5 eV aufweisen.

Bibliography

[1] T. Beier, Phys. Rep. Lett. **339**, 79, (2000).

[2] G. Soff, T. Beier, and C. Hofmann, Acta Phys. Pol. **B 27** (1996), 369.

[3] R.E. Marrs, Adv. At. Mol. Phys., **27**, 57 (1991).

[4] B. Franzke, Nucl. Inst. Meth. B **24/25**, 18 1987.

[5] B. Franzke, Phys. Scr. T **22**, 41 1988.

[6] H.F. Beyer, V.P. Shevelko (eds.) *Atomic Physics with Heavy Ions*(Springer, Berlin Heidelberg 1999).

[7] Th. Stöhlker, P.H. Mokler, K. Beckert, F. Bosch, H. Eickhoff, B. Franzke M. Jung, T.Kandler, O. Klepper, C. Kozhuharov, R. Moshammer, F. Nodeln, H. Reich, P. Rymuza, P. Spädtke, and M. Steck, Phys. Lett. A **71** (1993), 2184.

[8] H.F. Beyer, D. Liesen, F. Bosch, K.D. Finlyason, M. Jung, O. Klepper, R. Moshammer, K. Beckert, H. Eickhoff, B. Franzke, F. Nodeln, P. Spädtke, M. Steck, G. Menzel, R.D. Deslattes, Phys. Lett. **A 184**, (1994) 435.

[9] H.F. Beyer, IEEE Trans. Instrum. Meas. **44** (1995), 510; H.F. Beyer, G. Menzel, D. Liesen, A. Gallus, F. Bosch, R.D. Deslattes, P. Indelicato, Th. Stöhlker, O. Klepper, R. Moshammer, F. Nodeln, H. Eickhoff, B. Franzke, and M. Steck, Z. Phys. **D 35** (1995), 169.

[10] R.E. Marrs, S.R. Elliot, and T. Stöhlker, Phys. Rev. A **52** 3577 (1995).

[11] J. Schweppe, A. Belkacem, L. Blumenfeld, N. Claytor, B. Feinberg, H. Gould, V.E. Costram, L. Levy, S. Misawa, J.R. Mowat, and M.H. Prior, Phys. Rev. Lett. **66** (1991), 1434.

[12] I. Klaft, S. Borneis, T. Engel, B. Fricke, R. Greiser, G. Huber, T. Kühl, D. Marx, R. Neumann, S. Schröder, P. Seelig, L. Völker, Phys. Rev. Lett. **73** (1994), 2425.

[13] J.R. Crespo Lopez-Urrutia, P. Beiersdorfer, D. Savin and K. Widman, Phys. Rev. Lett. **77** (1996), 826.

[14] P. Seelig, S. Borneis, A. Dax, T. Engel, S. Faber, M. Gerlach, C. Holbrow, G. Huber, T. Kühl, D. Marx, K. Meier, P. Merz, W. Quint, F. Schmitt, L. Völker, H. Winter, M. Würtz, K. Beckert, B. Franzke, F. Nolden, H. Reich, and M. Steck, this volume.

[15] P. Beiersdorfer, A. Osterheld, J. Scofield, J.R. Crespo Lopez-Urrutia, and K. Widman, Lawrence Livermore National Laboratory report UCRL-JC-127437 (1997), p. 18.

[16] H. Häffner, T. Beier, N. Hermanspahn, H. -J. Kluge, S. Stahl, W. Quint, J. verdú, and G. Werth, Phys. Rev. Lett. **85** (2000), 5308.

[17] W.E. Lamb and R.C. Retherford, Phys. Rev. 72, 241(1947)

[18] S.S. Schweber *QED AND THE MAN WHO MADE IT: Dyson, Feynman, Schwinger, and Tomonaga*, Princeton University Press, Pinceteon (1994).

[19] P.J. Mohr, "Atomic, Molecular, & Optical Physics Handbook"(edited by G.W.F. Drake), (Woodbury, NY: AIP, 1996), ch. 28, p. 341.

[20] V.M. Shabaev, M. Tomaselli, T. Kühl, A.N. Artemyev, and V.A. Yerokhin, Phys. Rev. A **56**, 252-255, (1997).

[21] P.J. Mohr, Ann. Phys. **88**, 26, (1974); **88**, 52 (1974).

[22] P.J. Mohr, Phys. Rev. A **46**, 4421, (1992).

[23] P. Indelicato, and P.J. Mohr, Phys. Rev. A **58**, 165, (1998).

[24] P.J. Mohr, and G. Soff, Phys. Rev. Lett. **70**, 158, (1993).

[25] V.A. Yerokhin, and V.M. Shabaev, Phys. Rev. A **60**, 800, (1999).

[26] V.A. Yerokhin, V.M. Shabaev, Phys. Lett. A **207**, 274, (1995) **210**, 437 (1996).

[27] G. Soff, and P.J. Mohr, Phys. Rev. A **38**, 5066, (1988).

[28] N.L. Manakov, A.A. Nekipelov, and A.G. Fainshtein, Zh. Eksp. Teor. Fiz. **95**, 1167 (1989)[Sov. Phys. JETP **68**, 673 (1989)].

[29] H. Persson, I. Lindgren, S. Salomonson, and P. Sunnergren, Phys. Rev. A **48**, 2772, (1993).

[30] P.J. Mohr, G. Plunien, and G. Soff, Phys. Reports **293**, 227, (1998).

[31] T. Beier, *et al.* Phys. Lett. A **236**, 329, (1997).

[32] V.A. Yerokhin and V.M. Shabaev, Phys. Rev. A **64**, 062507-1 (2001).

[33] V.M. Shabaev, Theor. Math. Phys. **63**, 588 (1985).

[34] V.M. Shabaev, Phys. Rev. A **57**, 59 (1998).

[35] V.M. Shabaev, *et al.* Phys. Rev. A **57**, 4235 (1998).

[36] G. Plunien, and G. Soff, Phys. Rev. A **51**, 1119 (1995); **53**, 4614 (1996).

[37] A.V. Nefiodov, L.N. Labzowsky, G. Plunien, and G. Soff, Phys. Lett. A **222**, 227 (1996).

[38] P.J. Mohr, At. Data and Nucl. Data Tables **29**, 453, (1983).

[39] W.R. Johnson and G. Soff, At. Data and Nucl. Data Tables **33**, 405, (1985).

[40] S. Bourzeix, B. de Beauvoir, F. Nez, M.D. Plimmer, F. de Tomasi, L. Julien, F. Biraden, D.N. Stacey, Phys. Rev. Lett. **76**, 384 (1996).

[41] H. Persson , S. Salomonson, P. Sunnergren, I. Lindgren, M.G.H. Gustavsson, Hyperfine Interaction **108**, 3 (1997).

[42] H. Persson, I. Lindgren, L. Labzowsky, G. Plunien, T. Beier, G. Soff, Phys. Rev. A, in print.

[43] Th. Stöhlker, *et al.* GSI scientific report 1997, 99 (1998).

[44] Th. Stöhlker, P.H. Mokler, F. Bosch, R.W. Dunford, O. Klepper, C. Kozhuharov, T. Ludziejewski, B. Franzke, F. Nolden, H. Reich, P. Rymuza, Z. Stachura, M. Steck, P. Swiat, and A. Warczak, Phys. Rev. Lett. **85**, 3109, (2000).

[45] J.P. Briand, P. Chevallier, P.Indelicato, K.P. Ziock, and D. Dietrich, Phys. Rev. Lett. **65**, 2761 (1990).

[46] J.H. Lupton, D.D. Dietrich, C.J. Hailey, R.E. Stewart, K.P. Ziock, Phys. Rev. A **50**, 2150 (1994).

[47] P. Indelicato, private communication (1998).

[48] D.R. Plante, W.R. Johnson, J. Sapirstein, Phys. Rev. A, **49**, 3519 (1994).

[49] O. Gorceix, P. Indelicato, and J. P. Desclaux, J. Phys. B. **20**, 639 (1987); P. Indelicato, O. Gorceix, and J. P. Desclaux, *ibid.* **20**, 651 (1987).

[50] G.W. Drake, Can. J. Phys. **66**, 586 (1988).

[51] H. Persson , S. Salomonson, P. Sunnergren, I. Lindgren, Phys. Rev. Lett. **76**, 204 (1996).

[52] Th. Stöhlker, S.R. Elliott, R.E. Marrs, Hyperfine Interactions **99**, 217 (1996).

[53] S. MacLaren, P. Beiersdorfer, D.A. Vogel, D. Knapp, R.E. Marrs, K. Wong, and R. Zasadzinski Phys. Rev. A **45**, 329, (1992).

[54] P. Indelicato, J. P. Briand, M. Tavernier, and D. Liesen Z. Phys. D **2**, 249 (1986).

[55] Th. Stöhlker, P.H. Mokler, H. Geissel, R. Moshammer, P. Rymuza, E. M. Bernstein, C. L. Cocke, C. Kozhuharov, G. Münzenberg, F. Nickel, C.

Scheidenberger, Z. Stachura, J. Ullrich, and A. Warczak, Phys. Lett. A **168**, 285 (1992).

[56] P.H. Mokler, Th. Stöhlker, C. Kozhuharov, R. Moshammer, P. Rymuza, F. Bosch, and T. Kandler, Phys. Scr. **T51**, 28 (1994).

[57] P. Briand, P. Indelicato, A. Siminovici, V. San Vicente, D. Liesen, and D. Dietrich, Europhys. Lett. **9**, 225 (1989).

[58] T. Franosch and G. Soff, Z. Phys. D **18**, 219 (1991).

[59] G.W.F. Drake, Phys. Rev. A **34**, 2871 (1986).

[60] W.R. Johnson, Phys. Rev. Lett. **29**, 1123 (1972).

[61] R. Marrus, in: "Beam Foil Spectroscopy"(Edited by S. Bashkin) (Springer 1976), Topics in Current Physics 1, p. 209.

[62] R. Marrus, and P.J. Mohr, Adv. At. Mol. Phys. **14**, 181, (1978).

[63] M. Steck, K. Beckert, F. Bosch, H.Eickhoff, B. Franzke, O. Klepper, R. Moshammer, F. Nolden, P. Spädtke, and Th. Winkler, *Proc 4th Europ. Part. Accel. Conf., London 1994*, ed. V. Suller and Ch. Petit-Jean-Genaz (World Scientific, Singapore 1994), p. 1197.

[64] B.Franzke, Information about ESR Paramteres, GSI-ESR/TN-86-01, 1986 (Internal Report).

[65] Th. Stöhlker, D. Banaś, H. Beyer, and A. Gumberidze, Proceedings of "Simple Atomic Systems"conference, (2003).

[66] O. Klepper, C. Kozhuharov, Nucl. Instrum. Meth. B, (in print).

[67] G.I. Budker, in: Proc. Int. Sym. on Electron and Positron Storage Rings, Saclay, 1966 (PUF, Paris, 1967).

[68] H. Poth, Phys. Rep. **196**, 135 (1990).

[69] H.A. Kramers, Phil. Mag. **46**, 836 (1923).

[70] L.H. Andersen, J. Bolko and P. Kvistgaard, Phys. Rev. Lett. **64**, 729 (1990).

[71] L.H. Andersen, J. Bolko, Phys. Rev. A **42**, 1184 (1990).

[72] M. Stobbe, Ann. Phys. (Leipzig) **5**, 661 (1930).

[73] L.H. Andersen, J. Bolko, J. Phys. B **23**, 3167 (1990).

[74] L.H. Andersen, G.Y. Pan, and H.T. Schmidt, J. Phys. B **25**, 277 (1992).

[75] A. Wolf *et al.*, Z. Phys. D **21**, S69 (1991).

[76] A. Wolf, *Wechselwirkungen zwischen hochgeladenen Ionen und freien Elektronen in einem Ionenspeicherring: dynamische Reibung und Rekombination, Habilitation Thesis*, (Heidelberg, 1992).

[77] A. Müller *et al.*, Phys. Scripta T **37**, 62 (1991).

[78] A. Frank *et al.*, Contributed paper to *5-th Int. Conf. on Physics of Highly Charged Ions, Kansas State University, USA 1992.*

[79] Y. Hahn and K.J. LaGattuta, Phys. Rep. **166**, 195 (1990).

[80] F. Brouillard, in *Atomic Processes in Controlled Thermonuclear Fusion,* edited by C.J. Joachain and D.E. Post (Plenum, New York, 1983).

[81] L.H. Andersen, P. Hvelplund, H. Knudsen, and P. Kvistgaard, Phys. Rev. Lett. **62**, 2656 (1989).

[82] P.F. Dittner, S. Datz, P.D. Miller C.D. Moak, P.H. Stelson, C. Bottcher, W.B. Dress, G.D.Alton and N. Neskovic, Phys. Rev. Lett. **51**, 31 (1983).

[83] G. Kilgus *et al.*, Phys. Rev. Lett. **64**, 737 (1990).

[84] W. Spies *et al.*, Phys. Rev. Lett. **69**, 2768 (1992).

[85] G. Kilgus, D. Habs, D. Schwalm, A. Wolf, N.R. Bandell, and A. Müller, Phys. Rev. A **46**, 5730 (1992).

[86] C. Brandau *et al.*, Phys. Rev. Lett. **89**, 053201 (2002).

[87] D.A. Knapp, R.E. Marrs, M.A. Levine, C.L. Bennet M.H. Chen, J.R. Hendersen, M.B. Schneider, and J.H. Scofield, Phys. Rev. Lett. **62**, 2104 (1989).

[88] P. Mensbach and J. Keck, Phys. Rev. **181**, 275 (1969).

[89] D.R. Bates, A.E. Kingstone, and R.W.P. McWhirter, Proc. R. Soc. (London) A **267** 297 (1962).

[90] J. Stevefelt, J. Boulmer, and J.F. Delpech, Phys. Rev. A **12**, 1246 (1975).

[91] S. Byron, R.C. Stabler, and P.I. Bortz, Phys. Rev. Lett. **8**, 376 (1962).

[92] H.F. Beyer, D. Liesen, and O. Guzmann, Part. Accel. **24**, 1 (1989).

[93] W.J. Karzas and R. Latter, Astrophys. J. Suppl. Ser. **6**, 167 (1961).

[94] J.R. Oppenheimer, Phys. Rev. **31**, 349 (1928).

[95] W. Wessel, Ann. Phys. (Leipzig) **5**, 611 (1930).

[96] E.G. Stueckelberg and P.M. Morse, Phys. Rev. **36**, 16 (1930).

[97] W. Gordon, Ann. Phys. (Leipzig), **5**, 1031 (1929).

[98] D.R. Bates, R.A. Buckingham, H.S.W. Massey and J.J. Unwin, Proc. R. Soc. (London) **A170**, 322 (1939).

[99] A. Burgess, Mon. Not. R. Astron. Soc. **118**, 477 (1958).

[100] M.J. Seaton, Mon. Not. R. Astron. Soc. **119**, 81 (1959). (1930).

[101] H. Bethe and E. Salpeter, "Quantum Mechanics of One- and Two-Electron Systems", Vol. 35 of "Handbuch Der Physik"(Springer, Berlin 1957).

[102] M. Pajek and R. Schuch, Phys. Rev. A **45**, 7894 (1992).

[103] J. Eichler, A. Ichihara, and T. Shirai Phys. Rev. A **51**, 3027 (1995).

[104] A. Burgess, Mem. Roy. Ast. Soc. **69**, 1 (1964).

[105] O.C. Brinzanescu, Dissertation University Heidelberg, GSI-DISS 2000-13 (2002) .

[106] O. Brinzanescu and Th. Stöhlker Physica Scripta T **92**, 275 (2001) .

[107] Stöhlker, Th. *et al.,* Hyperfine Interactions **108**, 29 (1997).

[108] Stöhlker, Th. *et al.,* Phys. Rev. Lett. **79**, 3270 (1997).

[109] R.G. Helmer, R.C. Greenwood, R.C. Gehrke, Nucl. Instrum. Methods **124** 107, (1975).

[110] M. Bitter, H.Hsuan, V. Decaux, B. Grek, K.W. Hill, R. Hulse, L.A. Kruegel, D. Johnson, S. von Goeler and M. Zarnstroff, Phys. Rev. A **44**, 1796 (1991).

[111] L.C. Longoria, A.H. Naboulsi, P.W. Gray, and T.D. MacMahon, Nucl. Instrum. Methods Phys. Res. Sect. A **299**, 308, (1990).

[112] E.G. Kessler, L. Jacobs, W. Schwitz, and R.D. Deslattes , Nucl. Instrum. Methods **160** 435, (1979).

[113] W.R. Johnson and J. Sapirstein, Phys. Rev. A **46**, R2197 (1992).

[114] P.J. Mohr, Nucl. Instrum. Methods in Phys. Res. B **87**, 232-236 (1994).

[115] V.A. Yerokhin Phys. Rev. A **62**, 012508 (2000).

[116] A. Mitrushenkov, L. Labzowsky, I. Lindgren, H. Persson and S. Salomonoson, Phys. Lett. A **200**, 51 (1995).

[117] S. Mallampalli and J. Sapirstein, Phys. Rev. Lett. **80**, 5297 (1998).

[118] H.F. Beyer, *Physics with Multiply Charged Ions*, Edited by D. Liesen, (Plenum Press, New York 1995).

[119] H. Beyer, Nucl. Instr. Meth A **400**, 137 (1997).

[120] P. Egelhof, H.F. Beyer, D. McCammon, F.V. Feilitzsch, A.V. Kienlin, H.-J. Kluge, D. Liesen, J. Meier, S.H. Moseley, Th. Stöhlker, Nucl. Instr. Meth. A**370**, 26(1996).

[121] P. Egelhof, Adv. in Solid State Phys. **39**, 61 (1999).

[122] D. Protic, Th. Stöhlker, H. F. Beyer, et. al., IEEE Trans. Nucl. Sci. Vol. 48, No 4, pp. 1048-1052, 2001.

Acknowledgements

I dedicate this work to the memory of Prof. Boris Kikiani, whose help, support and contribution were essential for my PhD study.

I would like to express my very special thanks to my supervisor, Priv. -Doz. Thomas Stöhlker. His contribution is greatest in carrying out this work. His help, suggestions and encouragement throughout the years of my PhD work were absolutely crucial for me.

I direct many thanks to Prof. Dr. Heinz-Jürgen Kluge and to Prof. Dr. Horst Schmidt-Böcking for giving me the unique opportunity to do this PhD work.

I would like to express my gratitude to Prof. Anzor Khelashvili and to Prof. Simon Tsereteli, who have largely contributed to my understanding of physics and supported my study.

For the friendly environment and for their great help I would like to thank my colleagues from the Atomic Physics Department; Dr. D. Banaś, Dr. T. Beier, Prof. H.F. Beyer, Prof. F. Bosch, Dr. O. Brinzanescu, Prof. S. Hagmann , Priv. -Doz. D.C. Ionescu, Dr. O. Klepper, H. Kollmus, Prof. C. Kozhuharov, Dr. A. Krämer, Prof. D. Liesen, Dr. X. Ma, Prof. P.H. Mokler, A. Oršić-Muthig, U. Spillman, Dr. M. Steck, S. Tachenov, Dr. S. Toleikis as well as the external collaborators; D. Sierpowski, G. Bednarz, Prof. M. Pajek, Dr. Z. Stachura, Prof. A. Warczak, Dr. X. Cai, Prof. Y. Zou.

For support and for many happy moments we spent together I would like express my special thanks to Gosia Sudoł.

For being great friends I would like to thank; Dominik, Stanislav, Darek, Kasia & Zbyszek, Mateusz, Giorgios, Alejandro, Alberto, Juan, Gonzalo, Francois, Ahmed, Hayk, Andrey, Agnieszka, Fauzi, Kasia, Tania & Iura, Soso, Koba, Khati, Iona, Giorgi, Zura, Sakhela, Temo, Eka, Valeri, Gigi, Shala, Davita, Dima, Vaska, Stefana, Dito, Tamuna and Goga.

I would like to express my very special gratefulness to my parents, who have greatly supported me in everything, as well as to my family.

To everyone who helped me in carrying out this work, my sincere gratitude.

Lebenslauf

ALEXANDRE GUMBERIDZE

Verdistrasse 33
64291 Darmstadt

Geburtsdatum:	21. September 1976
Geburtsort:	Kutaisi, Georgien

1982-1990	Besuch der G. Tabidze Schule in Tbilisi
1990-1993	Besuch der Oberstufe mit phys. math. Schwerpunkt der G. Tabidze Schule in Tbilisi
Juni 1993	Abitur
1993	Beginn des Studiums an der "Tbilisi State University"
1997	Bachelor of Physics, Mathematics und Informatics (Tbilisi State University)
1998-1999	Anfertigung der Diplomarbeit mit dem Titel: "Nuclear Relaxation in Amorphous States With Paramagnetic Impurities"
1999	Master of Physics (Tbilisi State University)
seit 2000	Doktorand am Institut für Kernphysik der Johann Wolfgang Goethe-Universität Frankfurt und an der Gesellschaft für Schwerionenforschung (GSI)